Energy Research and Development Division

FINAL PROJECT REPORT

A Survey of Methane Emissions from the California Natural Gas System

California Energy Commission

Edmund G. Brown Jr., Governor

October 2017 | CEC-500-2017-033

PREPARED BY:

Primary Author(s):
Marc L. Fischer
Seongeun Jeong
Ian Faloona
Shobhit Mehrota

Lawrence Berkeley National Laboratory
1 Cyclotron Rd.
Berkeley, CA 94720
Phone: 510-486-5539
http://www.calgem.lbl.gov

University of California, Davis
Air Quality Research Center
Davis, California *95616*

Contract Numbers: 500-11-027 and 500-12-006

Prepared for:

California Energy Commission

Yu Hou
Contract Manager

Aleecia Gutierrez
Office Manager
Energy Generation Research Office

Laurie ten Hope
Deputy Director
ENERGY RESEARCH AND DEVELOPMENT DIVISION

Drew Bohan
Executive Director

DISCLAIMER

This report was prepared as the result of work sponsored by the California Energy Commission. It does not necessarily represent the views of the Energy Commission, its employees or the State of California. The Energy Commission, the State of California, its employees, contractors and subcontractors make no warranty, express or implied, and assume no legal liability for the information in this report; nor does any party represent that the uses of this information will not infringe upon privately owned rights. This report has not been approved or disapproved by the California Energy Commission nor has the California Energy Commission passed upon the accuracy or adequacy of the information in this report.

ACKNOWLEDGEMENTS

The authors gratefully acknowledge Stephen Conley and Scientific Aviation for airborne methane measurements; Donald Blake and his group for laboratory analysis of volatile organic compounds; Craig Clements, Ray Bambha, Brian LaFranchi, Hope Michelsen, Craig Clements, Pierre Glaize, Phil Martien, Abhinav Guha, and Jonathan Bower for assistance with measurements at Bay Area air quality measurement stations; and Jon Kofler, Arlyn Andrews, Ben Miller, Steve and Montzka for assistance with analysis of flask measurements at Walnut Grove and Sutro towers. The authors also thank Stephanie Detwiler, Joseph Fischer, Guido Franco, Yu Hou, Veronika Pesinova, François Rongere, Larry Sasadeusz, and Bill Winkler, and Gary Yowell for valuable advice and discussion. This analysis was supported by the California Energy Commissions Public Interest Environmental Research program, with work at Lawrence Berkeley National Laboratory (LBNL) conducted under U.S. Department of Energy Contract DE-AC02-05CH11231.

PREFACE

The California Energy Commission Energy Research and Development Division supports public interest energy research and development that will help improve the quality of life in California by bringing environmentally safe, affordable, and reliable energy services and products to the marketplace.

The Energy Research and Development Division conducts public interest research, development, and demonstration (RD&D) projects to benefit California.

The Energy Research and Development Division strives to conduct the most promising public interest energy research by partnering with RD&D entities, including individuals, businesses, utilities, and public or private research institutions.

Energy Research and Development Division funding efforts are focused on the following RD&D program areas:

- Buildings End-Use Energy Efficiency
- Energy Innovations Small Grants
- Energy-Related Environmental Research
- Energy Systems Integration
- Environmentally Preferred Advanced Generation
- Industrial/Agricultural/Water End-Use Energy Efficiency
- Renewable Energy Technologies
- Transportation

A Survey of Methane Emissions from the California Natural Gas System is a combined final report for projects Evaluation of Opportunities to Mitigate Fugitive Methane Emissions (contract number 500-11-027) from the California Natural Gas System and Source Sector Survey of Natural Gas Emissions from California Infrastructure (contract number 500-12-006) conducted by the Lawrence Berkeley National Laboratory and the University of California, Davis. The information from this project contributes to Energy Research and Development Division's Natural Gas Environmental Research Program.

For more information about the Energy Research and Development Division, please visit the Energy Commission's website at www.energy.ca.gov/research/ or contact the Energy Commission at 916-327-1551.

ABSTRACT

Methane is a potent greenhouse gas and the dominant constituent of natural gas. Measuring and controlling all methane sources, including natural gas, is necessary to limit the adverse consequences of global climate change. This report describes quantitative estimates of methane emissions from some of the California natural gas infrastructure with methane emissions occurring from "well to burner."

To establish a baseline, the research team used a 2013 U.S. Environmental Protection Agency (US EPA) inventory of national natural gas emissions to derive the California bottom-up model. The inventory suggests in-state emissions are about equally split between in-state production and the total of in-state transmission, processing, distribution, and consumption. The team investigated each area using atmospheric measurements and inverse modeling. At the regional level, emissions from production dominate in the Southern San Joaquin and Northern Sacramento Valleys, while distribution- and consumption-related emissions dominate in urban areas like San Francisco Bay Area. Methane emissions from natural gas distribution and consumption in the San Francisco Bay Area California are 1 to 1.6 times the 2013 US EPA bottom-up estimate. Emission measurements from eight natural gas storage fields are consistent with industry reporting to the US EPA, while emissions measured from three refineries were higher than the annual average. Leaks from nine compressed natural gas fueling stations were from 0.03 to 0.1 percent of annual average compressible natural gas retail fuel throughput (the amount of natural gas pumped by the compressors), and there were small but measurable leaks from plugged and abandoned dry-gas wells in the Sacramento River Delta. Finally, leakage measurements for 10 single-family houses were about 0.2 percent of consumption.

Benefits include improved knowledge to guide mitigation, identify measurement technologies to verify progress, and reduce the total societal costs of natural gas as an energy resource.

Keywords: Natural Gas, Methane, Emissions, Mapping, Measurements

Please use the following citation for this report:

Fischer, Marc, Seongeun Jeong, Ian Faloona, and Shobhit Mehrota. 2016. ***A Survey of Methane Emissions from the California Natural Gas System.*** California Energy Commission. Publication Number: CEC-500-2017-033.

TABLE OF CONTENTS

Acknowledgements i

PREFACE ii

ABSTRACT iii

TABLE OF CONTENTS v

LIST OF FIGURES viii

LIST OF TABLES viii

EXECUTIVE SUMMARY 1

Introduction 1

Project Purpose 1

Project Process and Results 1

Recommendations 2

Project Benefits 3

CHAPTER 1: Overview of California Natural Gas Emissions 5

1.1 Overview of California Natural Gas Infrastructure 5

1.2 Need to Survey Emissions From California's Natural Gas Infrastructure 6

1.3 Mapping Methane Emissions From California's Petroleum Production and Natural Gas System 6

1.3.1 Introduction 6

1.3.2 Methods and Data 7

1.3.3 Results and Discussion 15

CHAPTER 2: Inverse Analysis of Regional Natural Gas Emissions Using Multispecies Measurements 30

2.1 Atmospheric Inverse Method for Regional CH_4 Emission Estimates 30

2.2 Observations and Analysis of SFBA Natural Gas CH_4 32

2.2.1 Introduction 32

2.2.2 Data and Methods 33

2.2.3 Results 43

2.3 Sacramento Regional Emission Estimates Using Airborne CH_4 and VOC Measurements 52
2.3.1 Introduction 52
2.3.2 Data and Methods 52
2.3.3 Results and Discussion 60
CHAPTER 3: Facility-Scale Natural Gas Production and Processing Emissions 67
3.1 Overview of Non-Electricity California Natural Gas Facilities 67
3.2 Measurement Sites and Method 67
3.2.1 Measurements Sites 67
3.2.2 Aircraft Instrumentation 68
3.2.3 Airborne Estimation of Facility-Scale Emissions. 69
3.2.4 Error Analysis 70
3.3 Aircraft Mass Balance Emission Estimates 73
3.3.1 Storage Facilities. 73
3.3.2 Refineries. 74
3.3.3 Power Plants, Production Fields, and Processing/Compressor Stations. 75
Section 3.3.4 Analysis of Variability. 76
Section 3.3.5 Discussion 77
CHAPTER 4: Mobile Measurements of Distribution and Small Facility System Leakage 79
4.1 Introduction to Mobile Plume Measurements 79
4.2 Methods for Plume Integration Measurements 79
4.3 Mobile Plume Integration Results and Disussion 81
4.3.1 Bakersfield Production, Distribution, and Consumption Leakage 81
4.3.2 Sacramento Distribution and Consumption Leakage 82
4.3.3 Berkeley and Oakland Distribution and Consumption Leakage 85
4.3.4 Compressed Natural Gas (CNG) Fueling Stations 85
4.3.5 Abandoned Natural Gas Wells 87
CHAPTER 5: Residential Building Leakage 88
5.1 Introduction to Residential Building Leakage 88

5.2 Building Measurement Methods 88
5.2.1 Building Methane Leakage Measurements 88
5.2.2 Measurements at Residences 90
5.3 Building Leakage Results and Discussion 92
5.3.1 Observed CH_4 Enhancements and Leak Rates 92
CHAPTER 6: Summary of Natural Gas Emissions and Mitigation Costs 95
6.1 Summary of California Natural Gas Emissions 95
6.2 Assessment of Mitigation Options 98
REFERENCES 99
Glossary 108
APPENDIX A: Natural Gas Processing Facilities in California A-1
APPENDIX B: Population Density Map (persons per 0.1°×0.1° pixel) in California Based on CIESIN and CIAT B-1
APPENDIX C: Uncertainty Estimates for the Initial Bottom-Up Emissions C-1
APPENDIX D: Sensitivity Analysis D-1
APPENDIX E: Estimated Background Biases for SFBA Sites* E-1
APPENDIX F: Comparison of Bottom-Up Inventories between SFBA and SoCAB F-1
APPENDIX G: VOC Measurements at the THD Background Site G-1
APPENDIX H: Comparison of Measured and Predicted CH_4 Mixing Ratios and Estimated CH_4 Background for SFBA Analysis H-1
APPENDIX I: Correlation between the Landfill to Total Emission Ratios and the LF Emissions for SFBA I-1
APPENDIX J: Evaluation of SFBA Atmospheric Transport Using Carbon Monoxide J-1
APPENDIX K: High-Resolution Methane Emission Model for SFBA K-1
APPENDIX L: Details of Hierarchical Inversion Method L-1
APPENDIX M: Summary of Airborne Facility Measurements M-1

LIST OF FIGURES

Figure 1: Locations of Oil and Gas Wells in California for 2010 9

Figure 2: Natural Gas Transmission System in California 13

Figure 3: CH_4 Emission Maps (nmol m^{-2} s^{-1}; 0.1°×0.1°) by Sector 17

Figure 4: CH_4 Emission (nmol m^{-2} s^{-1}) Maps for the Production Sector 18

Figure 5: Major Natural Gas Pipelines by Size in California and Estimated CH_4 Emission Map 18

Figure 6: CH_4 Emission (nmol m^{-2} s^{-1}) Maps From the Transmission Sector 19

Figure 7: Total CH_4 Emission (nmol m^{-2} s^{-1}) Maps (0.1° resolution) From the Natural Gas System and Petroleum Production for 2010 and 2014 28

Figure 8: Ratios of 2014 to 2010 CH_4 Emissions for the Natural Gas System and Petroleum Production at the County Level 29

Figure 9: High-Resolution (0.01° × 0.01°) Prior Emission Flux (nmol/m^2/s) Maps by Sector 38

Figure 10: WRF Modeling Domain Configuration for the Inner Domains of 12 km (d02), 4 km (d03), and 1.3 km (d04 and d05) Resolutions 40

Figure 11: Simulated Monthly Mean Footprints (ppb/(nmol/m^2/s)) during 12 – 17 PST Hours* . 41

Figure 12: Posterior Distribution of the VOC Ratios Relative to CH_4 42

Figure 13: CH_4 Emissions in SFBA by Sector Using CH_4 Measurements Only 45

Figure 14: Dairy Livestock (DLS) and Landfill (LF) Emission Flux (nmol/m^2/s) Maps and Maps of Ratios of DLS and LF to the Total Emissions for Each 0.1º Pixel 46

Figure 15: Comparison of Posterior CH_4 Emissions* (at 95% confidence) by Source Sector Using CH_4, C_2H_6, i-C_5H_{12}, n-C_5H_{12}, and C_7H_8 Measurements 49

Figure 16: Comparison of Prior and Posterior Natural Gas Emissions (0.1° resolution) for SFBA 50

Figure 17: Measurement Campaign Area and Major Emission Sources in and Around the Measurement Area Over the 30-m Elevation Map 53

Figure 18: High-Resolution (0.1° × 0.1°) Prior Emission Flux (nmol/m^2/s) Maps Used in This Study by Sector 55

Figure 19: Simulated Footprints (ppb/(nmol/m^2/s)) at 1200 PST 57

Figure 20: Estimated C_2H_6:CH_4 Ratios Using Hierarchical Inverse Optimization 58

Figure 21: Estimated Background Values for VOCs During the Three-Day Campaign Period Using Hierarchical Inverse Optimization 59

Figure 22: Summer CH_4 Emissions in the Sacramento Valley by Sector Using CH_4 Measurements Only 61

Figure 23: Comparison of Posterior CH_4 Emissions (at 95% confidence) for the Sacramento Valley by Sector 63

Figure 24: Ratios of 2014 to 2010 CH_4 Emissions for the Natural Gas System in Counties Within the Sacramento Valley Air Basin (A) and Natural Gas Emission Comparison Between 2010 and 2014 by Subsector (B) 65

Figure 25: Flux Divergence Profiles 70

Figure 26: Observed CH_4 Mixing Ratios for Loops Surrounding Rodeo Refinery (May 23, 2016) 75

Table 18: F-Test Results for Facilities Sampled More Than Once 77

Figure 26:: Diagram of MPI System From Above Showing CH_4 Source and Plume (top) and From Side Showing Possible Measurements Taken From Three Levels by Driving Through Plume (bottom) 80

Figure 27: Example Cross Section Views of Measured Plumes by Mixing Ratio Above Background 81

Figure 28: Histogram of Plumes Observed in Bakersfield Area 82

Figure 29: Map of Mobile Survey Driving Route (blue) of the Sacramento Area 83

Figure 30: Isotope Ratio Comparisons for Large Plume Near Watt Avenue (Sacramento, Califoria) 84

Figure 31: Histogram of Estimated Plume Emissions Measured in the Sacramento Area 84

Figure 32: Map of Drives in Oakland and Berkeley, California, With Height Representing Measured CH_4 Concentrations 85

Figure 33: Histogram of Estimated CH_4 Emissions From Drives in Oakland and Berkeley, California 85

Figure 34: Driving Path of an Example CNG Filling Station Showing Multiple Passes 86

Figure 35: Driving Path of an Example Abandoned Well Showing CH_4 Enhancements for Multiple Passes 87

Figure 36: Diagram of the Total House Methane Leak Measurement Method 89

Figure 37: Time Series of Indoor (white background) and Outdoor (grey shaded) CH_4 Mixing Ratio During a Residential Measurement 93

Figure 38: Time Series Plot of CO_2 and CH_4 Concentrations in the Exhaust of an On-Demand Water Heater in Operation 94

LIST OF TABLES

Table 1: Summary of Sector, Subsector, and Activity Data for Estimation of CH_4 Emissions for Natural Gas System and Petroleum Production 8

Table 2: CH_4 Emission Factors for Natural Gas Production 10

Table 3: CH_4 Emission Factors for Petroleum Production 11

Table 4: Emission Factors for the Transmission Sector 14

Table 5: Comparison of Methane Emissions Estimates (Gg CH_4 yr^{-1}) in California's Petroleum Production and Natural Gas System 20

Table 6: Comparison of Natural Gas System CH_4 Emission Estimates in SoCAB (Gg CH_4 yr^{-1}) . 21

Table 7: State Total CH_4 Emission Estimates (Gg CH_4 yr^{-1}) From California's Natural Gas System and Petroleum Production Constrained by Measurements in SoCAB 24

Table 8: Comparison of CH_4 Emission Estimates (Gg CH_4 yr^{-1}) From California's Natural Gas System and Petroleum Production 27

Table 9: Prior Estimates of VOC Emission Ratios Relative to CH_4 Emissions for the Petroleum Sector* 32

Table 10: CH_4 and VOC Measurement Sites for SFBA 34

Table 11: Summary of CH_4 Prior Emissions for BAAQMD* 37

Table 12: Prior CH_4 Emissions for the Sacramento Valley by Sector (Gg CH_4) 54

Table 13: Location and Facility Type Targeted During the Field Campaign 68

Table 14: Storage Facility Characteristics, Measured and Reported Emissions (kg CH_4/hr) 73

Table 15: Measured and Reported Emissions From Refineries (kg CH_4/hr) 74

Table 16: Measured and Reported Emissions From Production, Compressor, and Power Stations (kg CH_4/hr) 75

Table 17: F-Test Results for Facilities Sampled More Than Once 77

Table 18: Building Characteristics for 10 Homes Measured in the San Francisco Bay Area* 90

Table 19 Estimated Regional NG CH_4 Emissions 97

EXECUTIVE SUMMARY

Introduction

While emissions of natural gas methane are uncertain, measurement and control of all methane (CH_4) sources, including natural gas, is recognized as necessary to limiting adverse consequences of global climate change. California receives about 40 percent of its fossil energy use from natural gas and is the second largest natural gas consumer in the United States. California imports about 90 percent of its natural gas supplies from out of state and produces the remaining 10 percent in state; mostly associated with the petroleum production. While inventories for California suggest that natural gas and petroleum systems contribute only about 15 percent of total CH_4 emissions, this distribution has not been explicitly tested except in the South Coast Air Basin. Additional evaluation for California natural gas emissions from transmission, storage, distribution, and consumption subsectors will be valuable to verify inventory estimates and identify opportunities for improvement.

Project Purpose

It is important for California climate action goals to evaluate where and how much natural gas methane is emitted to the atmosphere and identify ways to cut emissions. This report describes results from two California Energy Commission projects that surveyed sectors of California natural gas infrastructure where methane emissions are occurring and, to the extent possible, identify cost-effective opportunities for emissions reduction. The research team focused on measurements and models that provide a survey of infrastructure that might likely be responsible for the majority of California natural gas CH_4 emissions. Promising technologies were identified for future work to accurately quantify total natural gas emissions, verifying the success of specific mitigation activities and determine from previous work estimated costs to reduce these emissions.

Project Process and Results

The research team developed and applied measurement methods to show that CH_4 emissions occur throughout California natural gas infrastructure from "well-to-burner," looking at which areas might likely be responsible for most these natural gas CH_4 emissions. The measurement methods include aerial flight, ground mobile sampling, indoor sensors, and more. The team then identified promising technologies to use in future work to accurately quantify total natural gas emissions and to verify the success of specific mitigation activities.

The 2013 US Environmental Protection Agency (US EPA) emission factors were used in the bottom-up estimate to suggest that in-state emissions are about equally split between in-state production and transmission, processing, distribution, and consumption. Not surprisingly, at the regional level, emissions from production dominate in the Southern San Joaquin and Northern Sacramento Valley, while distribution and consumption related emissions dominate in urban areas like San Francisco Bay Area.

Based on the atmospheric measurements it is estimated the CH_4 emissions from San Francisco Bay natural gas infrastructure are 1 to 1.6 times the 2013 bottom-up estimate, and other work suggests higher values for the South Coast Air Basin. A similar analysis of three days of aircraft

data suggests CH_4 emissions from natural gas infrastructure in the Sacramento Valley, which has more production and storage compared to the San Francisco Bay Area, is consistent with the bottom-up estimates. From the facility-level measurements, emissions were roughly consistent with bottom-up estimates for eight natural gas storage fields, and a measurement of an oil and gas field was consistent with bottom-up estimates for production. In addition, limited airborne measurements show emissions from three refineries were larger than annual average facility reporting to U.S. EPA. At localized scales, distribution system leaks were measurable from roadways, with emissions varying with geographic region. A small sampling of nine natural gas-fueling stations exhibited leaks equivalent to less than one-tenth of 1 percent of average consumption and small but measurable leaks from capped dry-gas wells in the Sacramento River Delta. Last, measurements of leaks from 10 single-family homes suggest methane leaks were equal to about 0.2 percent of consumption, but some combustion appliances such as water heaters might add significantly to these leaks.

Project results and previous work suggest emissions from California's natural gas system are roughly consistent with or slightly larger than those in the current state inventory and the 2013 U.S. EPA inventory. However, they are likely higher for distribution then those estimated scaling from the 2016 U.S. EPA inventory. For planning future observations and mitigation activities, leakage from some subsectors likely contribute large emissions from a smaller number of leaks (for example, concentrated emissions from high-volume facilities), while other sectors likely contribute small leaks from a large number of locations (for example, distribution and consumer end use). Ongoing quantifications of total natural gas CH_4 leakage require a similarly diverse range of measurement methods and mitigation activities and should include improved component and management practices for all natural gas infrastructures, from production to consumption.

In summary, methane emissions from eight natural gas storage facilities were similar to industry reporting to U.S. EPA and CARB, while two others were variable and 2-3 larger than reported. In contrast, emissions from the three refineries measured were roughly an order of magnitude greater than reported. Emissions from eight compressor facilities were similar to that than reported, and measurement of one oil and gas production field was similar to a previous bottom-up estimate. This report also includes the first emission measurements of emissions from single-family homes and natural gas refueling stations, sectors that are not separately reported in current inventories.

Using existing information on costs to mitigate emissions from US gas production and processing, estimated costs to mitigate about 200 Gigagrams (this could be 200,000 metric tons) of CH_4 emitted is about $30 million per year for production and processing related CH_4 emissions. While the cost curves to mitigate emissions from the distribution and consumption sectors are not currently known. If the cost is similar to production and processing, the total mitigation cost for the entire NG system may be $60 million per year.

Recommendations

Based on the work reported in this study, the research team recommends a tiered measurement strategy is to measure and reduce natural gas CH_4 emissions:

- Continuous multispecies observations and atmospheric inversions can be expanded to quantify state total natural gas CH_4 emissions to verify inventory estimates.
- Gas plume imaging from ground, air, and space should be applied to identify local natural gas emission hot spots to measure emissions at the facility level.
- Periodic sensor measurements around facilities with potential leaks should be applied to assess the leaks and localized source emissions for greenhouse gas inventory reporting and reductions.
- Continuous sampling should be employed to monitor facilities that handle large quantities of natural gas.
- Additional work should identify the costs to reduce emissions from the distribution and consumption sectors. This work should expand beyond pipeline leak detection and repair.
- For mitigation activities, energy efficiency monitoring and retrofit programs might be enhanced to include leak detection and repair procedures within buildings.
- Finally, performance standards should be considered to encourage development and adoption of low-emission appliances.

Project Benefits

This project provides an assessment of the likely range of CH_4 emissions from different areas of California's natural gas infrastructure and identifies additional measurements that would improve future mitigation. These benefits include 1) improved understanding of the actual GHG emissions from natural gas infrastructures to help reduce impacts and costs, 2) identifying measurement technologies that improve public safety in areas near high-volume natural gas facilities and 3) avenues to reduce the energy costs of natural gas.

CHAPTER 1:
Overview of California Natural Gas Emissions

1.1 Overview of California Natural Gas Infrastructure

After 30 years of flat output, U.S. natural gas withdrawals increased by 27% between 2006 and 2012 [1] and are expected to increase in the coming years (United States Energy Information Administration [US EIA], 2013). While natural gas has the potential to reduce total greenhouse gas (GHG) emissions by displacing electrical power generation from coal, small emissions of methane (CH_4) during production and distribution could negate these benefits. In simple terms, the warming generated from a 4% leak of CH_4 generates a forcing equal to the remaining 97% of carbon in CH_4 combusted to carbon dioxide (CO_2) on a 20-year timescale, based on the relative molecular weights of CH_4 and CO_2 and the high 20-year global warming potential of CH_4 (84 grams of carbon dioxide equivalent per gram of methane [g CO2eq /gCH4], IPCC [2013]). For example, Alvarez et al. (2012) estimate leakage from well to power plant burner must remain below 3.2% for natural gas power generation to provide climate benefits relative to coal power generation over all time frames. The scientific community has not reached consensus regarding CH_4 emissions from natural gas systems; hence, the climate benefits of natural gas remain uncertain. National-scale estimates of CH_4 emissions as a percentage of gas produced vary significantly. Burnham et al. (2011) estimate emission rates of 0.97% to 5.47% for conventional gas production and 0.71% to 5.23% for shale gas production, while Howarth et al. (2011) estimate relatively high emission rates 1.7% to 6% for conventional gas and 3.6% to 7.9% of shale gas. Allen et al. (2013) estimate emissions from the natural gas production sector to be 0.42% of total production.

In California, GHG emissions from natural gas and petroleum systems are influenced by federal and state policies and historical practices. California consumes more natural gas than any state except Texas,[2] importing 85% of natural gas consumed. California is the second largest oil producer after Texas and has potential for greater production from the Monterey Shale formation (estimated to contain 15 billion barrels of recoverable oil).[3] Much of California's oil production involves enhanced recovery with steam injection. Regarding regulations, California's oil and gas infrastructure has the most comprehensive emissions control regulations in the United States, with Assembly Bill 32 (Núñez, Chapter 488, Statutes of 2006) requiring state total emissions reduced to 1990 levels by 2020.

---

1 U.S. Natural Gas Gross Withdrawals, http://www.eia.gov/dnav/ng/hist/n9010us2a.htm (accessed April 2014)

2 Natural Gas Consumption by End Use, http://www.eia.gov/dnav/ng/ng_cons_sum_a_epg0_vc0_mmcf_a.htm (accessed April 2014).

3 Review of Emerging Resources: U.S. Shale Gas and Shale Oil Plays, http://www.eia.gov/analysis/studies/usshalegas/(accessed April 2014).

1.2 Need to Survey Emissions From California's Natural Gas Infrastructure

There is significant uncertainty in California's CH_4 emission estimates for natural gas and petroleum systems. A series of measurement campaigns in the South Coast Air Basin (SoCAB), including work by Wunch et al. (2009), Hsu et al. (2010), Townsend-Small et al. (2012), Wennberg et al. (2012) and Peischl et al. (2013), and recently Wunch et al. (2016), suggest varying contributions to total CH_4 emissions from petroleum and natural gas activities.

Motivated by these concerns, the California Energy Commission authorized investigations to quantify methane emissions from different subsectors of California's natural gas infrastructure. Two Energy Commission projects focused on surveying the subsectors of California natural gas infrastructure where methane emissions are occurring (contract number 500-11-006) and, to the extent possible, identify cost-effective opportunities for emissions mitigation (contract number 500-11-027). This report focuses on measurements and modeling that provide a survey of infrastructure that might likely be responsible for a majority of California natural gas CH_4 emissions and then identifies promising technologies for use in future work to accurately quantify total natural gas emissions and to verify the success specific of mitigation activities. Efforts have also been recently conducted at the national scale, focusing primarily on quantifying upstream production (e.g., Zavala-Araiza et al., 2015), and includes studies of storage (Subramanian et al., 2015), distribution (Lamb et al., 2015), and regional CH_4 emissions attributed to natural gas using ethane as a fossil fuel-specific tracer (McKain et al., 2015).

1.3 Mapping Methane Emissions from California's Petroleum Production and Natural Gas System

1.3.1 Introduction

Methane emissions from petroleum and natural gas activities were reported in the state's official GHG inventory (California Air Resources Board [CARB], 2013; CARB, 2016) and a CARB equipment survey of gas and petroleum producers (CARB, 2013). However, spatially explicit CH_4 emission maps are required to compare state total oil and gas infrastructure CH_4 emission estimates with regional to local measurement campaigns. Furthermore, a spatially explicit inventory can assist local planning estimates of GHG emissions and is an essential input to atmospheric inverse modeling techniques used to develop emission estimates from limited observations. The Emission Database for Global Atmospheric Research[4] includes emission estimates for natural gas and petroleum systems but the spatial apportionment is primarily based on population (Wunch et al., 2009). The California Greenhouse Gas Emission Measurements (CALGEM, calgem.lbl.gov) project inventory provides some refinement compared with the EDGAR inventory but was based on production data limited to Northern California (Jeong et al., 2012a).

---

4 EDGAR; Global Emissions EDGAR v4.2, http://edgar.jrc.ec.europa.eu/overview.php?v=42 , accessed April 2014.

This work provided an updated, spatially explicit bottom-up estimate of CH_4 emissions from the production, transmission, processing, and distribution of natural gas and petroleum production in California using spatially resolved activity information, disaggregated, or broken down, by sector and facility based on publically available data and published emissions factors[5], and (2) characterized the implications of local measurement campaigns in Southern California on state total emission estimates.

The Methods section details the data and emission factors used to develop the spatially explicit emissions inventory. The Results and Discussion section is subdivided to highlight estimated emission totals, compare this work to other bottom-up inventories, and explore the differences between the bottom-up inventories and top-down measurement campaigns.

1.3.2 Methods and Data

Overall Approach

Spatially explicit emissions for oil production and the natural gas system were estimated from four primary sectors: production, processing, transmission, and distribution. Emission estimates were compared with existing statewide inventories and with top-down measurement campaigns in SoCAB. Total state emissions were scaled from the spatial inventory by sectors; so the SoCAB totals match top-down estimates by sector and estimate a range of revised state total emissions (Section 1.3.3). Although the team estimated uncertainty for the initial bottom-up CH_4 emissions, the primary goal is to estimate the uncertainty in the emission estimates by combining the spatially explicit bottom up emissions with emission measurement from the top-down analyses. To compare the bottom-up CH_4 emission estimates from the natural gas system and petroleum production with the 2010 measurement-based top-down estimates (Peischl et al., 2013), the team focused on estimating emissions for 2010. Researchers estimated emissions for 2014 using the most recent U.S. Environmental Protection Agency (U.S. EPA) inventory (EPA, 2016; data available up to 2014) and discussed the difference in emissions between 2010 and 2014 at the subsector level.

Generally, emissions were disaggregated to the finest scale provided by mostly publicly available activity datasets. For example, processing sector emissions were estimated based only on the volume of gas processed by each facility, while production sector emissions were estimated based on multiple factors, including well type, workovers, frequency of liquid unloadings, and other activity information. The sectors, subsectors, and associated activity data considered in this study are summarized in Table 1.

5 Such as U.S. Environmental Protection Agency (US EPA), 2012; US EPA, 2013; US EPA, 2016).

Table 1: Summary of Sector, Subsector, and Activity Data for Estimation of CH_4 Emissions for Natural Gas System and Petroleum Production

Sector	Subsector	Activity Data[b]
Production	Conventional/unconventional production, associated/non-associated/offshore production[a]	Frequency of liquid unloading, well completion, frequency of well work over, oil and gas production volume, and other activities for fugitive emissions used in the standard EPA emission estimates[d]
Processing	Processing	Number of processing facilities and processing volume
Transmission	Pipeline, compressor station, metering station, and storage facility	Pipeline length, number of compressor/metering stations, number of storage facilities
Distribution	Distribution	Population density and natural gas consumption

[a]The production sector was divided into different subsectors depending on the extraction method (e.g., conventional well) and production type (e.g., associated well).

[b]Activity data are compiled for each grid cell of 0.1°×0.1° to produce spatially explicit emission maps.

[c]Applied to dry gas wells only.

[d]Source: US EPA (2012; 2013; 2016)

Emissions estimates from the product of emission factors and activity data:

$$E_X = E_f \times D_a \quad (1.1)$$

where E_X is the emission of species X (e.g., CH_4), E_f is the emission factor, and D_a is the associated measure of activity (e.g., annual volume of gas produced).

The research team then grids emissions at a 0.1°×0.1° (roughly 10×10 km^2) resolution as

$$E_X^p = \sum_{k=1}^{n} \sum_{j=1}^{m} \sum_{i=1}^{l} E_f^{i,j,k} \times D_a^{i,j,k} \quad (1.2)$$

where E_X^p is the emission of species X for grid cell p, $E_f^{i,j,k}$ is the emission factor for activity i, subsector j, and sector k with $\{i, j, k\} \in p$ and $D_a^{i,j,k}$ is the activity data for activity i, subsector j, and sector k. For example, for the pipeline subsector of the transmission sector, $D_a^{i,j,k}$ represents the total length of pipelines within grid cell p. Therefore, given {i = pipeline length, j = pipeline, k = transmission}, $D_a^{i,j,k}$ itself can be calculated as $D_a^{i,j,k} = \sum_{s=1}^{S_n} L_{s|p}$ where $L_{s|p}$ is the length of a pipeline segment belonging to grid cell p and S_n is the total number of pipeline segments in grid cell p. state total emissions for the entire system can be calculated as $\sum_{p=1}^{T} E_X^p$ where T is the total number of grid cells.

Data and Emission Factors

Production well activities are reported by the California Department of Conservation, Division of Oil, Gas, and Geothermal Resources (DOGGR).[6] DOGGR provides well locations, production volume for each well, well type, and other related information. Figure 1 shows the locations of natural gas wells (active and new) that produced natural gas. This map does not include the many abandoned or plugged wells. Emission factors are adopted from EPA for most activities (Tables 2 and 3).[7]

Figure 1: Locations of Oil and Gas Wells in California for 2010

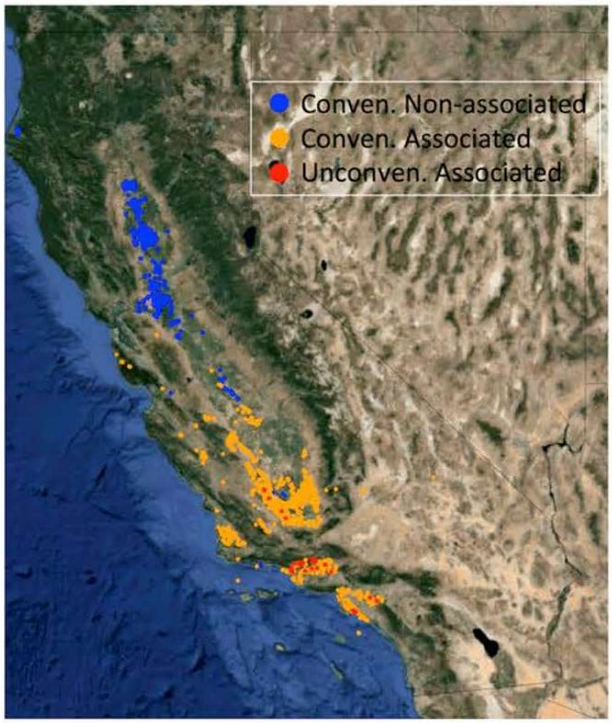

Only active and new wells were shown and no unconventional nonassociated wells were identified.

6 http://www.conservation.ca.gov/dog/Pages/Index.aspx, accessed April 2014.

7 (US EPA, 2012; US EPA, 2013; US EPA, 2016).

Table 2: CH_4 Emission Factors for Natural Gas Production

Emission Source	Emission Factor for 2010 from the 2012 EPA Inventory[a]	Emission Factor for 2014 from the 2016 EPA Inventory[b]	Units	Notes
Liquid unloading	0.83	0.57	Mg CH_4/well	Due to the lack of spatially disaggregated liquid unloading data, the emission factor was calculated by dividing the total CH_4 emissions from EPA by the total number of wells (US EPA, 2013; 2016)
Well completion	0.02	0.02	Mg CH_4/well completion	
Well workover	0.06	0.05	Mg CH_4/ workover	0.04 workovers per well-year applied for both 2010 and 2014 (US EPA, 2012; 2016)
Other fugitive emissions	0.02	0.08	Mg CH_4/ Mg natural gas	Includes fugitive emissions from pneumatic devices, other point source and fugitive emissions based on EPA total emissions (US EPA, 2012; 2016) and the total produced natural gas from US EIA and DOGGR[c]
Offshore production	5.28×10^{-3}	4.35×10^{-3}	Mg CH_4/Mg natural gas	Based on the total emissions from EPA (US EPA, 2012; 2016) and total natural gas production from USEIA[d]

[a]These emission factors (i.e., net emission factors for 2010) for the natural gas system are for the West Coast region. Emission factors for the production sector are taken from the US EPA 2012 inventory (for 2010; U.S. EPA, 2012) except for liquid unloading, which is based on the 2013 inventory (for 2011; U.S. EPA, 2013). Although the research team finds that in general there is no significant difference between the 2010 and 2011 emissions from the 2012 and 2013 inventories, respectively, there is a large discrepancy for liquid unloading between the 2010 and 2011 emissions, which is discussed in the sensitivity analysis (see Appendix D).

[b]Based on the 2016 US EPA inventory for 2014 (US EPA, 2016). These emission factors are for potential emissions (as opposed to those in the 2012 inventory). To obtain net emission factors, researchers multiplied these values by 0.88 because the emission reduction rate for the natural gas production sector was 12%.

[c]Natural gas production for Oregon (1.4 Bcf / year for 2010 and 1.0 Bcf/year for 2014; Bcf = 109 cubic feet) is from US EIA (Natural Gas Gross Withdrawals and Production for Oregon; http://www.eia.gov/dnav/ng/ng_prod_sum_a_EPG0_FGW_mmcf_a.htm). For 2010, California's total production (71 Bcf / year) is from the 2010 DOGGR preliminary report (DOGGR, 2011). The DOGGR report includes production from state offshore, which is assumed to be negligible as shown in the 2009 DOGGR final report (DOGGR, 2010). For 2014, 35 Bcf natural gas was produced in California (DOGGR, 2014).

[d]Natural Gas Gross Withdrawals and Production for Offshore; http://www.eia.gov/dnav/ng/ng_prod_sum_dcu_rusof_a.htm.

Table 3: CH_4 Emission Factors for Petroleum Production

Emission Source	Emission Factor for 2010 from the 2012 EPA Inventory[a]	Emission Factor for 2014 from the 2016 EPA Inventory[b]	Units	Notes
Well completion	0.014	0.014	Mg CH_4/well completion	Used 733 cf / completion from EPA (US EPA, 2012; 2016)
Well workover	1.85×10^{-3}	1.83×10^{-3}	Mg CH_4/workover	0.16 workovers per well-year for 2010 (US EPA, 2012) and 0.13 workovers per well-year for 2014 (US EPA, 2016)
Other emissions	5.98×10^{-4}	8.43×10^{-4}	Mg CH_4/barrel oil	Includes fugitive emissions from pneumatic devices, other point source and fugitive emissions based on EPA total emissions (US EPA, 2012; 2016) and total produced oil[c]
Offshore production	1.04×10^{-3}	3.27×10^{-4}	Mg CH_4/barrel oil	Based on the total emissions from EPA (US EPA, 2012; 2016) and total offshore oil production[c]

[a]These emission factors for petroleum production are national averages. These values for 2010 from the 2012 inventory represent net emission factors.

[b]The 2016 EPA inventory (for 2014) provides emission factors for potential emissions. To obtain net emission factors, a factor of 0.99 was multiplied to these emission factors because voluntary reductions were only 1% of the total potential emissions.

[c]Crude Oil Production; http://www.eia.gov/dnav/pet/pet_crd_crpdn_adc_mbbl_a.htm.

California wells are categorized into conventional and unconventional wells depending on the drilling/extraction method of gas or oil. In this study, unconventional wells are hydraulically fractured wells. The DOGGR database[8] "does not identify hydraulically fractured as wells that are fractured vertically or horizontally" (personal communication with DOGGR staff). EPA also attributes all emissions from dry-gas production to conventional wells for the West Coast, including California (U.S. EPA, 2012; U.S. EPA, 2013). Associated gas production is distinguished from wells producing gas and petroleum and nonassociated gas (dry gas) production, from wells producing only gas. Region-specific (West Coast) emission factors are applied to nonassociated gas production available from U.S. EPA (2012; U.S. EPA, 2013), while national average emission factors are used for petroleum production (not available for individual regions).

[8] http://www.conservation.ca.gov/dog/Pages/Index.aspx, accessed April 2014

The activity data gathered for the production sector vary by well type. For example, activity data for all active well types include production volumes of individual wells, well work over, and time of well completion, while liquid unloadings data are compiled only for dry gas wells. Production is 187.7 billion cubic feet (Bcf) and 70.0 Bcf for associated and nonassociated natural gas, respectively, by summing all wells within California.[9] These totals are slightly different from the DOGGR preliminary report, which estimated 184.6 and 70.9 Bcf, respectively.[10] Associated production n was mostly from conventional wells (186.5 Bcf), with 1.2 Bcf produced from unconventional wells. All nonassociated gas was produced from the conventional wells, and most was produced in Northern California.

Processing stage emissions are based on the volume of natural gas processed at each facility. Natural gas processing facility information is reported in the Natural Gas Annual Respondent Query System of Energy Information Administration (EIA).[11] Processing facility locations are provided in Appendix A. Because detailed component-level emission factors are not available for each facility, national average emissions factors used here are calculated based on the ratio of US EPA's processing sector emission estimates to total natural gas processed (0.96 Tg CH_4 / 308 Tg natural gas = 3.1×10^{-3} Mg CH_4 / Mg natural gas; natural gas density of 19.05 g / cf used throughout the study) (US EPA, 2012; US EIA Natural Gas Annual Respondent Query System, http://www.eia.gov/cfapps/ngqs/ngqs.cfm?f_report=RP9, accessed April 2014). The estimated emission factor is applied to the volume of natural gas processed at each facility.

Transmission emissions include emissions from pipelines, compressor stations, metering stations, and storage facilities, which are estimated using national average emission factors. The major transmission pipelines are included but not those used for local natural gas distribution. It is assumed all other local pipes belong to the distribution sector, and this categorization may be different from that of U.S. EPA.

Georeferenced transmission sector data were obtained from the California Energy Commission, which are similar to available data from the Energy Commission [12] and PG&E.[13] Figure 2 shows spatial data for the transmission sector in California, including pipelines, compressor stations, storage stations, and metering stations. (Distribution metering stations are not included.) The

---

9 (DOGGR, http://www.conservation.ca.gov/dog/Pages/Index.aspx, accessed April 2014)

10 (DOGGR,2011)

11 Natural Gas Annual Respondent Query System of Energy Information Administration, http://www.eia.gov/cfapps/ngqs/ngqs.cfm?f_report=RP9 (accessed April 2014).

12 Map of Major Natural Gas Pipelines in California, http://www.energy.ca.gov/maps/infrastructure/natural_gas.html (accessed April 2014).

13 Western North American natural gas pipelines, http://www.pge.com/pipeline/about/system_maps/western_pipelines_2011.pdf (accessed April 2014); California pipeline/storage facilities, http://www.pge.com/pipeline/about/system_maps/statemap.pdf (accessed April 2014).

total length of pipelines is 11.81×10^3 miles (excluding pipes marked with size of < 0), slightly larger than US EIA's estimate of 11.77×10^3 miles. [14]. Table 4 summarizes emission factors for transmission stage subsectors.

Figure 2: Natural Gas Transmission System in California

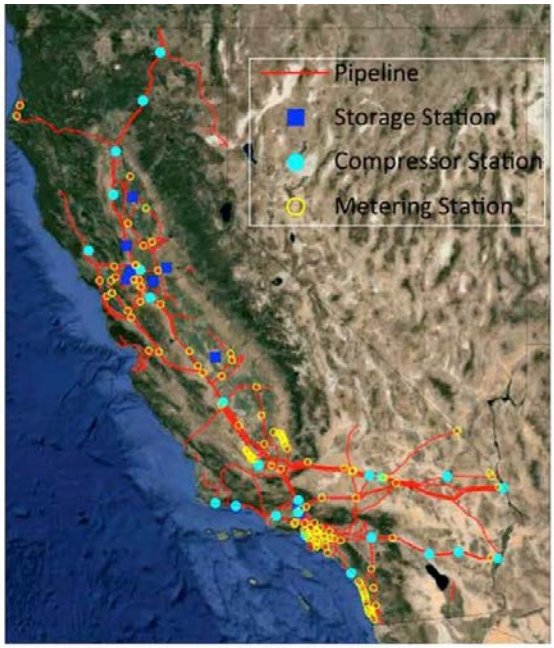

Based on the Energy Commission GIS Database

California compressor station locations are also included. There were some unknown compressor stations listed in the Energy Commission GIS database, and the research team checked and identified the unknown stations by referring to information from US EIA[15] and PG&E.[16] Compressor station subsector emissions were estimated based on the simple emission factor of 571 Mg CH_4/station-year from the Interstate Natural Gas Association of America (INGAA, 2005), as information regarding subcomponents for each compressor station was not available (i.e., "Tier 1" approach).

---

14 Estimated Natural Gas Pipeline Mileage in the Lower 48 States, Close of 2008, http://www.eia.gov/pub/oil_gas/natural_gas/analysis_publications/ngpipeline/mileage.html (accessed April 2014).
15 U.S. Natural Gas Pipeline Compressor Stations Illustration, 2008, http://www.eia.gov/pub/oil_gas/natural_gas/analysis_publications/ngpipeline/compressorMap.html (accessed April 2014).
16 PG&E compressor stations, http://www.pge.com/mybusiness/environment/taking-responsibility/compressor-stations/ (accessed April 2014).

Table 4: Emission Factors for the Transmission Sector

Transmission Subsector	Emission Factor	References
Pipeline	1.55 Scfd[a]/ mile	INGAA (2005) and EPA (2012)
Compressor station	571.25 Mg CH_4/station-year	INGAA (2005)
Metering station	1.15 Mg CH_4/station-year	INGAA (2005)
Storage facility	675.40 Mg CH_4/station-year	INGAA (2005)

[a]Scfd = standard cubic feet per day

Metering station and storage facility information is also available from the Energy Commission GIS database and is included. An emission factor of 1.15 Mg CH_4/station-year (INGAA, 2005) for identified metering stations was used. Identified storage facilities in the Energy Commission GIS database are similar to storage facilities mapped by US EIA[17] and PG&E.[18] Lacking detailed storage facility information (e.g., counts of pumps), researchers use an emission factor of 675 Mg CH_4/station-year from INGAA (2005).

Estimating emissions from the distribution of natural gas requires detailed geospatial information of distribution pipelines and metering stations. This information, especially detailed geospatial information, is not readily available. Therefore, the population density of California was used as a proxy for natural gas distribution. Population data were derived from the Center for International Earth Science Information Network (CIESIN) and Centro Internacional de Agricultura Tropical (CIAT)[19] (Appendix B). There is a correlation between fractional county natural gas consumption and fractional county population (regression of consumption versus population = 1.07±0.08, R^2=0.66). No adjustment, however, has been made to the distribution estimates for large gas consumers such as power plants or industrial facilities because there is little knowledge of emissions from large gas consumers. A simple distribution emission rate of 0.3% of natural gas delivered to consumers is estimated by comparing the total

17 U.S. Underground Natural Gas Storage Facilities, Close of 2007, http://www.eia.gov/pub/oil_gas/natural_gas/analysis_publications/ngpipeline/undrgrndstor_map.html (accessed April 2014).

18 California pipeline/storage facilities, http://www.pge.com/pipeline/about/system_maps/statemap.pdf (accessed April 2014).

19 Gridded Population of the World (GPW), v3, http://sedac.ciesin.columbia.edu/gpw (accessed April 2014).

natural consumption (24.09×10^{12} cf for 2010[20]) and the EPA-estimated CH_4 emissions for the natural gas distribution sector (1410 Gg CH_4 for 2010; US EPA, 2012).

Similarly, a U.S. EPA study estimated an emission rate (emission as percentage of produced or consumed gas) of 0.35% of the gross U.S. natural gas production for the 1992 base year (U.S. EPA, 1997). This emission rate is equivalent to 0.38% of the total U.S. natural gas consumption for 1992 (20.2 × 1012 cf) [21] which is similar to the simple emission rate of 0.3%. The emission rate for the distribution sector is uncertain, so the research team used the national average emission rate of 0.3% in its initial estimation of distribution emissions. The initial estimate based on results from a California-specific top-down analysis is adjusted. A sensitivity analysis of emissions for the distribution sector to emission rates is also presented in the Appendix D. Total CH_4 distribution emissions are allocated according to population density in California as in Jeong et al. (2012a). This simplification does not capture variations in the age or maintenance characteristics of both utility-side and customer-side infrastructure.

1.3.3 Results and Discussion

Initial Bottom-up Estimation of Spatially Explicit Emissions

Spatially disaggregated CH_4 emission estimates for petroleum production and the production, processing, transmission, and distribution sectors of the natural gas system were reported. As described previously, the focus is on the emission estimates for 2010 based on the 2012 U.S. EPA inventory because the top-down estimates by Peischl et al. (2013), which are used for scaling of the bottom-up estimates, are based on atmospheric measurements in 2010. Furthermore, the emission estimates for the distribution sector based on the most recent 2016 U.S. EPA inventory are significantly lower compared to those based on the 2012 inventory, which are not consistent with recent top-down studies (e.g., Wennberg et al., 2012, Peischl et al., 2013). More discussion is provided on the difference in CH_4 emission estimates between 2010 and 2014.

Emission maps using the emission factors and activity data described in Section 1.3.2 were constructed showing estimated CH_4 emissions from production based on well locations, well type and other activity data (Figure 3). CH_4 emissions from non-associated gas wells are dominant in northern California (mostly Sacramento Valley) while CH_4 emissions from associated gas wells are concentrated in the southern San Joaquin Valley and SoCAB. No unconventional non-associated gas wells from the DOGGR database were identified. US EPA also reports that there is no unconventional non-associated gas well in the West Coast region (US EPA, 2012; US EPA, 2013). For oil wells (including associated gas production), emission factors were used for the petroleum system from EPA where there is no distinction in emission factors between conventional and unconventional wells.

---

20 Natural gas consumption by end use, http://www.eia.gov/dnav/ng/ng_cons_sum_dcu_SCA_a.htm (accessed April 2014).

21 U.S. Natural Gas Total Consumption, http://www.eia.gov/dnav/ng/hist/n9140us2a.htm (accessed April 2014).

Using the 2010 DOGGR database for oil and gas wells, total California CH_4 emissions (including offshore emissions) were estimated at 140.2 and 27.7 Gg CH_4 yr^{-1} for associated wells and nonassociated wells, respectively. Although offshore petroleum production is 15% of California total production (nationally 29%), offshore oil well emissions account for 26% (offshore gas well emission = 1% of total gas well emission) of the total CH_4 emissions from oil wells.[22] The reason for high CH_4 emissions from offshore petroleum production is that U.S. EPA emission factors for the offshore petroleum production are 1.7 times higher than those of the onshore production (U.S. EPA, 2012; U.S. EPA, 2013).

The team estimated 12.10 Gg CH_4 yr^{-1} for California's processing sector, or about 4% of the initial total CH_4 emission estimated in this study. Although total emissions from processing are relatively small, localized emissions are comparable to CH_4 emissions from small landfills in California (Jeong et al., 2012a).

For the transmission sector, estimates have been made for CH_4 emissions from major pipelines (local distribution pipelines are included in the distribution estimate), compressor stations, metering stations, and storage stations. Methane emissions for the pipeline subsector are estimated as a function of pipeline length, as described in Section 1.3.2. As size-dependent emission factors were unavailable, a uniform emissions factor was applied to all pipelines. Annual state total CH_4 emissions from pipelines were estimated at 0.12 Gg CH_4, a fraction of the total transmission related emissions (20.90 Gg CH_4) (Figure 5). Applying the emission factor from INGAA (2005) to compressor stations uniformly, the research team estimated 13.14 Gg CH_4 emitted from compressor stations. Although fewerless than 30 grid cells (0.1°×0.1°) contained compressor stations, an accurate spatial characterization of these stations is important for research using top-down inverse modeling approaches. The team estimated 0.14 and 7.50 Gg CH_4 for the metering station and storage facility subsectors, respectively. Among the four subsectors of the transmission sector, compressor stations account for the largest portion of the CH_4 emissions (63%) followed by storage facilities (36%) (Figure 6). Pipelines and metering stations emit less than 2% of the transmission sector total.

---

22 US EPA, 2012; US EPA, 2013; DOGGR, 2011; Crude Oil Production, http://www.eia.gov/dnav/pet/pet_crd_crpdn_adc_mbbl_a.htm, accessed April 2014.,

Figure 3: CH_4 Emission Maps (nmol m^{-2} s^{-1}; 0.1°×0.1°) by Sector

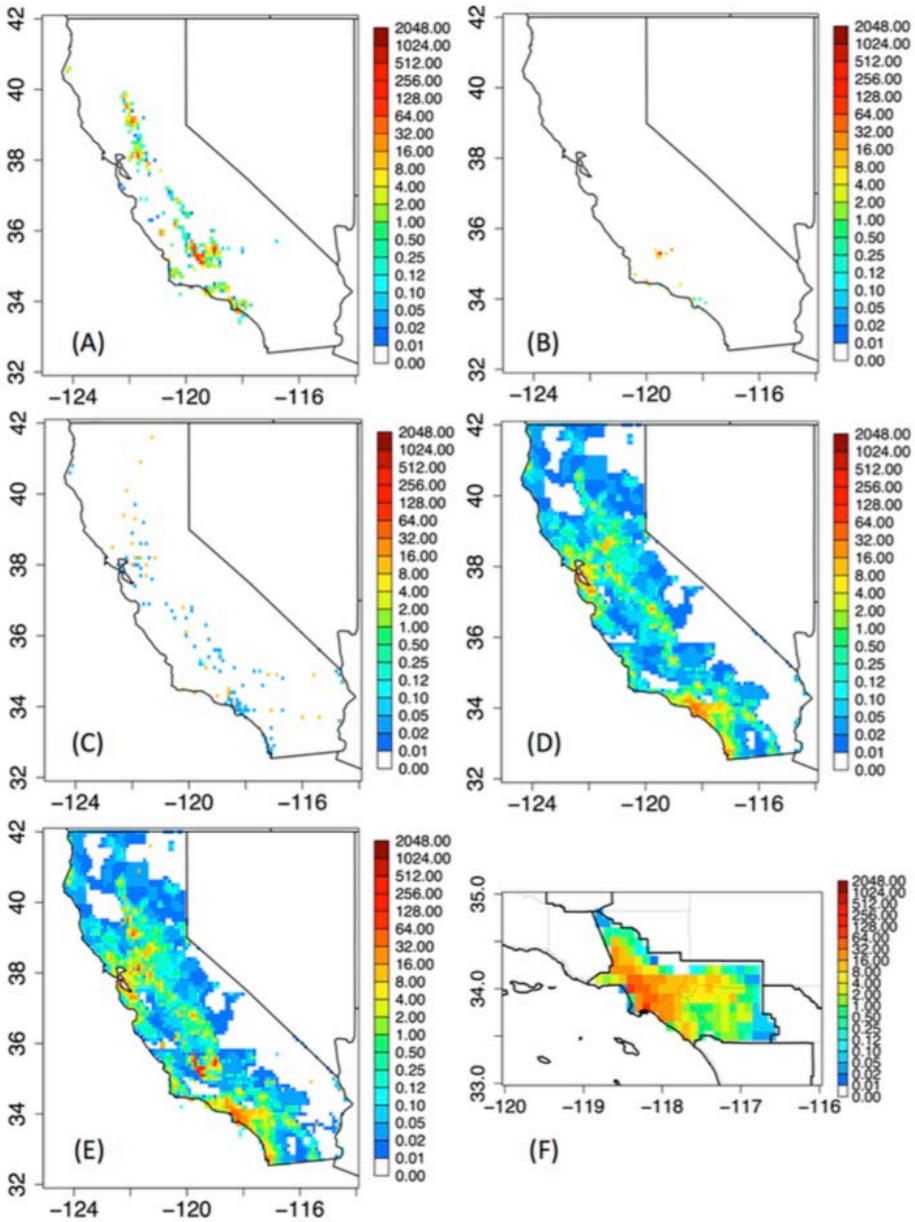

(A) production, (B) processing, (C) transmission, (D) distribution sectors in California, (E) state total CH4 emissions, and (F) SoCAB total CH4 emissions from petroleum production and the natural gas system.

The state total emissions for the distribution sector were estimated at130.0 Gg CH_4 yr^{-1}, assuming a 0.3% emission rate (ratio of CH_4 emissions to natural gas consumption - Section 1.3.2). Emissions were allocated in proportion to population density. Distribution accounts for 39% of the initial total CH_4 emission from oil production and the natural gas system in California, the number driven by the large amount of natural gas that is consumed. Uncertainty in distribution (and other) sector emission estimates were evaluated in relation to field measurement campaigns in the following sections.

Figure 4: CH_4 Emission (nmol m^{-2} s^{-1}) Maps for the Production Sector

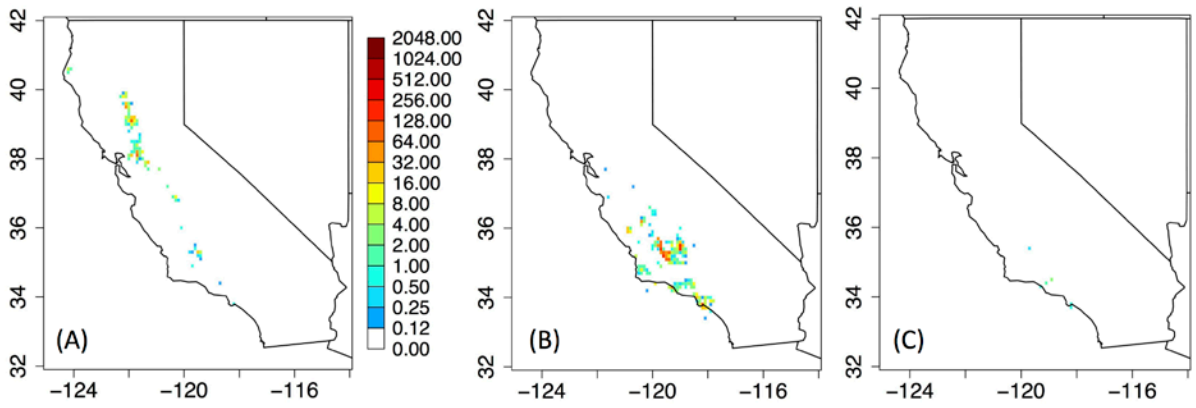

CH4 emission maps for the production sector from: (A) conventional non-associated wells, (B) conventional associated wells, and (C) unconventional associated wells. Federal offshore emissions are not included in these emission maps, but are calculated separately.

Figure 5: Major Natural Gas Pipelines by Size in California and Estimated CH_4 Emission Map

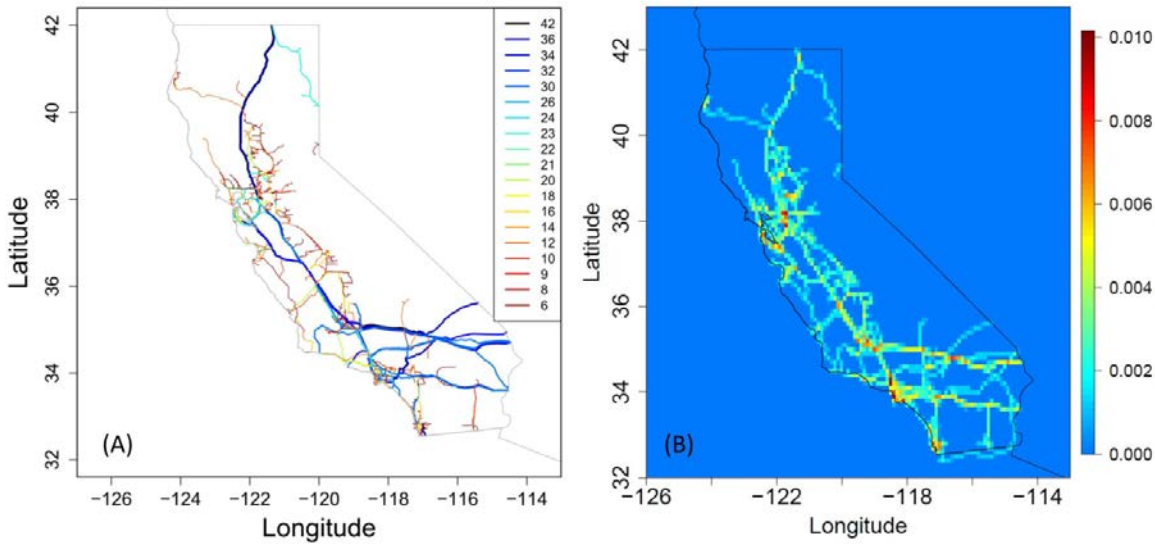

(A) Major natural gas pipelines in California (shown for pipelines greater than five inches in diameter) and (B) CH4 emission (nmol m-2 s-1) map from transmission pipelines (emissions are shown to be zero outside California).

Figure 6: CH_4 Emission (nmol m^{-2} s^{-1}) Maps from the Transmission Sector

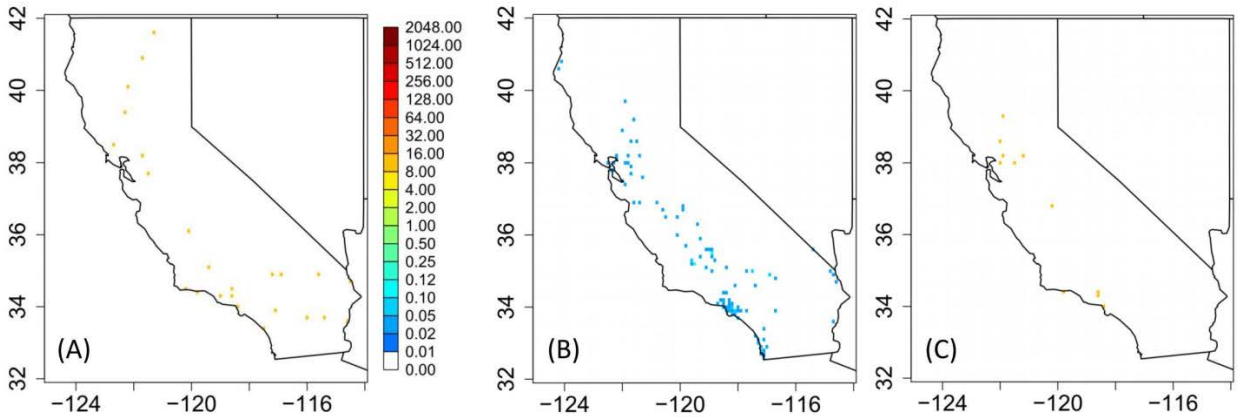

(A) compressor stations, (B) metering stations, and (C) storage facilities in California.

Initial Bottom-up State Total Emissions

State total emissions from petroleum production and the natural gas system are 222 – 518 Gg CH_4/yr (Table 5). The uncertainty estimate, shown in Table 1.5, is based on U.S. EPA's uncertainty estimates, which provides the overall uncertainty for the natural gas and petroleum systems as the percentage deviation from the mean estimates (Appendix C). Later, however, adjusted emissions with uncertainties were calculated based on results from a top-down study in SoCAB and reported as the final estimates because of the lack uncertainty estimates specific to California's activity data and emission factors.

Analysis of sensitivity of emission estimates were included to selected factors, for example liquid unloadings and well completions (Appendix D). CH_4 emissions at the production, processing, transmission, and distribution stages account for 50.7, 3.7, 6.3, 39.3% of the initial state total emissions from petroleum production and the natural gas system, respectively.

The initial bottom-up state total estimates were compared to two other bottom-up estimates, the CARB Oil and Gas Survey (CARB-OGS; ARB, 2013) estimate and California's official greenhouse gas (CARB-GHG) inventory (CARB, 2013). Despite differences in method and in sector categorization, the bottom-up inventories are in rough agreement with each other, except for emissions from petroleum production and, to a lesser extent, emissions from dry-gas production. The CARB-OGS was based on detailed information regarding equipment, equipment components, and activity in oil and gas production and processing facilities in California. By gathering such detailed equipment information, CARB-OGS was able to apply detailed and activity-based emission factors and develop GHG emission estimates for facilities across the state. However, the specific facility data CARB-OGS gathered are confidential, and the reproduction of this type of bottom-up inventory would not be feasible for outside institutions.

The estimate of total CH_4 emissions from petroleum and associated gas production is 4.3 times that of CARB-OGS. The emission estimates from nonassociated gas production is 1.7 times that

of CARB-OGS. The estimate of total production emissions (petroleum-based + dry natural gas) is 6.7 times larger than total production emissions from the CARB-GHG inventory, although the CARB-GHG production categories may not match exactly with the research team's categories. These estimates for emissions related to processing are double those of the CARB-OGS inventory, but the estimates for storage are within 20% of the CARB-OGS inventory. The estimates of total transmission and distribution emissions are within 20% of CARB-GHG estimates. (CARB-OGS did not estimate transmission and distribution emissions.)

Table 5: Comparison of Methane Emissions Estimates (Gg CH_4 yr^{-1}) in California's Petroleum Production and Natural Gas System

Sector	Initial Bottom-Up Emission Estimates for 2010 from This Work	2007 Emission Estimates from CARB-OGS[a]	2011 Emission Estimates from the 2013 CARB-GHG Inventory	2014 Emission Estimates from the 2016 CARB-GHG Inventory
Production: Associated	140.2	32.3[b]	38.8[c]	72.9[e]
Production: Non-associated	27.7	16.2	--	--
Processing	12.1	6.1	--	--
Transmission: Storage	7.5	6.3	--	--
Transmission: All other sources	13.4	--	171.9[d]	159.7[f]
Distribution	130.0	--	--	--
Total	330.9 (222 – 518)[g]	204.3[h]	210.7	232.6

[a]Summary of CARB's Oil and Gas Industry Survey Results (CARB, 2013)

[b]Includes all CH_4 emissions associated with gas and (on and offshore) crude oil production.

[c]The GHG inventory groups oil and gas extraction (associated + non-associated) into one category. This category also includes emissions from processing.

[d]This includes the residential leakage and distribution pipelines as well as transmission pipelines because CARB used total organic gases emissions for specification of CH_4 emissions based on California Emission Inventory Development and Reporting System (CEIDARS) database. Storage emissions are also included in this category.

[e]Includes emissions from production and processing.

[f]Includes fugitive emissions from transmission and distribution pipelines.

[g]This range of emissions (in the parentheses) were calculated by incorporating uncertainty estimates for the natural gas (lower bound = 19%, upper bound = 30% as percentage deviation from the mean at 95% confidence interval) and petroleum (lower bound = 24%, upper bound = 149%) systems from the EPA inventory (US EPA, 2012; 2013), on which most of the emission factors are based. See Appendix C.

[h]This total is calculated by including the estimates from this work for the sectors where the CARB-OGS did not contain estimates.

Comparison to Top-Down Estimates in SoCAB

Based on the initial bottom-up approach, the research team estimated a total of 83.2 Gg CH_4 yr^{-1} for the entire natural gas system and oil production in SoCAB (Table 6). By subsectors, the team estimated 24.0 and 59.2 Gg CH_4 yr^{-1} for natural gas production/processing and transmission/distribution, respectively. The bottom-up CH_4 emission estimates in SoCAB were compared to several top-down studies that have been conducted in the basin. Comparison with these top-down studies allowed evaluate of the uncertainty in the bottom-up approach.

Table 6: Comparison of Natural Gas System CH_4 Emission Estimates in SoCAB (Gg CH_4 yr^{-1})

Study	Method	Comments and Sector Specific Totals	Total Emissions (all sources)	Time Period
Townsend-Small et al. (2012)	Top-down: Isotopic measurements	Majority of all CH_4 emissions from geologic seeps, pipelines, fossil fuels refining		Aug. 2009
Wunch et al. (2009)	Top-down: FTS, CH_4/CO_2 and CH_4/CO correlation	Two different estimates: relative to CO and CO_2	400±100 (CO-based) 600±100 (CO_2-based)	2007 - 2008
Hsu et al. (2010)	Top-down: CH_4/CO correlation	NA	380±100[a]	2007-2008
Wennberg et al. (2012)	Top-down: $CH_4/C_2H_6/CO$ correlation	Natural gas (NG) system total: 390±150[b]	440±150	2008, 2010
Peischl et al (2013)	Top-down: $CH_4/CO/CO_2$ correlation combined with light alkanes	NG transmission and distribution + local seeps: 192±54[c] Landfills, dairies, wastewater: 182±54 NG production/processing: 32±7	410±40	2010
This Work	Bottom-up	NG production/processing: 24.0[d] NG storage: 2.0 NG transmission and distribution[e]: 57.2 NG system total: 83.2	NA	2010
CARB-GHG from CARB's 2013 Inventory (CARB, 2013)	Bottom-up[f]	NG production/processing: 5.2 NG transmission and distribution: 67.4 NG system total: 72.6	NA	2011
CARB-OGS (CARB, 2013)	Bottom-up[g]	NG production/processing/storage: 6.8	NA	2007
CARB-GHG	Bottom-up[f]	NG	NA	2014

Study	Method	Comments and Sector Specific Totals	Total Emissions (all sources)	Time Period
from CARB's 2016 Inventory (CARB, 2016)		production/processing: 9.7 NG transmission and distribution: 62.6 NG system total: 72.4		
EDGAR42[h]	Bottom-up	NG system total: 229.5	630	2008

[a]Originally Hsu et al. (2010) reported total LA County emissions (at 200 Gg CH_4 yr^{-1}), Wennberg et al. (2012) expanded the Hsu et al. (2010) results to the full SoCAB.

[b]An upper bound estimate.

[c]Peischl et al. (2013) suggest an important portion of local seeps come from the La Brea Tar Pits as estimated by Farrell et al. (2013) to be ~1/6 kiloton per day or ~61 Gg CH_4 yr^{-1}. This leaves 131 Gg CH_4 yr^{-1} from transmission and distribution and seeps other than the La Brea Tar Pits.

[d]This includes CH_4 emissions from petroleum production.

[e]Distribution estimated based on an initial assumption of 0.3% emission rate of total consumption. Storage not included in this line.

[f]State totals from CARB (Table 1.5) are scaled by spatial distribution from this work: 1) production and processing (corresponding to CARB's oil and gas extraction sector) and 2) transmission and distribution (CARB's pipelines sector) (as opposed to population as in past work).

[g]Summarized from CARB's Oil and Gas Industry Survey Results, Final Report (Revised) (CARB, 2013).

[h]Global Emissions EDGAR v4.2, http://edgar.jrc.ec.europa.eu/overview.php?v=42.

Recently, Wennberg et al. (2012) estimated CH_4 emissions from the natural gas sector to be 390±150 Gg CH_4 using atmospheric measurements of CH_4 and other trace gases. Wennberg et al. used the ratio of C_2H_6 to CH_4 to estimate CH_4 emissions from natural gas, assuming natural gas systems are the only significant source of C_2H_6 in SoCAB. The Wennberg et al. estimate is significantly larger (a factor of 4.7±1.8) than the SoCAB estimate, suggesting the U.S. EPA-based emission factors applied in the initial bottom-up estimate are too low, at least for SoCAB. Shorter et al. (1997) reported 1.6±0.6% of total natural gas produced in the United States was leaked during the production, processing, transport and distribution of the gas, roughly in line with the 2% leakage estimate from Wennberg et al. (2012).

Peischl et al. (2013) estimated separate CH_4 emissions in SoCAB for production and processing (32±7 Gg CH_4) and natural gas transmission, distribution, and local seeps (192±54 Gg CH_4), using measured ratios of alkanes (C_2-C_5) and published estimates for the alkane ratios of different sources in SoCAB. The total, 224 Gg CH_4, is lower than that of Wennberg et al. (2012). Peischl et al. (2013) estimated a 17% CH_4 emission rate for natural gas produced in SoCAB. In explaining this high emission rate, they suggested that their estimate is within a factor of 1.5 of the CARB-OGS estimate. However, recent changes to the CARB-OGS (CARB, 2013) have reduced estimated emissions from SoCAB production and processing so that they are lower than the estimates by Peischl et al. (2013). The team's analysis suggests that one possible reason for this difference is the relatively high offshore emissions. This estimate, based on U.S. EPA emission estimates, for offshore production emissions in California (37.2 Gg CH_4 yr^{-1}) is 21 times higher than that of CARB-OGS, and 38% of the total is concentrated in SoCAB, where associated

gas production is dominant. Because different sets of emission factors for the natural gas and petroleum systems (effectively higher emission factors for associated gas produced with petroleum) were used, direct comparison of emissions with natural gas produced may not be appropriate for regions where associated gas production is significant. Another possible explanation for the high emission rate for natural gas production reported by Peischl et al. is that a large fraction of dry natural gas entering SoCAB is temporarily stored in depleted petroleum reservoirs, where it has been found to be enriched in heavier alkanes (L. Sasadeusz, personal communication), such that leakage of stored gas may have an alkane profile similar to that locally produced associated natural gas. The volume of gas flow from storage wells is around 72 Bcf for 2010 in SoCAB, compared to roughly 17 Bcf from production wells (DOGGR, 2011). If the production and processing category in Peischl et al. (2013) is redefined to include emissions from production, processing, and storage, then total emission rate is less than 3% of local associated gas production.

Assuming a similar alkane profile between stored and produced gas and including the storage sector with the production and processing sectors from Peischl et al. (2013), total emissions from those sectors were estimated at 1.2 times the SoCAB inventory, while the emissions from transmission and distribution (not including storage or Tar Pit emissions) are 2.2 times greater in Peischl et al. (2013) than in the SoCAB inventory.

Adjusted State Emissions Based on SoCAB Measurements

Based on this discussion of the SoCAB field campaigns the general observation is the field campaigns find higher emissions (2 to 10 times larger, depending on which inventories are compared) from natural gas systems and petroleum production than are indicated in the bottom-up inventories. In this section, the spatially resolved bottom-up inventory developed is used to ask the question: if the leak rates implied by the SoCAB measurement campaigns represent the leak rates throughout the state, how much should the estimates of total statewide emissions be increased?

The team focused primarily on the top-down analysis in SoCAB by Peischl et al. (2013) because, although Wennberg et al. (2012) estimates total emissions from the natural gas system, Peischl et al. (2013) attribute emissions separately to two different categories within the natural gas system: the production/processing/storage sectors and the transmission/distribution sectors. As discussed, group storage emissions with production and processing emissions were grouped based on the reported alkane profiles of storage gas. Gas production in SoCAB is almost entirely associated with petroleum production, and no changes were made to the bottom-up estimates of dry-gas production emissions.

A simple way to adjust the bottom-up estimate to be consistent with the measurements described by Peischl et al. (2013) is to scale the bottom-up emissions so the totals in SoCAB match the measurements. Emissions from production, processing, and storage are multiplied by 1.2 and emissions from transmission and distribution by 2.2. After this scaling, the inventory will reflect the application of the emission rates implied by Peischl et al. (2013) to the state total emissions.

Table 7 presents adjusted state-total emission estimates, where the total emissions within SoCAB are held equal to the emissions found by Peischl et al. (2013). For reference, the first column shows the initial bottom-up estimate based on U.S. EPA emission factors. The second column shows an even scaling (1.2 and 2.2, respectively) across sectors within the two categories: emissions from the production, processing, and storage sectors; and emissions from transmission and distribution sectors. The initial estimates of emissions from dry-gas production were retained.

Table 7: State Total CH_4 Emission Estimates (Gg CH_4 yr^{-1}) from California's Natural Gas System and Petroleum Production Constrained by Measurements in SoCAB

Category	2010 Emissions Based on EPA's 2012 Inventory	Bottom-Up (2010 Emissions) Scaled to Match Measurement-Based Emission Estimates
Category 1[a]		
Production (dry gas)	28±8	28±8
Category 2		
Production associated	140	172
Processing	12	15
Storage	8	9
Sub-total:	160	196±40
Category 3[b]		
Transmission	13	30
Distribution	130	288
Sub-total:	143	317±138
Total	331	541±144

[a]Currently there are no top-down estimates of dry gas emissions in California, so the bottom-up estimates are left unchanged. The uncertainty in this category is based on EPA's uncertainty estimates for the natural gas system (an upper limit of 30%).

[b] The research team attempts to isolate emissions from transmission and distribution by subtracting from the Peischl et al. (2013) total major "local seep" emissions from the La Brea Tar Pits, (~1/6 kiloton per day) or ~61 Gg CH_4 yr^{-1} as estimated by Farrell et al. (2013).

An adjusted state total emission estimate of 541±144 Gg $yr^{-1}$was found, where the uncertainty is derived solely from propagating uncertainties reported by Peischl et al. (2013). Transmission and distribution emissions represent 59% of California's total and the majority of the uncertainty. Additional uncertainties are described; however, the team emphasizes that uncertainties, relative to mean estimates in a given region of the state, are likely larger than that for California's total. This highlights the necessity of making additional measurements in other regions.

There are two additional sources of uncertainty that have not been quantified. One source of uncertainty (Appendix D) relates to which subsector is responsible for differences between the

bottom-up and the top estimates. Sensitivity tests show variation in the adjusted state total of ±7% related to this source of uncertainty, which are within the uncertainty associated with the adjusted state total emission estimate. An additional source of uncertainty is related to the degree to which emissions in SoCAB represent emissions across the state. "How well do measurements in SoCAB represent emissions elsewhere in California?" cannot not be definitively answered without additional top-down measurement campaigns or inverse modeling. California has begun top-down measurement campaigns and inverse modeling efforts. To date, there have been only a limited number of studies focused on CH_4 emissions from the oil and gas industry in locations in California outside SoCAB. In a recent example, Gentner et al. (2014) conclude, "The vast majority of CH_4 enhancements observed in the San Joaquin Valley (SJV) are due to emissions from dairy operations," as opposed to petroleum operations. After adjusting the initial bottom-up estimates as described above, researchers estimated emissions in the SJV from the production, processing, and storage sectors to equal 128.2 Gg yr^{-1}, and emissions from the transmission and distribution sectors of 34.4 Gg yr^{-1}, combined for a total 162.6 Gg yr^{-1}, 30% of the state total estimate. Jeong et al. (2013) estimate emissions from dairy sources in SJV to be 1130±205 Gg yr^{-1}, 7.0 times larger than the research team's petroleum and natural gas estimate in SJV, in agreement with the qualitative conclusions by Gentner et al. (2014).

Furthermore, all the SoCAB measurement studies are consistent with the general conclusion that top-down estimates indicate a higher rate of emissions than is assumed in bottom-up inventories, similar to results from recent top-down studies of air basins in Colorado by Pétron et al. (2012) and in Utah by Karion et al. (2013).

California reports 193.8 billion cf of associated gas production (onshore and offshore) in 2009, or 3.69 Tg yr^{-1}. (The research team used 2009 data because federal offshore production is not included in 2010 data; DOGGR, 2010). The team estimated 5.3±1.1% (196 Gg / 3.69 Tg) of this associated gas production total is leaked during associated production and all processing and storage phases of the natural gas system. (See Table 1.7 for emission estimates.) Leakage during the associated production phase can be estimated only by subtracting the emissions the team attributes to storage and processing to find an emission rate of 4.7% (172 Gg / 3.69 Tg) for associated production only. However, researchers did not provide quantitative uncertainty for the leak rate estimate for associated production alone, as top-down estimates of emissions from the associated production sector alone are missing.

Regarding dry gas, the bottom-up estimate indicates leakage of 1.8% of the DOGGR-reported production (28 Gg yr^{-1} / 1.58 Tg yr^{-1}; DOGGR, 2010). The dry-gas estimate is based solely on the initial bottom-up estimate as opposed to the associated production emission estimate, which was adjusted to reflect the implications of the work by Peischl et al. (2013).

Comparison with Bottom-up Estimates from Updated EPA Inventory

The initial bottom-up estimates described in the previous sections are compared with those estimated based on the updated 2016 US EPA inventory (for 2014; US EPA, 2016). For this comparison, the 2014 oil and gas production activity data from DOGGR were used[23] for the production sector. For processing, researchers used the facility information for 2014 from U.S. EIA was used.[24] For the transmission sector, the same activity data were used as those used for 2010, except for the storage facilities for which the storage volume from the 2014 DOGGR databases used. As in 2010, the 2014 distribution emission map was generated apportioning emissions in proportion to the population density.

Table 8 shows the comparison between 2010 and 2014 emission estimates for California's natural gas system and petroleum production. Although the difference in the total emissions between 2010 and 2014 is around 15%, there are larger differences in the subsector total. In particular, the distribution emission for 2014 decreased significantly compared to that of 2010 (39 vs. 130 Gg CH_4/yr) because U.S. EPA's total 2014 distribution emission for the United States is only 33% of that of 2010. Figure 7 shows the total CH_4 emissions from the natural gas system and petroleum production for 2010 and 2014. The difference in urban region emissions between the two maps is noticeable due to the change in the emission factors for the distribution sector.

---

23 (http://www.conservation.ca.gov/dog/Pages/Index.aspx, accessed May 2016.

24http://www.eia.gov/cfapps/ngqs/ngqs.cfm?f_report=RP9&f_sortby=&f_items=&f_year_start=&f_year_end=&f_show_compid=&f_fullscreen=, accessed May 2016.

Table 8: Comparison of CH_4 Emission Estimates (Gg CH_4 yr^{-1}) from California's Natural Gas System and Petroleum Production

Sector	Subsector	2010 Emissions Based on EPA's 2012 Inventory (Gg CH_4/yr)[a]	2014 Emissions Based on EPA's 2016 Inventory (Gg CH_4/yr)[b]	2013 Emissions from CARB's 2015 Inventory (Gg CH_4/yr)[c]	2014 Emissions from CARB's 2016 Inventory (Gg CH_4/yr)[d]
Production	Non-associated production	27	49		
	Associated production	103	158		
	Offshore production	37	8		
	Subtotal	168	215	96[e]	73[e]
Processing		12	7		
Transmission		21	24		
Distribution		130	39	152[f]	160[f]
Total[g]		331	286	249	233

[a]From Jeong et al. (2014) using emission factors from US EPA 2010 and 2011 emission estimates (available in the 2012 and 2013 EPA inventories, respectively). As described previously, the transmission emissions for 2010 were estimated using emission factors from INGAA as well as the U.S. EPA inventory.

[b]Estimated using the US EPA 2016 inventory (for 2014). The 2016 (for 2014) EPA inventory reports only national average emissions for non-associated gas production (contrary to previous years). Thus it is assumed that the West Coast emission is 1.3% of the national total as reported in the 2015 U.S. EPA inventory (US EPA, 2015) and derived regional emission factors based on this assumption

[c]CARB's April 2015 inventory (for 2013); http://www.arb.ca.gov/cc/inventory/data/graph/treemap/ghg_2000-13.htm (accessed May 2016).

[d]CARB's June 2016 inventory (for 2014); http://www.arb.ca.gov/cc/inventory/data/graph/treemap/ghg_2000-14.htm (accessed July 2016).

[e]CARB's oil and gas extraction sector.

[f]CARB's estimate for the distribution sector includes emissions from the "pipelines" sector (transmission + distribution).

[g]Due to rounding, the sum of subsector emissions may not match the total.

Figure 7: Total CH_4 Emission (nmol m^{-2} s^{-1}) Maps (0.1° resolution) from the Natural Gas System and Petroleum Production for 2010 and 2014

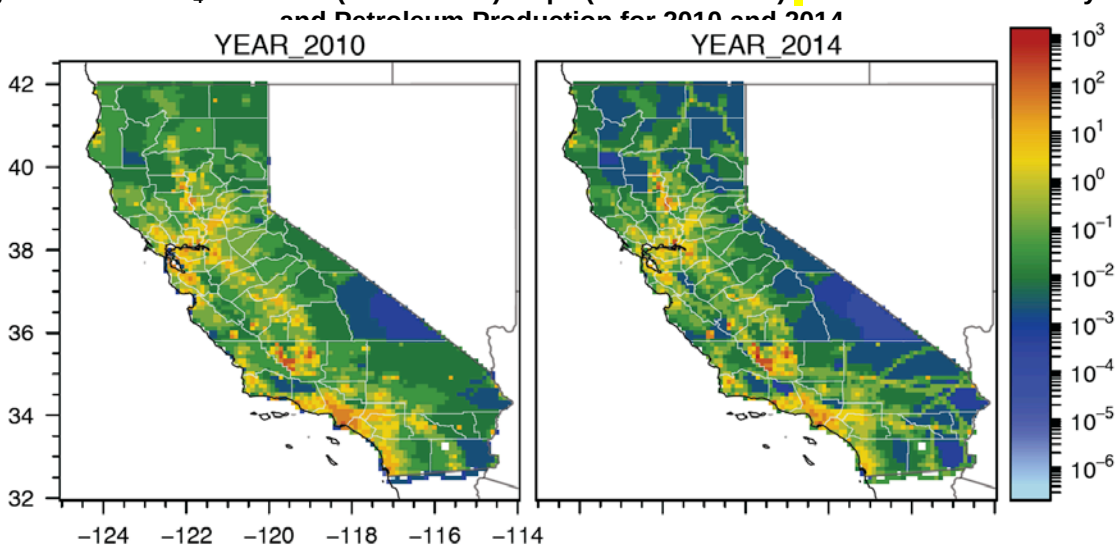

2010 (left) and 2014 (right) total CH_4 emissions from the natural gas system and petroleum production (see Table 1.8 for summary).

The ratios of 2014 to 2010 CH_4 emissions for the natural gas system and petroleum production at the county level are depicted, aggregating the emissions and comparing them (Figure 8). The differences between the two emissions are shown more clearly, in particular for the counties where oil and natural gas production is active and the distribution emissions are dominant. For example, the Kern County (southern end of the San Joaquin Valley) shows higher emissions in 2014 than in 2010 due to increase in the associated production emissions. On the other hand, the San Francisco Bay Area counties, which are dominated by the distribution emissions, show significantly lower emissions in 2014 than 2010 due to the decrease in the distribution sector. In Chapter 2, using a top-down analysis, the different CH_4 emission estimates for the natural gas system and petroleum production will be evaluated focusing on the San Francisco Bay Area and the Sacramento region.

Figure 8: Ratios of 2014 to 2010 CH_4 Emissions for the Natural Gas System and Petroleum Production at the County Level

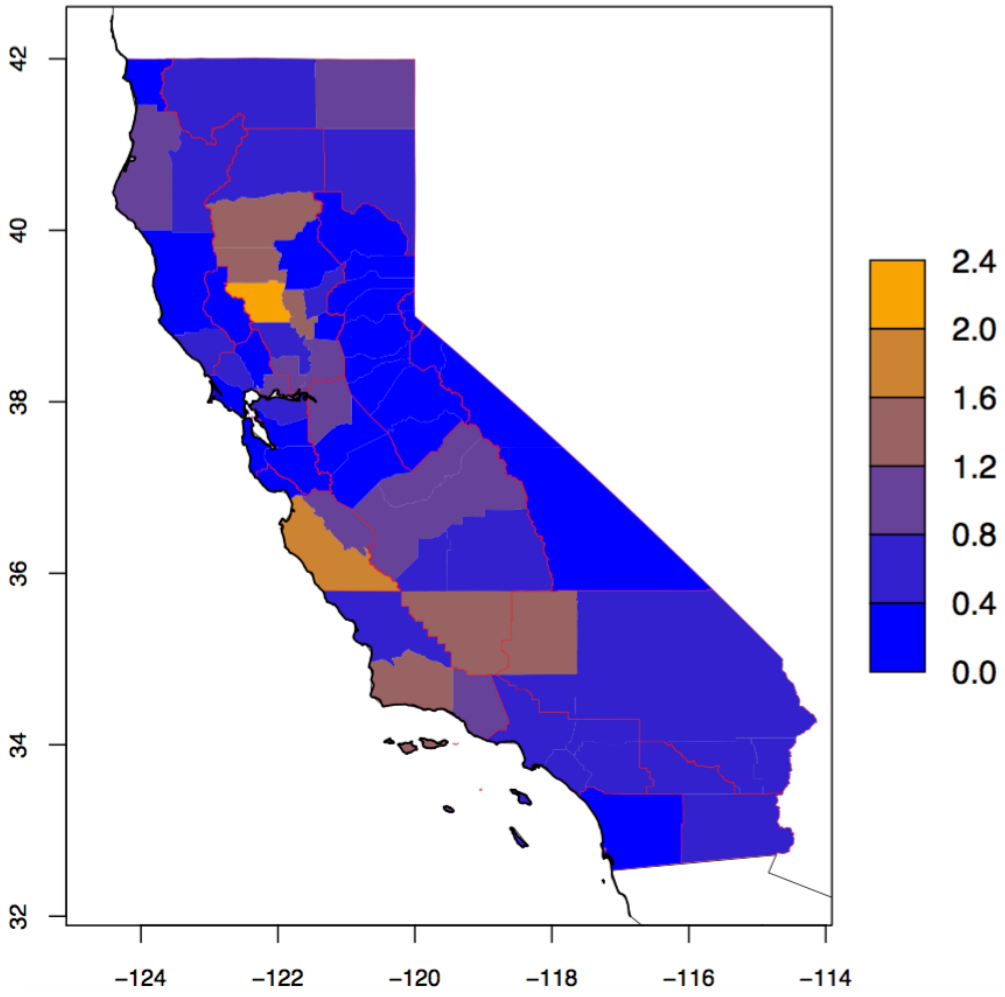

The red lines represent the California's air basins. There are a total of 15 air basins including the Bay Area Air Basin which itself includes nine counties within its boundary.

CHAPTER 2:
Inverse Analysis of Regional Natural Gas Emissions Using Multispecies Measurements

2.1 Atmospheric Inverse Method for Regional CH_4 Emission Estimates

An atmospheric inversion method was developed combining CH_4 and volatile organic compound (VOC) measurements to attribute emissions sources between biological and fossil-fuel sources. This method was applied to estimate regional emissions for the San Francisco Bay Area and the Sacramento region, which are described in the following sections of this chapter and reported in Jeong et al. (2017).

A hierarchical inversion method was developed to estimate various parameters including model-measurement mismatch uncertainty, VOC:CH_4 ratios, and uncertainty for the prior emissions and scaling factors (i.e., adjustment to the prior emissions to derive posterior emissions). The details of the hierarchical inverse method are provided in the Appendix L, and here researchers describe the expanded equation that relates predictions to measurements to incorporate VOC measurements.

The following linear model was used for estimating emissions at various spatial scales (Zhao et al., 2009; Jeong et al., 2012a; 2012b; 2013; Wecht et al., 2014) (2.1) and expand it in this study):

$$\mathbf{y} = \mathbf{K}\boldsymbol{\lambda} + \mathbf{v} \qquad (2.1)$$

where $\mathbf{y}$ is the measurement vector, $\mathbf{K} = \mathbf{FE}$, $\mathbf{F}$ is the footprint, $\mathbf{E}$ is prior emissions, $\boldsymbol{\lambda}$ is a vector for scaling factors with a covariance matrix $\mathbf{Q}$, and $\mathbf{v}$ is a vector representing the model-measurement mismatch with a covariance matrix $\mathbf{R}$. In this study, researchers solve for $\boldsymbol{\lambda}$ at 0.1° resolution for the San Francisco Bay Area (SFBA; 0.3° for the Sacramento Valley region) after aggregating predictions, based on the high-resolution prior emissions, and for regions outside SFBA, regions were aggregate grid cells at the subregion scale (i.e., California's air basins) in a similar way to that of Jeong et at. (2013) so that the number of parameters can be reduced for those regions. Similarly, for the Sacramento analysis, researchers solve for $\boldsymbol{\lambda}$ at 0.3° resolution for the Sacramento Valley and the regions directly adjacent to it (i.e., SFBA and the northern San Joaquin Valley) and for other regions, it was estimated $\boldsymbol{\lambda}$ at the regional level. Solving for $\boldsymbol{\lambda}$ and multiplying it by $\mathbf{E}$, posterior emissions can be obtained.

The linear model in Equation (2.1) is expanded to solve for $\boldsymbol{\lambda}$ specific to biological, natural gas, and petroleum sources for source partitioning:

$$\begin{bmatrix} \boldsymbol{C}_{CH_4} - C^*_{bg} \\ \boldsymbol{C}_{C_2H_6} - C^*_{bg} \\ \boldsymbol{C}_{iC_5H_{12}} - C^*_{bg} \\ \boldsymbol{C}_{nC_5H_{12}} - C^*_{bg} \\ \boldsymbol{C}_{C_7H_8} - C^*_{bg} \end{bmatrix} = \begin{bmatrix} \boldsymbol{FE}_{BIO} & \boldsymbol{FE}_{NG} & \boldsymbol{FE}_{PL} \\ \mathbf{0} & \boldsymbol{FE}_{NG} f^*_{C_2H_{6NG}} & \boldsymbol{FE}_{PL} f^*_{C_2H_{6PL}} \\ \mathbf{0} & \mathbf{0} & \boldsymbol{FE}_{PL} f^*_{iC_5H_{12PL}} \\ \mathbf{0} & \mathbf{0} & \boldsymbol{FE}_{PL} f^*_{nC_5H_{12PL}} \\ \mathbf{0} & \mathbf{0} & \boldsymbol{FE}_{PL} f^*_{C_7H_{8PL}} \end{bmatrix} \begin{bmatrix} \boldsymbol{\lambda}_{BIO} \\ \boldsymbol{\lambda}_{NG} \\ \boldsymbol{\lambda}_{PL} \end{bmatrix} + \mathbf{v} \quad (2.2)$$

where $\boldsymbol{C_X}$ is the measurement vector (n × 1) for gas species X, and $\boldsymbol{C^*_{bg}}$ is the background vector (n × 1) for each species. In this study, researchers adjust the background (as indicated in the asterisk in $\boldsymbol{C^*_{bg}}$) by estimating the systematic bias along with other parameters using the hierarchical Bayesian inversion. In simple form, Equation 2.1 is modified to incorporate the background adjustment as

$$\mathbf{y} = \mathbf{K}\boldsymbol{\lambda} + \mathbf{D} + \mathbf{v} \qquad (2.3)$$

where **D** is a vector for mean adjustments, which is estimated during the hierarchical inverse process. Each element of **D** represents the mean background adjustment for each combination of sites and species. For the matrix that constitutes predictions (first term in the right-hand side of Equation 2.2), $\boldsymbol{FE_{BIO}}$ (n × k matrix; k is the number of pixels (0.1°) or subregions) is the predicted mixing ratio (**F** is the footprint and **E** is the surface emission) for biological sources (i.e., all source sectors except for the natural gas and petroleum sectors), $\boldsymbol{FE_{NG}}$ (n × k matrix) is the predicted mixing ratio for the natural gas sector, and $\boldsymbol{FE_{PL}}$ (n x k matrix) is the predicted mixing ratio for the petroleum sector. **0** is a zero matrix with a dimension of n × k. Applying this inversion scheme, inversions are performed for two seasons of early fall (September – October) and late fall (November – December), and estimated emissions are summarized for the combined fall-winter season.

The research team uses the matrix equation in Equation (2.2) to solve for scaling factors and VOC:CH_4 ratios. $\boldsymbol{\lambda_{BIO}}$ (k × 1 vector) is the scaling factor for the biological source sector, $\boldsymbol{\lambda_{NG}}$ (k × 1 vector) is the scaling factor for the natural gas sector, and $\boldsymbol{\lambda_{PL}}$ (k × 1 vector) is the scaling factor for the petroleum sector. $f^*_{C_2H_{6_NG}}$ and $f^*_{C_2H_{6_PL}}$ are the C_2H_6:CH_4 emission ratios for the natural gas and petroleum sectors, respectively, which are updated based on the VOC measurements during the inverse optimization. As shown in Equation (2.2), for example, the C_2H_6:CH_4 emission ratio, $f^*_{C_2H_{6_NG}}$, is used to derive C_2H_6 emission maps for the natural gas sector by multiplying it by the natural gas CH_4 emission map. The prior value for $f^*_{C_2H_{6_NG}}$ is sampled from a truncated normal distribution with mean 0.04 and standard deviation 0.005, which is a typical value for C_2H_6:CH_4 reported for the natural gas distribution system in northern California (PG&E, 2015). Here, the value of 0.04 for $f^*_{C_2H_{6_NG}}$ means that C_2H_6 emissions for the natural gas sector are 4% of those of the natural gas CH_4 on average. $f^*_{iC_5H_{12PL}}$ and $f^*_{nC_5H_{12PL}}$ are the i-C_5H_{12}:CH_4 and n-C_5H_{12}:CH_4 emission ratios for the petroleum sector. $f^*_{C_7H_{8PL}}$ is the C_7H_8:CH_4 ratio. The VOC emission ratios relative to CH_4 for the petroleum sector are summarized in Table 9. These emission ratios were adopted from Kirchstetter et al. (1996), which were estimated for light-duty vehicles. The C_2H_6 and C_5H_{12} emissions relative to CH_4 are similar to those used in Peischl et al. (2013). The emission maps from Jeong et al. (2014) show there are some natural gas production activities within the BAAQMD boundary. However, the total CH_4 emissions from natural gas production are estimated to be 2 Gg/yr; these emissions are mostly from dry gas production (Jeong et al., 2014). Thus, the authors use all VOCs except for C_2H_6 to constrain the petroleum sector, which includes the on-road mobile and refinery subsectors. As described, the VOC:CH_4 emission ratios from previous studies are used as prior estimates (as hyperparameters) to derive VOC emission maps, and the related posterior values are inferred based on the VOC measurements during the hierarchical inversion process.

Table 9: Prior Estimates of VOC Emission Ratios Relative to CH_4 Emissions for the Petroleum Sector*

VOCs	Molar Ratio (%)**
ethane	7.0 ± 1.1†
n-pentane	4.7 ± 0.4
i-pentane	18.0 ± 1.3
toluene	15.5 ± 1.2

*The petroleum sector includes the on-road mobile and refinery subsectors.

**The authors use these values for both on-road mobile and refinery subsectors.

†These uncertainty values are multiplied by a factor of 2 to broaden the uncertainty and then used as hyper-parameters to estimate posterior VOC:CH_4 ratios.

2.2 Observations and Analysis of SFBA Natural Gas CH_4

2.2.1 Introduction

California's Global Warming Solutions Act of 2006 (Assembly Bill 32, Núñez, Chapter 488, Statutes of 2006) mandates that greenhouse gas (GHG) emissions be reduced to 1990 levels by 2020, requiring accurate accounting of CH_4 emissions for effective mitigation planning and verification of future emissions reductions. Although both California's official GHG inventory (CARB, 2016) and recent top-down studies using atmospheric measurements (Wennberg et al., 2012; Jeong et al., 2013; Peischl et al., 2013; Hopkins et al., 2016) suggest that California's Central Valley is the major source of the state's CH_4 emissions, California's large metropolitan regions are increasingly considered to be an important component of the state's CH_4 budget.

California emits roughly 459.3 Tg CO_2 (1 Tg = 10^{12} g) equivalent GHGs each year (CARB, 2015). Among the reported GHGs, about 9% of total GHG emissions are attributed to CH_4, which is the second largest contributor to climate-forcing emissions in California behind CO_2 (CARB, 2015). As reported in recent studies (e.g., Jeong et al. [2013, 2014]), however, CH_4 emissions in California are relatively uncertain compared to those of CO_2 because of a lack of activity data and incomplete understanding of emission processes. At the subregional scale (e.g., air basins of California), CH_4 emissions are more uncertain than at the state level. Recent studies in the South Coast Air Basin (SoCAB) of California, which includes Los Angeles, suggest that the state inventory underestimates CH_4 emissions in the region (Wunch et al., 2009; Hsu et al., 2010; Wennberg et al., 2012; Jeong et al., 2013; Peischl et al., 2013; Wong et al., 2015; Cui et al., 2015). More importantly, multiple recent studies for SoCAB suggest that at the subregional or city scale, identifying CH_4 emissions sources is important, but source partitioning is much more uncertain than the total CH_4 budget (Wennberg et al., 2012; Jeong et al., 2013; Peischl et al., 2013; Wong et al., 2015, Cui et al., 2015; Hopkins et al., 2016; Conley et al., 2016).

Few studies have been conducted to estimate CH_4 emissions in the San Francisco Bay Area (SFBA), despite the fact that the region's total CH_4 emissions are substantial and are estimated to be nearly 30% of SoCAB, based on the CARB and Bay Area Air Quality Management District

(BAAQMD) inventories (CARB, 2014; BAAQMD, 2015). Zhao et al. (2009) and Jeong et al. (2012a, 2013) estimated CH_4 emissions from SFBA, but these studies used towers in the Central Valley and have not fully constrained the urban emissions in the region. Fairley and Fischer (2015) reported a study on CH_4 emissions in SFBA using CH_4:CO enhancement ratios from 14 air quality sites in SFBA spanning two decades from 1990 to 2012. They estimated a total of 240±60 Gg/yr (at 95% confidence) for the most recent period (2009 - 2012), which is about 1.5 to 2.4 times higher than that of BAAQMD's inventory (BAAQMD, 2015). Given the discrepancy between the bottom-up inventory and the top-down analysis, it is important to verify the estimate by Fairley and Fischer (2015) and identify potential emissions sources that dominate the region's CH_4 total emissions for efficient mitigation planning.

To address this challenge, a short-term study was conducted to quantify CH_4 emissions from SFBA using atmospheric observations of CH_4 and volatile organic compounds (VOCs) from six ground sites from September to December 2015. In particular, this study combines CH_4 with four VOC species (ethane (C_2H_6), i-pentane (i-C_5H_{12}), n-pentane (n-C_5H_{12}), and toluene (C_7H_8)) for source partitioning of CH_4 emissions. Expanding on previous work by Jeong et al. (2012a; 2012b; 2013; 2014) and Ganesan et al. (2014), a hierarchical Bayesian method was developed. For the first time, incorporating both CH_4 and VOC measurements into a full Bayesian inverse analysis where uncertainty is thoroughly characterized, the authors illustrate how VOC measurements can be used to separate fossil-fuel emissions from biological emissions (e.g., dairy emissions). In Section 2.2.2, the methods employed were described, including atmospheric measurements, previous CH_4 emissions, transport modeling, and the hierarchical Bayesian inverse method. Section 2.2.3 presents results, including the inferred CH_4 emissions from SFBA for different sources. Section 2.2.4 further discusses the results and presents conclusions for CH_4 emissions in SFBA.

2.2.2 Data and Methods

Atmospheric Measurements and Boundary Conditions

For this study, a measurement intensive including CH_4, selected VOC, and CO measurements from September to December 2015 was conducted. The CH_4 and VOC measurements were made at five sites within the BAAQMD and at a SFBA outflow site near Walnut Grove (Sacramento County – WGC). The locations of the six sites are provided in Table 10. Two of the sites (STR and WGC) are tall towers, where automated flasks are collected in collaboration between the Lawrence Berkeley National Laboratory (LBNL) and the National Oceanic and Atmospheric Administration's (NOAA) Earth System Research Laboratory (NOAA-ESRL). Two sites are BAAQMD's air quality monitoring sites (Oakland and Livermore [OAK, LVR]), a fifth site is a two-story home with a 5-m mast (henceforth designated as "BWT") providing samples at 9 m a.g.l. (above ground level), and the sixth site is a 10-story building with a 9-m mast (SJSU) sampling at 45 m agl. With the exception of LVR, CO flask sampling or continuous CO measurements were made at all sites. To capture CO measurements in the Livermore Valley, continuous measurements of CO were also collected at 27 m on a seventh tower (Sandia National Laboratory [SNL]) for model-measurement comparison of CO mixing ratio signals.

Measurement methods varied between the different sites for the CH_4, CO, ethane, pentane, and toluene analyses. For WGC and STR, air samples were collected near 2200 GMT in glass flasks and subsequently measured at NOAA-ESRL (e.g., Petron et al., 2012). For the BWT, OAK, and San Jose State University (SJSU) sites, samples were collected near 2200 GMT, either daily (BWT, SJSU) or bi-daily (OAK), into steel canisters and subsequently analyzed at UC Irvine (Colman et al., 2001). For the LVR site, the BAAQMD operates a calibrated gas chromatography mass spectrometry (GC-MS) () providing calibrated hourly measurements of ethane, pentane, and toluene (BAAQMD, 2016), while LBNL operated a calibrated off-axis laser CH_4 spectrometer (Los Gatos Research) providing hourly averaged CH_4 measurements. In general, CH_4 measurements had a precision of 1 ppb and accuracy of 3 ppb (based on drift in target gas), which were sufficient to capture variations at the urban and suburban sites. Similarly, the precision and accuracy of the VOC measurements was 0.1 ppb or better based on laboratory testing (NOAA and UCI) or on-site calibration tests (BAAQMD). At the SNL site, the Sandia team operates a calibrated CO instrument (Ecotech Model EC 9830T) providing hourly averaged CO measurements for comparison with transport model predictions.

Table 10: CH_4 and VOC Measurement Sites for SFBA

Site Name	Location	Longitude	Latitude	Height (m a.g.l.)	Gas Analysis
BWT	Berkeley, CA	-122.26	37.85	9	UCI
LVR	Livermore, CA	-121.78	37.69	10	LBNL-BAAQMD
OAK	Oakland, CA	-122.17	37.74	10	UCI
SJSU	San Jose, CA	-121.88	37.33	45	UCI
STR	San Francisco, CA	-122.45	37.76	232	NOAA
WGC	Walnut Grove, CA	-121.49	38.26	91	NOAA

Background mixing ratios for CH_4 were estimated for each site using a method simplified from that described by Jeong et al. (2013), which estimates background concentrations at the receptor sampling NOAA's three-dimensional curtain of CH_4 background across the Pacific Ocean based on the WRF-STILT back trajectories. Because the most recent NOAA background curtain does not cover the analysis period, the previous year's (2014) curtain was used after adding an average of 5 ppb. For possible additional biases in background, the team estimated systematic mean biases for each site while performing hierarchical inversions and adjusting the bias. The estimated systematic background biases are provided in Appendix E. For background concentrations for VOCs, measurements from a coastal site in Trinidad Head (THD) were used. To estimate daily background values from a limited number of available data points during 2015, a linear model was fit to the THD measurements because the measured data show a clear linear trend (Appendix G). As in CH_4 background, systematic mean biases for VOC species were estimated by site during the inversion (Appendix E).

Prior Emission Model

A high-resolution (1 km × 1 km) CH_4 emissions prior model was developed for SFBA. The SFBA-specific prior emissions model is based on the California Greenhouse Gas Emission Measurements (CALGEM) project prior CH_4 emissions model (CALGEM model, available at calgem.lbl.gov) described by Jeong et al. (2012a, 2013, 2014) and inventories from BAAQMD and CARB with some modifications. For sectors (e.g., wastewater) with spatial information from BAAQMD's inventory, spatially explicit prior emissions for those sectors based on BAAQMD's inventory were generated. For other sectors (e.g., dairy) for which spatial information is not readily available from BAAQMD's inventory, the emissions factors from CARB or BAAQMD were combined with the spatial distribution of the CALGEM emission model to generate spatially disaggregated emissions.

The CALGEM emissions model provides emissions by sector at a high spatial resolution (0.1° × 0.1°) for California. The CALGEM model has seasonal components for wetlands and crop agriculture only, and these seasonal emissions are combined with nonseasonal emissions to construct monthly emission maps for inversions. The inversion approach using nonseasonal prior emissions is widely used (e.g., Zhao et al. [2009], Jeong et al. [2012a; 2012b; 2013], Wecht et al. [2014], Cui et al. [2015]). The CALGEM prior emissions are scaled to match 2012 CARB state totals for anthropogenic emissions sectors (CARB, 2014; March 2014 version), with small (< 50 Gg CH_4/yr) adjustments for some regions and sectors (per CARB staff private communication).

The BAAQMD CH_4 inventory provides facility-level emissions for some subsectors (e.g., emissions from fuel combustion and wastewater). Spatially explicit CH_4 emission maps were generated using the detailed facility-level information in the BAAQMD inventory (Appendix K). For the subsectors lacking detailed spatial information in the BAAQMD inventory, the spatial distribution of the CALGEM prior model was modified or it was used to generate new emission maps for some sectors (e.g., on-road mobile emissions). For some subsectors, the emissions at the county level were uniformly allocated.

In total, the anthropogenic emissions for BAAQMD were estimated at 116.4 Gg (1 Gg = 10^9 g) CH_4/yr. The total CH_4 emissions estimate for BAAQMD is 120.1 Gg CH_4/yr including the emissions from wetlands (Jeong et al., 2013). This is only slightly smaller than the BAAQMD's official inventory, which is 125.5 Gg CH_4/yr (BAAQMD, 2015). Table 11 summarizes the estimated CH_4 emissions by sector that was used as prior emissions in the inversion. The sectors were categorized following those that are used in recent regional emissions quantification studies (e.g., Jeong et al., 2013, Peischl et al., 2013, Wecht et al., 2014). Using a combination of CH_4 and VOC measurements, emissions for biological, natural gas, and petroleum source sectors are assumed. The emission maps for these three sectors are shown in Figure 9. The CH_4 emissions from the SFBA region are dominated by urban activities, with agricultural activities (e.g., dairy farming) occurring in suburban areas of the region. Landfill emissions account for 53% of BAAQMD's total emissions, followed by livestock (16%) and natural gas (15%). These three dominant sectors account for 84% of the total anthropogenic emissions in BAAQMD. The total emissions (17 Gg) for the natural gas distribution sector (based on BAAQMD's inventory) are smaller than that of the 2010 emissions (26 Gg; using the 2012 EPA inventory) that were

estimated in Chapter 1 (i.e., Section 1.3). The spatial pattern of emissions closely follows the density of population, while strong point sources are distributed in the suburban areas of BAAQMD.

Table 11: Summary of CH_4 Prior Emissions for BAAQMD*

Sector	Subsector	Mg CH_4/yr
Livestock	Dairy	9219
	Major non-dairy	8471
	Poultry (broiler, layer&pullets, turkey)	62
	Domestic and Other Animals	505
	Sector total	18257
Landfill	Point source	56888
	Fugitive area source	4590
	Sector total	61478
Natural gas	Distribution	17287‡
	Domestic natural gas	52
	Other external combustion	160
	Sector total	17499
On-Road Mobile	On-road mobile	2164
	Sector total	2164
Refinery	Refinery	1931
	Sector total	1931
Wastewater	Domestic anaerobic digester	427
	Domestic central anaerobic	3370
	Domestic septic system	1230
	Industrial non-refinery wastewater	894
	Industrial refinery wastewater	1063
	Sector total	6984
Others**	Point source	2945
	Area source	4705
	Sector total	7650
Anthropogenic Total†		115963
Wetland¶		3738
Total		119701

*The high-resolution spatially explicit emissions were developed for 2011 to be consistent with BAAQMD's official inventory while some sector emissions were derived based on 2012 activity data. See Appendix F for comparison with SoCAB.

**BAAQMD's estimates for miscellaneous emissions including emissions from wood stove and fireplace combustion, other stationary combustion (e.g., liquefied petroleum gas), and off-highway mobile sources. Excluding wood stove and fireplace combustion, the emissions total from all miscellaneous fossil sources is 3.7 Gg CH_4/yr.

†Includes anthropogenic emissions only. Excluding the natural gas, petroleum (on-road mosbile + refinery) and miscellaneous fossil source emissions, the total emission for the anthropogenic biological source is 94 Gg CH_4/yr.

‡If the authors apply the emission factors from the 2012 EPA inventory (for 2010) derived in Chapter 1, they estimate a total of 26 Gg CH_4 for the distribution sector for SFBA, which is 1.5 times larger than this estimate (i.e., 17 Gg) based on BAAQMD's inventory.

¶Taken from Jeong et al. (2013) for BAAQMD.

Figure 9: High-Resolution (0.01° × 0.01°) Prior Emission Flux (nmol/m^2/s) Maps by Sector

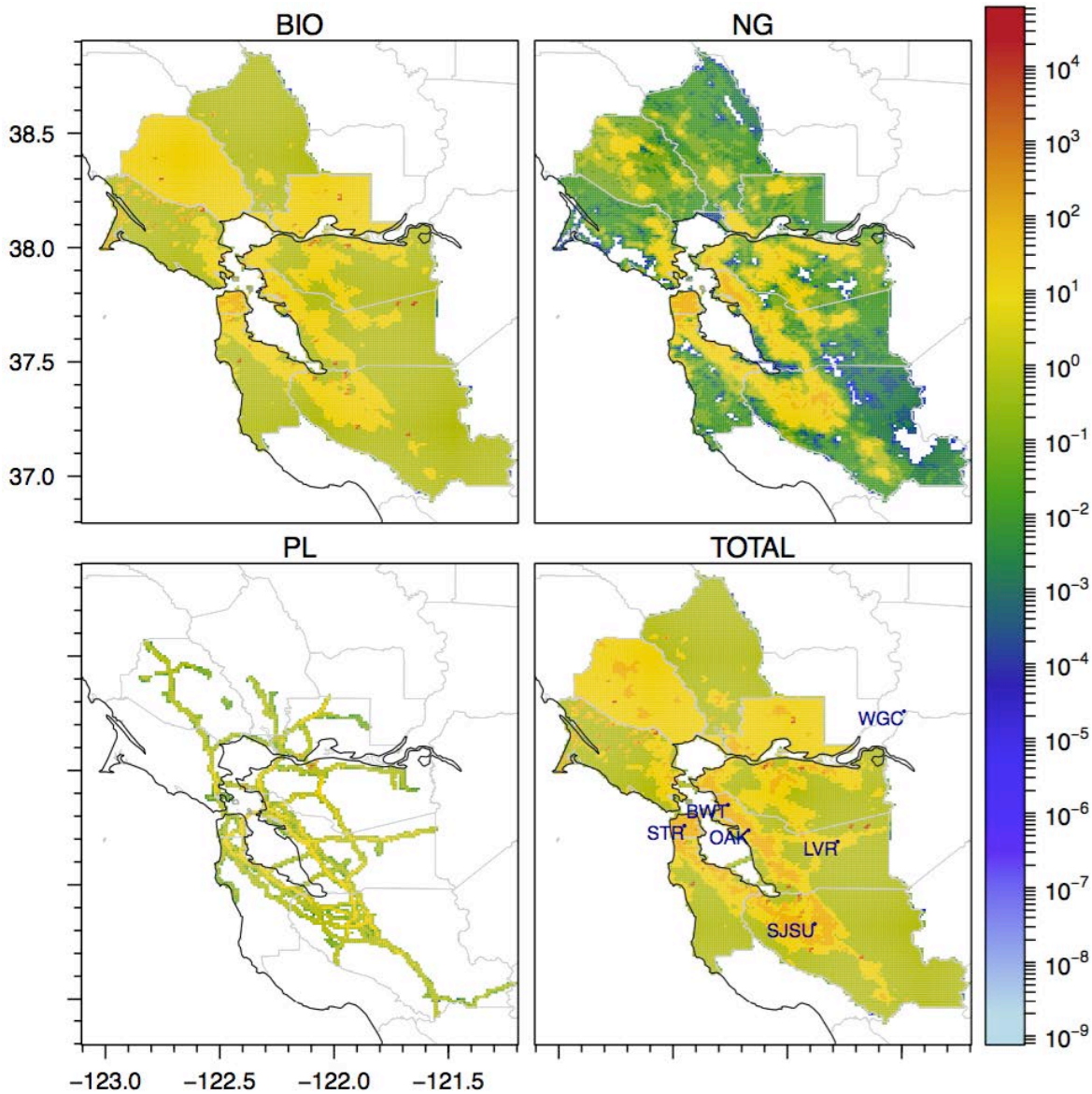

High-resolution (0.01° × 0.01°) prior emission flux (nmol/m^2/s) maps used in this study by sector: biological (BIO), natural gas (NG), petroleum (PL), and total (TOTAL). The PL sector includes on-road mobile and refinery emissions (see Table 2.3). The emission maps show emission fluxes only within the BAAQMD's boundary for which researchers developed the high-resolution emission maps. For the regions outside BAAQMD's boundary, 10-km CALGEM emission maps are used.

Atmospheric Transport Modeling

The coupled Weather Research and Forecasting and Stochastic Time-Inverted Lagrangian Transport (WRF-STILT) model for atmospheric transport was used (Lin et al., 2003; Skamarock et al., 2008; Nehrkorn et al., 2010). The WRF-STILT model has been used to constrain GHG emissions in many studies including airborne measurement-based (e.g., Gerbig et al., [2003]; Kort et al., [2008]) and tower measurement-based (e.g., Zhao et al., [2009]; Jeong et al., [2012a];

Jeong et al., [2012b]; Newman et al., [2013]; Jeong et al., [2013]) applications. The setup adopted used in Jeong et al. (2013) to run the STILT model. In this setup, an ensemble of 500 STILT particles are run backward in time for seven days driven with meteorology from the WRF model (version 3.6.1) (Skamarock et al., 2008). Except for the LVR site, one measurement is available each day from the flask sampling around 14 PST. Thus, the corresponding predictions from WRF-STILT to compare with the available measurements (Jeong et al., 2012b) were used. For the LVR site, hourly predicted CH_4 mixing ratio signals based on WRF-STILT are aggregated into 3-hour averages, which are compared with 3-hour measurements in inverse modeling following methods described in Jeong et al. (2012a, 2013).

The WRF model simulations closely follow those described in Jeong et al. (2012a, 2012b, 2013) with some modifications. The team used Version 3.6.1 of the WRF model (Skamarock et al., 2008). As in Jeong et al. (2013), the team stimulated meteorology for four horizontal resolutions of 36, 12, 4, and 1.3 kilometers (km) (vertical levels = 50) using initial and boundary meteorological conditions provided by the North American Regional Reanalysis (NARR) dataset (Mesinger et al., 2006). The configuration of the four inner domains is shown in Figure 10. In this study, the 1.3-km domain is used for the observation sites in BAAQMD to better represent the region's complex terrain and land-sea interactions whereas, the 4-km domain is used to simulate predicted mixing ratios for the WGC site. As in Jeong et al., (2013) a two-way coupling was applied between domains and 3-D analysis nudging at the outer domain every three hours using the NARR product. For surface physics, following Jeong et al. (2013) the Noah land surface model (LSM) (Chen and Dudhia, 2001) was used, except for WGC during September for which the team used the five-layer thermal diffusion LSM (5-L LSM) to account for irrigation in the land surface process during the late summer – early fall period. For the planetary boundary layer (PBL) scheme, the 2.5 level MYNN (MYNN2) PBL scheme (Nakanishi and Niino, 2006) was employed coupled with the Noah LSM. The monthly mean footprint simulated by WRF-STILT is provided in Figure 11.

Figure 10: WRF Modeling Domain Configuration for the Inner Domains of 12 km (d02), 4 km (d03), and 1.3 km (d04 and d05) Resolutions

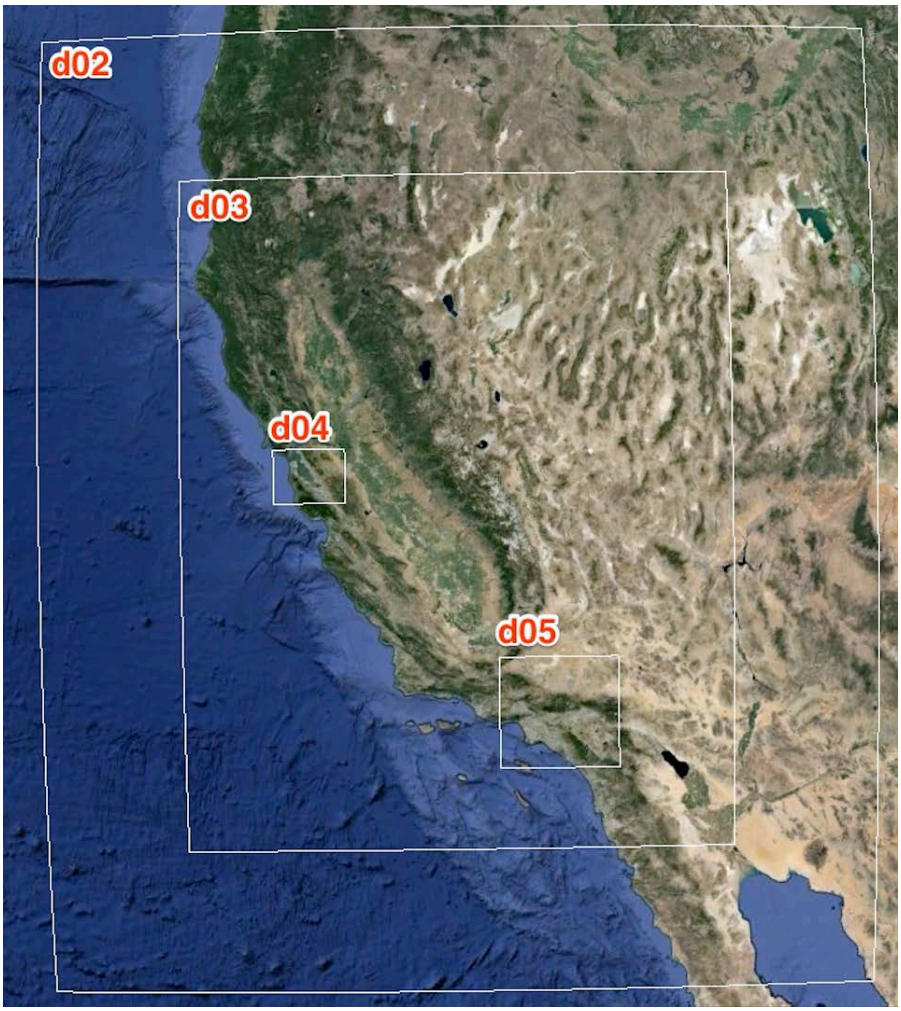

Figure 11: Simulated Monthly Mean Footprints (ppb/[nmol/m^2/s]) during 12 – 17 PST Hours*

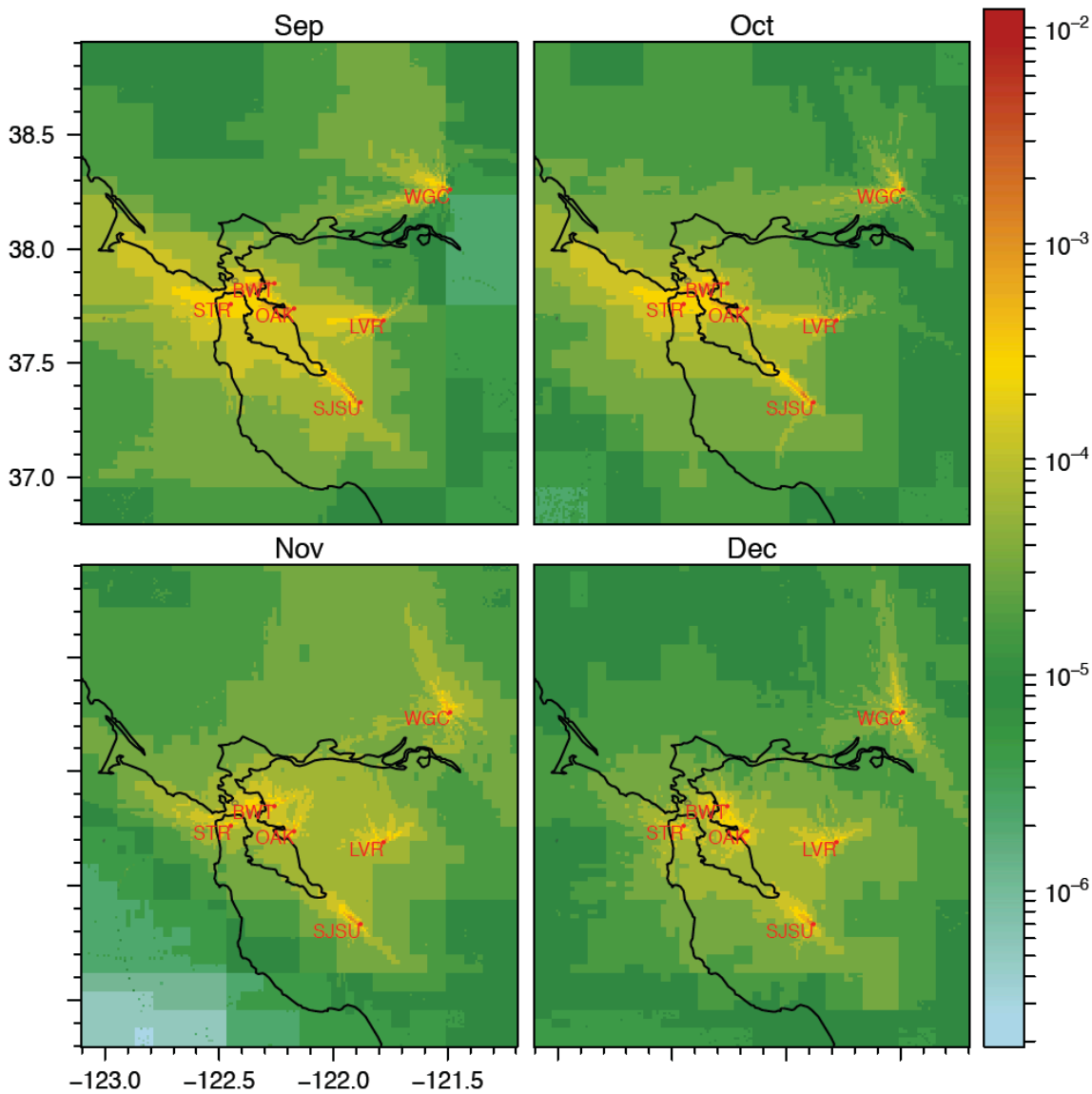

*The footprint is strongest over the Bay during September while the November footprint is spread over a larger area in the region. Although there is no measurement site in the North Bay (a sub-region north of San Francisco), the monthly footprint shows some sensitivity in the northern region of the Bay Area where dairy emissions sources are concentrated, in particular during September. As reported in Jeong et al. (2012a, 2012b, 2013), the footprint for WGC in the Central Valley is strong in the north-south direction during early winter, changing from the dominant west-east direction during the early fall.

Estimates of VOC Ratios Relative to CH_4

Posterior VOC:CH_4 ratios (e.g., $f^*_{C_2H_6_NG}$) are estimated using hierarchical inverse optimization. Figure 12 shows the posterior VOC:CH_4 ratios estimated from the hierarchical inversion. In HBI, the prior information is provided as a probability distribution using hyper-parameters (e.g., mean 0.04 for $f^*_{C_2H_6_NG}$ in a normal distribution) instead of a fixed value. For each probability

density plot for the VOC:CH_4 ratios, the median values and the 95% confidence intervals (CI) are presented, which are derived from posterior Markov chain Monte Carlo (MCMC) samples. For $f^*_{C_2H_6_NG}$, the median value from the posterior samples is similar to the prior assumption of 0.04. The median value for the posterior estimate for $f^*_{C_2H_6_PL}$ is also similar to the prior assumption of 0.07 (i.e., C_2H_6:CH_4 = 0.07 for the petroleum sector). For other VOCs, the estimated VOC:CH_4 ratios from HBI are consistent with the prior values except for C_7H_8, which shows somewhat lower posterior estimates for its ratio relative to CH_4 compared to the prior value (0.155 or 15.5%). One possible explanation is that this may reflect the change in the C_7H_8 composition relative to CH_4 in the on-road emission since the study by Kirchstetter et al. (1996), probably due to California's reformulation of gasoline (Kirchstetter et al., 1999). To verify this change in the VOC composition, more studies on VOC composition in on-road and refinery emissions are needed.

Figure 12: Posterior Distribution of the VOC Ratios Relative to CH_4

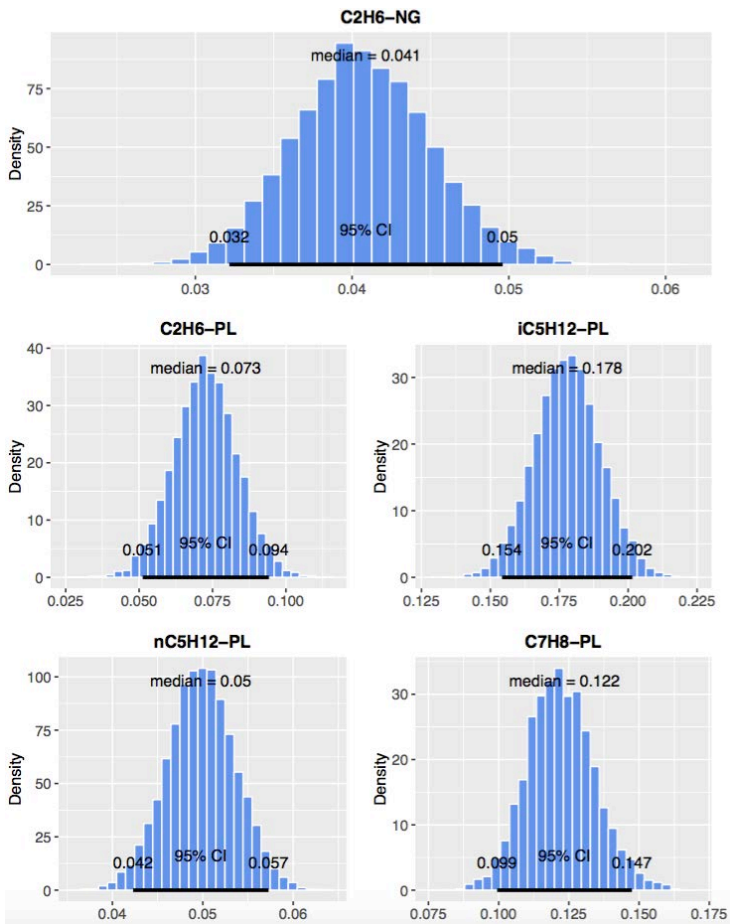

*C_2H_6 ratios are associated with both natural gas (NG) and petroleum (PL), and the other VOCs are used for PL only. The petroleum sector includes refinery and on-road emissions.

Estimates of Systematic Background Bias

The systematic mean bias in the background is estimated using the HBI method, which considers the mean bias as a subset of the entire parameter set solved during the inversion (Equation 2.3). For VOCs, the mean background bias is expected because the authors used a linear model to generate continuous VOC background mixing ratios for each site, fitting measurements at THD with data available only for a limited number of days (see THD VOC measurements in Appendix G). The details for the estimated mean bias are provided in Appendix E. The sites that are located in the heavily populated areas (e.g., East Bay, east of San Francisco Bay) show relatively larger mean biases compared to the coastal site (STR) and the Central Valley site (WGC). This difference in the mean bias is likely due to the use of different measurement systems. The small bias at STR suggests that on average the measurements at THD are representative of background concentrations for the SFBA region compared to those of a similar coastal site. On the other hand, the relatively large biases at other sites indicate that the linear fit using THD measurements cannot entirely capture the background variability of the sites located in densely populated areas. This HBI method corrects the systematic biases that could affect the inversion result.

2.2.3 Results

CH_4 Emissions in SFBA

Using atmospheric observations from six sites (LVR sites with hourly data) during September 2015 – December 2015, the team estimated CH_4 emissions in SFBA. In this section, the inversion results are presented using CH_4 only, and the results on source partitioning using CH_4 and VOCs are described.

This hierarchical Bayesian inversion analysis estimates that SFBA's CH_4 emissions (including wetland, 3% of the anthropogenic total in the prior emission) are 174 to 282 Gg CH_4/yr (median = 225, at 95% confidence), higher (1.4 to 2.2 times) than the recent inventory (126 Gg CH_4/yr in 2011) from BAAQMD (BAAQMD, 2015). A simple regression analysis of WRF-STILT predictions on measurements also indicates that actual CH_4 emissions are more than two times higher than those from the prior emission model (see Appendix H). These inverse estimates also agree with those reported by Fairley and Fischer (2015) where they reported a total of 240±60 Gg/yr (at 95% confidence) for the period from 2009 to 2012 using CH_4:CO enhancement ratios from 14 air quality sites in SFBA.

Figure 13 shows the median posterior emissions after inversion by sector, adjusting the prior emissions for individual 0.1º pixels based on the corresponding posterior scaling factors (i.e., posterior $\boldsymbol{\lambda}$). As expected from the higher SFBA's total posterior emission than the prior, the posterior median emissions for individual sectors are higher than those of the prior emission model. In particular, this HBI analysis suggests the posterior landfill (LF) emissions are much higher than those of the prior although the ratio of LF to total (51%) in the posterior estimate is similar to the one prior (54%). In deriving sector emissions it is assumed the ratios of individual source emissions relative to the total for each 0.1° pixel are known in the prior emission model, as in previous studies (e.g., Jeong et al., 2013, Wecht et al., 2014). Thus, source partitioning using this method depends on the accuracy of the relative source composition in the prior

emission model and cannot be used as an independent one; for this reason, the confidence interval is not shown.

A further analysis on the spatial distribution of emissions suggests that inversions using a high resolution as in this study can be useful to separate emissions for some source sectors from those of other sources. Figure 2.6 shows the LF emission map and the ratio of LF to total emissions for each 0.1° pixel in SFBA. Many of the pixels, which have high emission fluxes, also show high ratios of LF to the total. By summing emissions from the pixels with greater than 0.8 in the LF ratio relative to the total, researchers found that the total from those high-emitting pixels account for 85% of the total LF emissions in SFBA (see Appendix I). This result indicates that the higher LF emissions in the posterior estimate than the prior are likely attributable to the pixels with high ratios of LF to the total emissions. A similar analysis to the dairy livestock (DLS) sector is applied, which has been reported to emit more CH_4 emissions than the inventory in California (Jeong et al., 2013; Johnson et al., 2014) although in SFBA the difference between the prior and posterior DLS emissions is less noticeable than the LF sector. As shown in Figure 14, the dairy emission sources in SFBA are concentrated in Marin and Sonoma counties, and in the majority of those pixels with DLS emission sources the ratios of DLS to the total are greater than 0.5. More quantitative source partitioning using VOC measurements are provided in the following section.

Figure 13: CH_4 Emissions in SFBA by Sector Using CH_4 Measurements Only

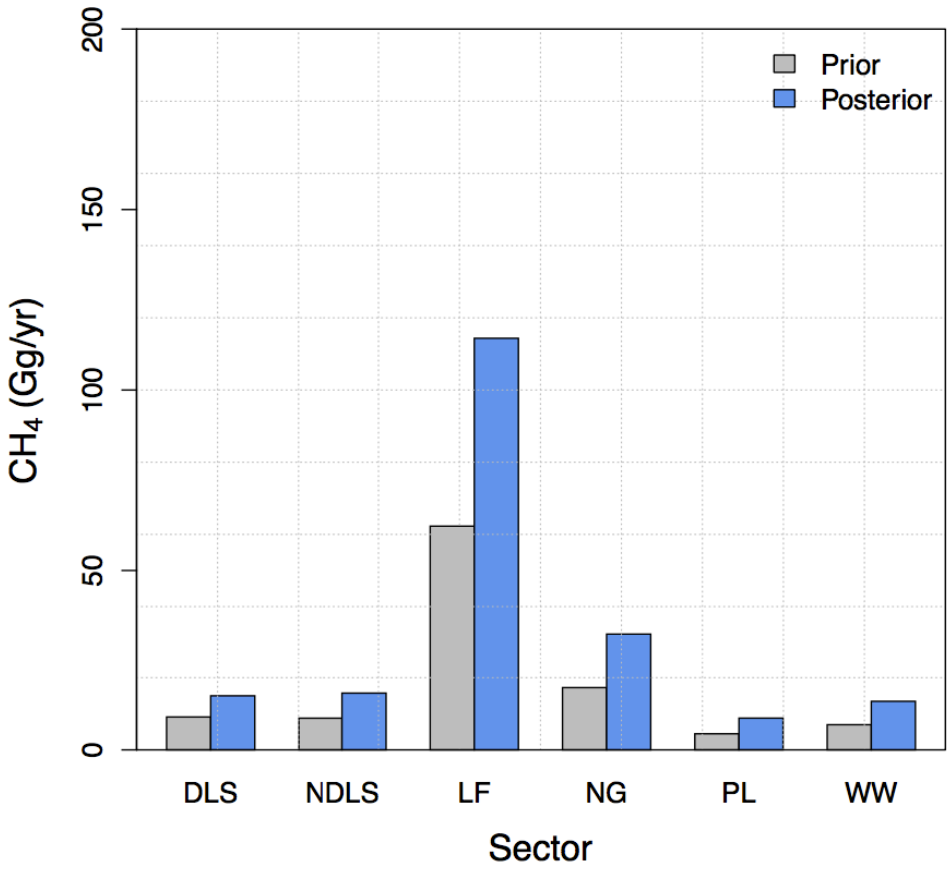

Only posterior median emissions are shown for sectors: dairy livestock (DLS), non-dairy livestock (NDLS), landfill (LF), natural gas (NG), petroleum refining and on-road mobile sources (PL), and wastewater (WW). For this result, researchers assume that the ratios of individual sector emissions to the total for each 0.1° pixel is known from the prior CH_4 emission map. Then they scaled each sector prior within each pixel by the corresponding posterior scaling factor to obtain posterior emissions.

Figure 14: Dairy Livestock (DLS) and Landfill (LF) Emission Flux (nmol/m^2/s) Maps and Maps of Ratios of DLS and LF to the Total Emissions for Each 0.1º Pixel

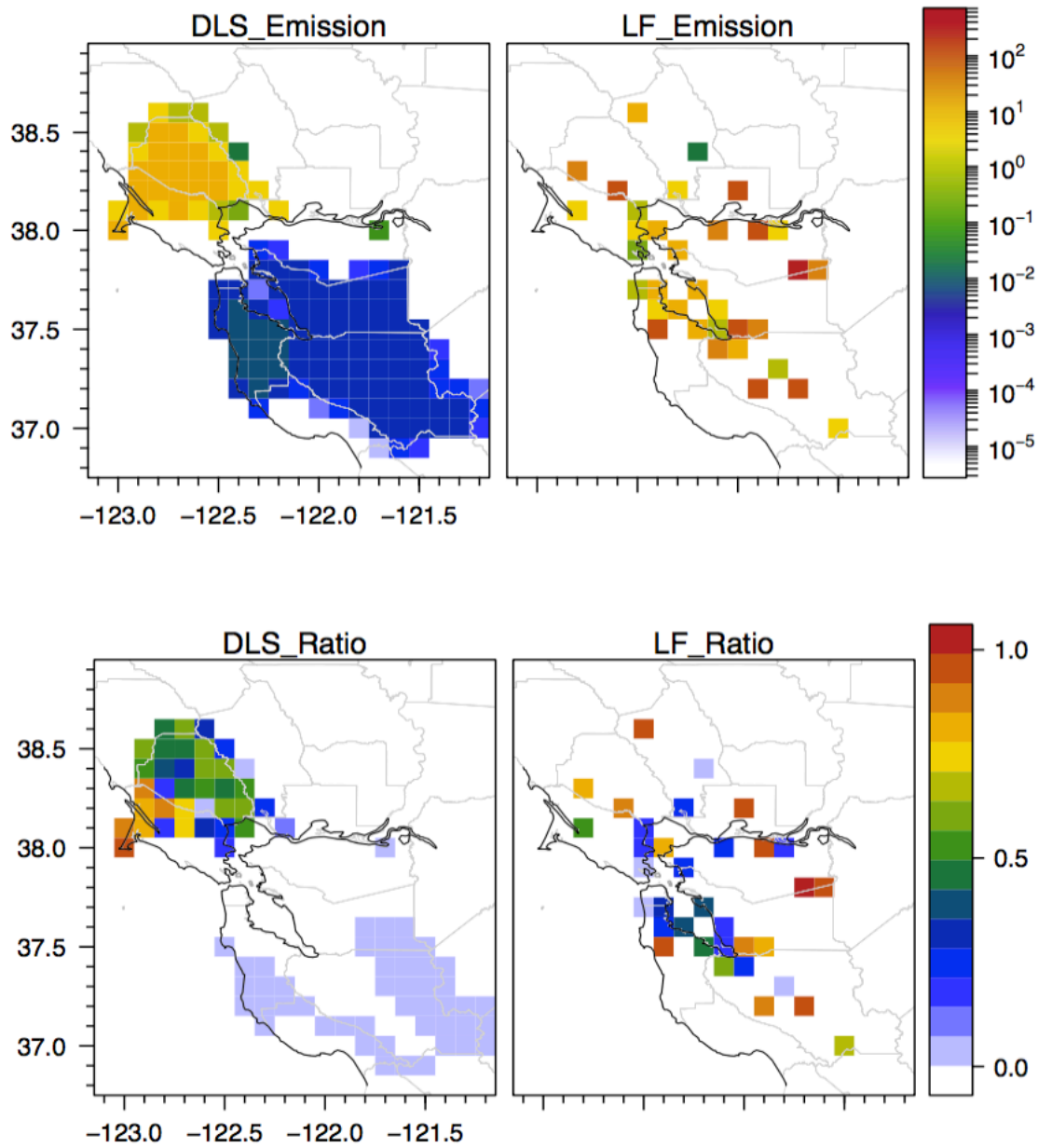

Dairy livestock (DLS) and landfill (LF) emission flux (nmol/m^2/s) maps at 0.1º × 0.1º resolution (top panel), and maps of ratios of DLS and LF to the total emissions for each 0.1º pixel (bottom panel). Note that the inversion is performed at 0.1º (~10 km) resolution for SFBA aggregating original emissions at 0.01º (~1 km) resolution.

Source Apportionment Using VOCs

Combining CH_4 and VOC measurements, a more robust method is used for source attribution than applied in the previous section and separate CH_4 emissions into biological, natural gas (NG), and petroleum (PL) sectors. VOC compositions relative to CH_4 are used to derive

predicted concentrations of VOCs to be compared with VOC measurements. Measurements of C_2H_6, i-C_5H_{12}, n-C_5H_{12}, and C_7H_8 from six sites are used to separate fossil-fuel sources (NG and PL) from the biological source sector, which includes all other sources except for NG and PL (see Table 2.3). If more VOC measurements linked with other biological sources, such as dairy and landfill emissions, are available, the inversion system developed here can be used to distinguish those sources from other sources.

Figure 15 shows the estimated emissions by sector based on different sets of VOC measurements. When the inversion was performed with CH_4 and C_2H_6 only, and i-C_5H_{12} and n-C_5H_{12} was then added to further constrain the petroleum sector. A third inversion was conducted combining CH_4 and all four VOCs. When i-C_5H_{12}, n-C_5H_{12}, and C_7H_8 are used in addition to C_2H_6, the posterior uncertainty for the petroleum sector emissions are significantly reduced compared to the case with C_2H_6 only. As expected, the biological and natural gas emissions do not vary much across different inversions because the same CH_4 and C_2H_6 measurements are used for all inversions. The uncertainty for the biological source emission is slightly reduced when the PL sector is further constrained by addition of more VOCs. The inversion results using CH_4 and all four VOC measurements suggest that SFBA CH_4 emissions (including wetlands, ~3% of total) are 166 - 289 Gg CH_4/yr (median = 226, at 95% confidence) and 1.3 – 2.3 times higher than a recent inventory (126 Gg CH_4/yr in 2011) from BAAQMD. This estimate for total CH_4 emissions is very similar to the one estimated using CH_4 measurements only (174 - 282 Gg). It is noted that, if the additional uncertainty of 8% (about the median estimate) is incorporated based on the CO measurement-prediction comparison assuming the CO analysis is applicable to CH_4, the estimated CH_4 emissions are 154 – 297 Gg CH_4/yr (1.2 – 2.4 times the BAAQMD inventory, 95% confidence) (Appendix J). Undiagnosed sources of uncertainty may increase these error bounds beyond that indicated here. It is also noted that the transport error analysis based on CO rests on an assumption that *a priori* CO emissions in SFBA are known to better than 10%, though Brioude et al. (2013) found that a comparison of measured and predicted CO agreed to within about 15% for aircraft flights over SoCAB conducted in May and June, 2010.

Attributing the total CH_4 emissions to different sources, researchers estimate that the biological, natural gas, and petroleum emissions in SFBA account for 82, 15, and 2% of the total (remaining 1% from other miscellaneous sources), respectively, suggesting the biological source CH_4 emissions are much higher than fossil-fuel-based emissions. Similarly, the prior emission model suggests that the biological source was dominant (78%) in SFBA. The HBI analysis estimates that the posterior emission for the biological source sector is 126 – 249 Gg CH_4/yr (at 95% confidence), higher than the prior (94 Gg CH_4/yr) by factors of 1.3 – 2.6.

Total NG emissions for SFBA are estimated at 26 – 42 Gg CH_4/yr, 1.5 – 2.4 times higher than the prior (17 Gg CH_4/yr). The spatial distribution of CH_4 emissions for the natural gas sector is compared between prior and posterior estimates in Figure 16, where emissions in some pixels are elevated after inversion. According to the previous model, 99% of the NG emissions in SFBA are from the NG distribution sector, and the elevated emissions in the posterior NG emission map indicate the prior emissions for the NG distribution sector are underestimated. This conclusion is consistent with the results from recent studies in SoCAB that CH_4 emissions

from NG distribution are generally higher than the inventory (Wennberg et al., 2012; Peischl et al., 2013).

In a recent study aimed at estimating spatially explicit natural gas emissions across California, Jeong et al. (2014) estimates a total of 30 Gg CH_4/yr for SFBA from the natural gas sector, 93% of which are from the NG transmission and distribution subsectors. In comparison, the total for the natural gas sector in the prior emission model is 17 Gg CH_4/yr, which is based on BAAQMD's inventory and lower than that of Jeong et al. (2014). The team's posterior estimate for the natural gas sector is 0.87 – 1.4 times the total in Jeong et al. (2014). The NG CH_4 emission for SFBA, based on the updated 2016 EPA inventory, is estimated to be 11.6 Gg CH_4/yr, which is only about 40% of that estimated by Jeong et al. (2014) (see Section 1.3 in Chapter 1). The inverse analysis results suggest that the new EPA inventory underestimates CH_4 emissions from the natural gas distribution sector even further, compared to the previous inventory.

Overall, the posterior estimate for the NG sector supports the finding of Jeong et al. (2014) that their SoCAB total for NG distribution was lower than the top-down estimate (for the year 2010) (Peischl et al., 2013) by a factor of ~2. A possible explanation for the more modest underestimate of NG CH_4 emissions in SFBA than in SoCAB might be due to effective control of NG CH_4 leakage in SFBA following the 2010 natural gas pipeline explosion in San Bruno (located south of San Francisco). However, this hypothesis must be confirmed with further investigation. Using all four VOCs, the posterior PL emission is estimated at 3 – 4 Gg CH_4/yr (at 95%), which is consistent with the prior (4 Gg CH_4) estimate. Compared to the result from the inversion with CH_4 only, the new approach with VOCs constrains PL CH_4 emissions with much high confidence.

Figure 15: Comparison of Posterior CH_4 Emissions* (at 95% confidence) by Source Sector Using CH_4, C_2H_6 , i-C_5H_{12}, n-C_5H_{12} and C_7H_8 Measurements

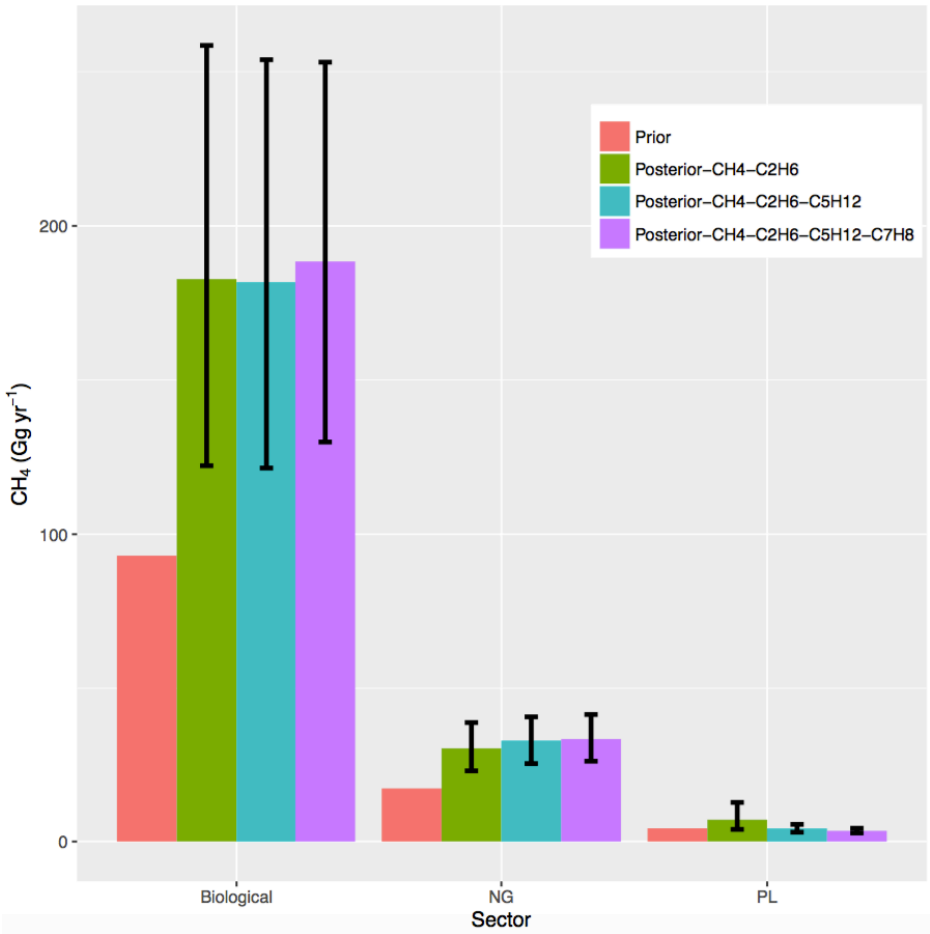

*The posterior emissions are estimated by solving for the scaling factors specific to the biological sources (livestock, wastewater, landfill, wetland), natural gas (mostly distribution) and petroleum (refinery and on-road mobile) emissions.

Figure 16: Comparison of Prior and Posterior Natural Gas Emissions (0.1° resolution) for SFBA

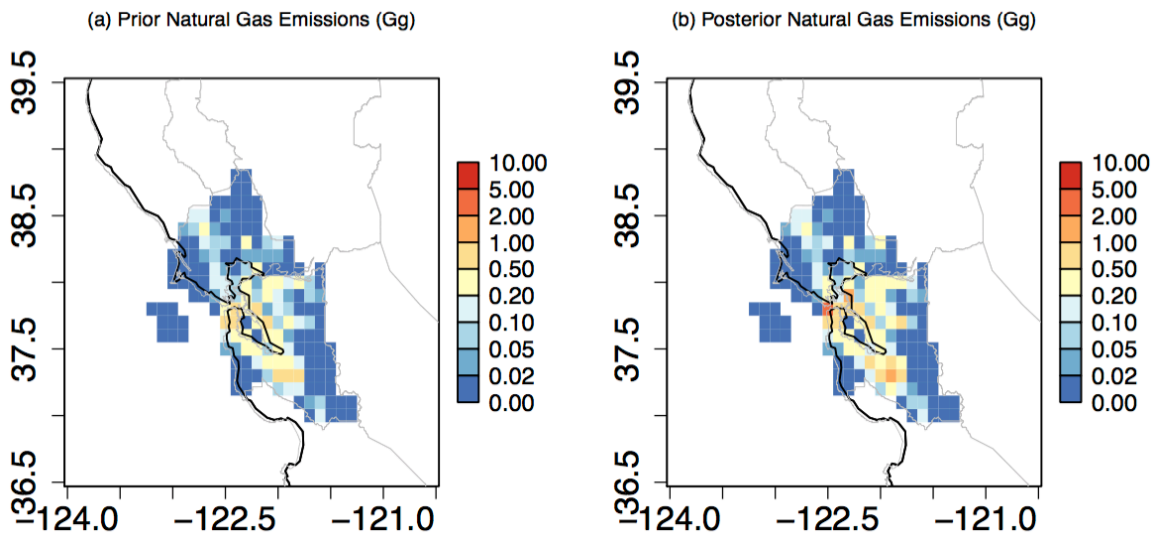

(a) NG CH_4 emissions (Gg) from the prior model and (b) the posterior emissions (Gg CH_4).

Discussion

The multi-tracer method used in this study is effective in separating biological source CH_4 emissions from NG and PL source emissions in SFBA. This study estimates that 82% (i.e., median ratio of 185/226 in posterior estimates) of the total emissions in SFBA is from biological sources, suggesting that the ratio of biological vs. fossil emissions in SFBA is different from that of SoCAB, where multiple studies suggest the proportion of fossil-fuel CH_4 is considerably higher (58 – 65% (Hopkins et al., 2016); ~70%, (Wennberg et al., 2012); and 41 - 68% (Peischl et al., 2013)). Similarly, the CALGEM prior model, which is scaled to match the 2012 CARB state inventory (CARB, 2014) based on the spatial distribution from Jeong et al. (2013; 2014), the fossil-fuel sources for SoCAB account for 35% of the total (349 Gg CH_4/yr), which is higher than that (22%) of the previous model for SFBA (Appendix F) and slightly lower than the lower bound of Peischl et al. (2013).

Among the biological sources, this analysis shows the landfill sector is underestimated in the prior emission, contributing significantly to the large discrepancy between the prior and posterior emissions estimates. This result for SFBA is different from the SoCAB where Peischl et al. (2013) suggested that landfill emissions in SoCAB are generally consistent with ARB's inventory estimate. In comparison, the CALGEM prior model estimates that the combined total for landfill, wastewater, and livestock in SoCAB is 224 Gg CH_4/yr, which is consistent with that (182±54 Gg, at 68% confidence) of Peischl et al. (2013). Both this study and the Fairly and Fischer (2015) study show that the prior emissions are underestimated, and the VOC-based analysis indicates that emissions from the fossil-fuel sources in SFBA are relatively small, compared to the biological sources. These results suggest that landfill emissions are likely a dominant source of the total emissions in SFBA, consistent with the prior model. Further studies using facility-

level measurements of CH_4 and relevant VOCs (e.g., landfill flux measurements) would be useful to verify the results of this study.

Recent studies reported that livestock is the main source of CH_4 emissions in California and are likely underestimated in the ARB inventory (Jeong et al., 2012a; 2013; Johnson et al., 2014). In this study, dairy emissions have not been separated from other sources, although it's suggested that, given the spatial distribution of dairy farms in SFBA, the posterior emissions estimate for dairy livestock can be relatively independent compared to other sources, such as non-dairy livestock. Because the emission factors for dairy livestock were derived based on CARB's inventory, it is possible that the dairy emissions in SFBA are also higher than the prior estimate. This explanation for the underestimation of emissions from the biological sources in the prior emission model merits further verification.

The inversion result based on VOC measurements suggests that the emission rate in SFBA is relatively lower than other urban regions in the United States. Natural gas consumption in SFBA shows seasonality with winter having the highest consumption (about two times that of summer). If the entire year is divided into three seasons, the first (January – April) and second season (May – August) NG consumptions are 1.2 and 0.5 times that of the study period (September – December). If the seasonal consumption is applied relative to that for the study period to the posterior emissions (26 – 42 Gg CH_4), it is estimated that annual natural gas emissions for SFBA are 23 – 38 Gg CH_4 (95% confidence; mostly distribution emissions). These annual estimates are equivalent to 0.3 – 0.5% (in mass ratio of CH_4 per unit NG) of the total NG consumption, which is estimated to be 4.4×10^{11} cubic feet for 2011 in BAAQMD's official inventory (BAAQMD, 2015).

For comparison, SoCAB NG emissions are estimated to be 0.7 – 3% of the total NG consumption; in SoCAB, however, separating distribution NG emissions from other NG sources is more challenging than in SFBA because of oil and gas production (Wennberg et al., 2012; Peischl et al., 2013). McKain et al. (2015) reported that the emission rate in the Boston urban area is 2.7±0.6% (at 95% confidence) of NG consumption. As pointed out in the previous section, the relatively low emission rate in SFBA may be possibly due to the effective control of NG CH_4 leakage in SFBA following the 2010 natural gas pipeline explosion in San Bruno, which requires further verification in future regional studies.

In summary, one of the first analyses is presented that involves a full Bayesian inverse model using a combination of a high-resolution (1 km × 1 km) prior emission model and CH_4 and VOC measurements. The GHG measurement network constrains CH_4 emissions from the urban and suburban areas of SFBA, separating fossil-fuel source emissions from those of biological sources. The estimated total emissions from this study are consistent with a recent independent study (Fairly and Fischer, 2015), suggesting that the inverse framework based on the measurement network can be an effective approach to quantifying emissions and potentially monitoring long-term spatial and temporal changes in SFBA emissions. However, it is possible that undiagnosed sources of error affect the CH4 emissions estimates. In the future, a combination of improved prior emissions and meteorological models, expanded multi-gas measurements (e.g., additional VOC measurements), and inverse model analyses will reduce

uncertainty in SFBA's GHG emissions. In SFBA and across the state, where livestock emissions are important, additional measurements of VOC can be incorporated into the inversion system developed in this study to separate dairy emissions from other emissions sources. Given the importance of distinguishing dominant CH4 sources for prioritizing mitigation efforts and large-scale events, such as the well failure at Aliso Canyon (Conley et al., 2016), a combination of facility specific emission measurements and regionally representative measurements of source-specific tracers (e.g., CO, VOCs, and potentially CH4 isotopes) (Townsend-Small et al., 2012; Peischl et al., 2013; Guha et al., 2015) are likely to prove useful in the future.

2.3 Sacramento Regional Emission Estimates Using Airborne CH_4 and VOC Measurements

2.3.1 Introduction

The Sacramento Valley region has complex emission sources including seasonal rice cultivation, livestock, non-associated dry gas production as well as urban sources from the Sacramento metropolitan area. However, few studies have been conducted to estimate CH_4 emissions in this region, despite that the Sacramento Valley is likely the third largest emission source region in California following the San Joaquin Valley and the South Coast Air Basin (ARB, 2014). Zhao et al. (2009) and Jeong et al. (2012a, 2013) estimated CH_4 emissions from this region, but these studies focused on quantifying regional total emissions, not separating emissions between different sources. Given the multiple strong emission sources and the substantial total emission in the region, it is important to further verify emissions estimated from previous work and identify potential emission sources that dominate the region's CH_4 total emissions for efficient mitigation planning.

A short-term airborne campaign was conducted in June 2014 to quantify CH_4 emissions from the Sacramento Valley. This study combines CH_4 with four VOC species (ethane (C_2H_6), i-pentane (i-C_5H_{12}), n-pentane (n-C_5H_{12}), and toluene (C_7H_8)) for source partitioning of CH_4 emissions in this region. Expanding on previous work by Jeong et al. (2012a; 2012b; 2013; 2014) and Ganesan et al. (2014), researchers developed a hierarchical Bayesian method to combine CH_4 with VOC measurements for source apportionment of CH_4 emissions. Incorporating both CH_4 and VOC measurements into a full Bayesian inverse analysis where uncertainty is thoroughly characterized, researchers illustrate how VOC measurements can be used to separate fossil-fuel emissions from biological emissions (e.g., dairy emissions).

2.3.2 Data and Methods

Atmospheric Measurements

The short-period airborne measurement campaign was conducted in the Sacramento metropolitan area. The area is surrounded by various emission sources including natural gas production, natural gas facilities, rice cultivation, dairy farm operation and landfill (Figure 17).

A Mooney TLS M20 high performance single engine aircraft modified was used for air sampling. The wings have either eighth inch stainless steel or quarter inch (outer diameters) Teflon tubing for the air sampling inlets (Conley et al., 2016). The air inlets are routed through the plane and the stainless tubing is connected to a continuous flow pump. Periodic air samples

were then collected manually into steel canisters and subsequently analyzed at UC Irvine for CH_4 , ethane, pentane, and toluene (Colman et al., 2001).

Figure 17: Measurement Campaign Area and Major Emission Sources in and around the Measurement Area over the 30-m Elevation Map

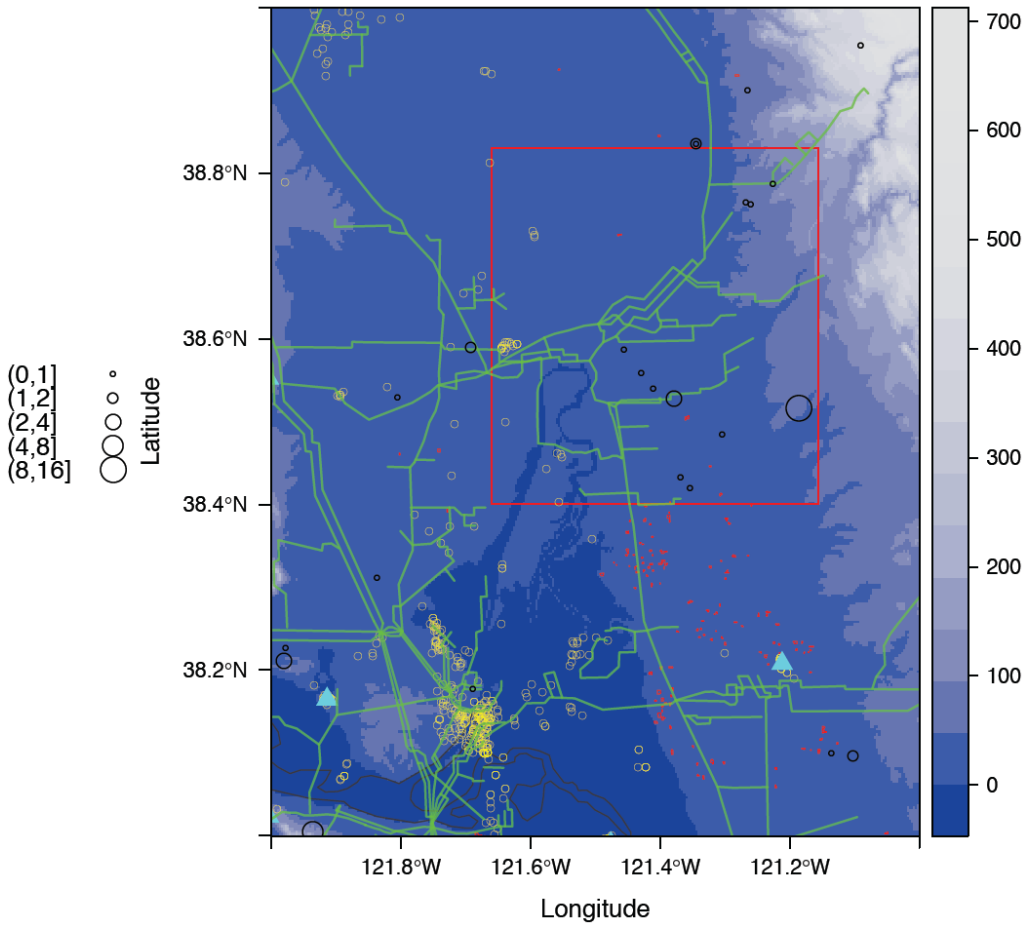

The red rectangular box shows the campaign area and the color scale bar shown on the right is for the elevation map in meters. The open black circles represent the landfill point sources with circle sizes proportional to emissions (Gg CH_4/yr ; the legend shown on the left), the yellow open circles show the active natural gas wells, the cyan filled triangles show the natural gas storage facilities, and the red dots indicate the dairy farm locations. The green lines show the major transmission pipelines.

Prior Emission Model

This work used the California Greenhouse Gas Emission Measurements (CALGEM) project, a prior CH_4 emission model (CALGEM model, available at calgem.lbl.gov) described by Jeong et al. (2012a, 2013, 2014) with some modifications. The CALGEM emission model provides emissions by sector at a high spatial resolution (0.1° × 0.1°) for California. The CALGEM model has seasonal components for wetlands and crop agriculture only, and these seasonal emissions are combined with non-seasonal emissions to construct monthly emission maps for inversions. The inversion approach using non-seasonal prior emissions is widely used (e.g., Zhao et al. (2009), Jeong et al. (2012a; 2012b; 2013), Wecht et al. (2014), Cui et al. (2015)).

In this study, the CALGEM prior emission distributions are scaled to match 2012 CARB state totals for anthropogenic emission sectors (CARB, 2014), with small (< 50 Gg CH_4/yr) adjustments for some regions and sectors (per ARB staff private communication). The spatial distribution of the dairy livestock emissions was revised by incorporating the 2012 county-level dairy statistics from USDA (2013).[25] For natural wetlands, researchers used the prior emission map from Jeong et al. (2013). Table 12 provides the prior emissions used in this study by source, and Figure 18 shows the emission maps for the biological, natural gas, petroleum and total sectors. Note the prior emissions reflect the summer-season emissions for seasonally varying source sectors (i.e., rice and wetland) which are significantly higher than those of the other seasons.

Table 12: Prior CH_4 Emissions for the Sacramento Valley by Sector (Gg CH_4)

Source[a]	CH_4 Emissions
DLS	31
LF	27
NDLS	20
NG	30
RM	3
WW	3
WL[b]	9
CP[b]	126
Total	**249**

[a]Sectors include dairy livestock (DLS), landfill (LF), non-dairy livestock (NDLS), natural gas including petroleum production and local processing (NG), petroleum refining and mobile sources (RM), wastewater (WW), wetland (WL), and crop agriculture (CP, largely rice).

[b]Summer season emissions

[25] United States Department of Agriculture, http://www.nass.usda.gov/Statistics_by_State/California/Publications/County_Estimates/ to the spatial distribution from Jeong et al.

Figure 18: High-resolution (0.1° × 0.1°) Prior Emission Flux (nmol/m^2/s) Maps Used in This Study by Sector

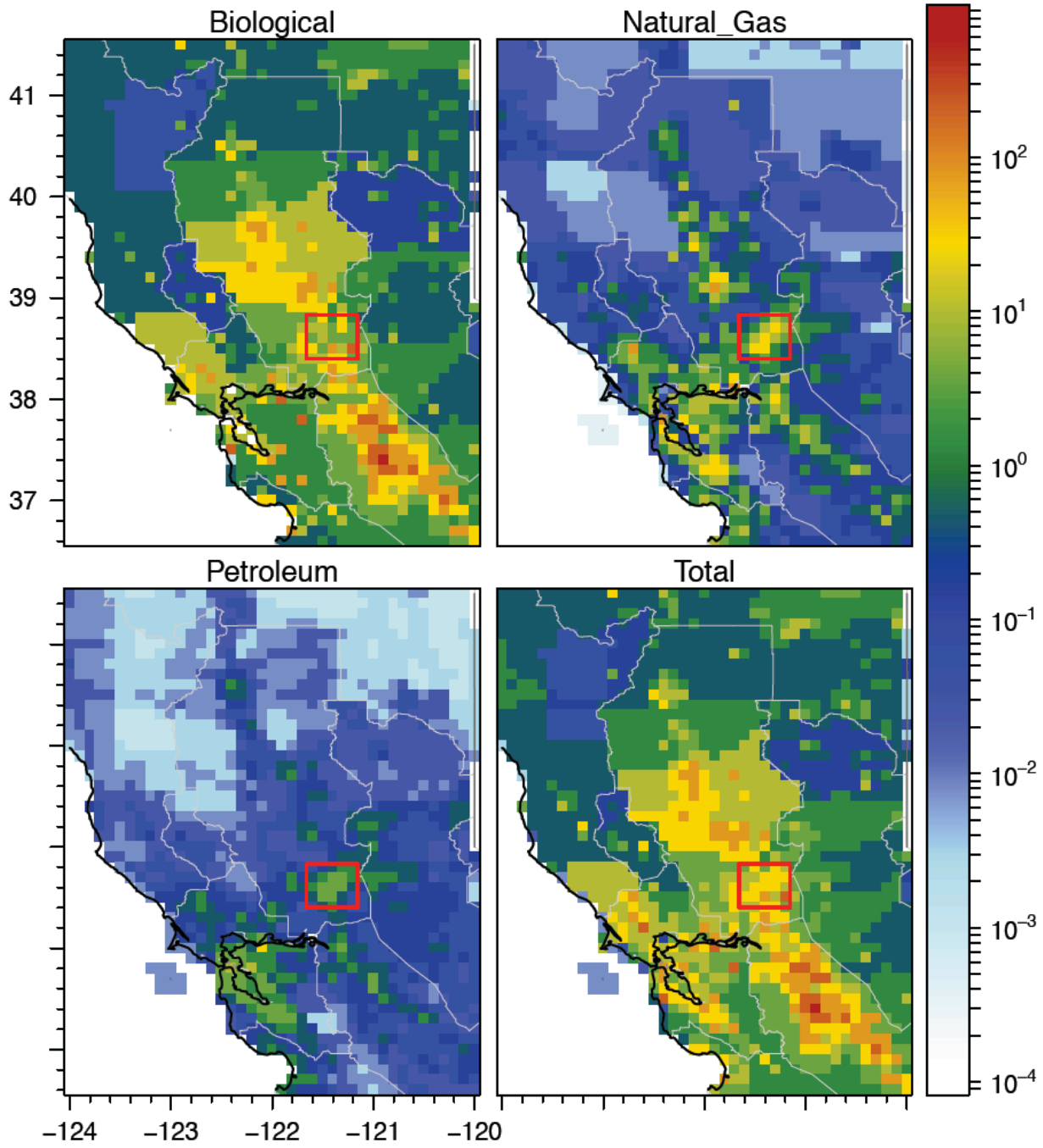

The emissions maps are shown for the biological, natural gas, petroleum, and total sectors. The petroleum sector includes on-road mobile and refinery emissions (see Table 2.4). The red rectangular box indicates the area where the airborne measurements were made and the light grey lines represent California's air basin (http://www.arb.ca.gov/ei/maps/statemap/abmap.htm). The measurement campaign was conducted in the Sacramento Valley Air Basin that includes the red rectangular box; the analysis focuses on this air basin.

Atmospheric Transport Modeling

The coupled WRF-STILT (Weather Research and Forecasting and Stochastic Time-Inverted Lagrangian Transport) model was used for atmospheric transport (Lin et al., 2003; Skamarock et al., 2008; Nehrkorn et al., 2010). The WRF-STILT model has been used to constrain GHG emissions in many studies including airborne measurement-based (e.g., Gerbig et al., (2003); Kort et al., (2008)) and tower measurement-based (e.g., Zhao et al., (2009); Jeong et al., (2012a); Jeong et al., (2012b); Newman et al., (2013); Jeong et al., (2013)) applications. The set-up adopted was used in Jeong et al. (2013) to run the STILT model. In this set-up, an ensemble of 500 STILT particles are run backwards in time for seven days driven with meteorology from the WRF model (version 3.6.1) (Skamarock et al., 2008). Figure 19 shows the mean footprint for each day (Noon local time) during the measurement campaign simulated by WRF-STILT. The simulated footprint for each receptor is combined with the prior emissions to calculate predicted mixing ratio concentrations.

The WRF model simulations closely follow those described in Jeong et al. (2012a, 2012b, 2013) with some modifications. The Version 3.6.1 of the WRF model (Skamarock et al., 2008) is used. As in Jeong et al. (2013), the meteorology was simulated for four different horizontal resolutions of 36, 12, 4, and 1.3 km (vertical levels = 50) using initial and boundary meteorological conditions provided by the North American Regional Reanalysis (NARR) dataset (Mesinger et al., 2006). In this study, the 4-km domain covers the entire Sacramento Valley region and most of California. As in Jeong et al., (2013) a 2-way coupling was applied between domains and 3-D analysis nudging at the outer domain every three hours using the NARR product. Following Jeong et al. (2013) the team used the five-layer thermal diffusion for the land surface model (5-L LSM) to account for irrigation in the land surface process during the early summer and use the MYJ scheme (Mellor and Yamada, 1982; Janjić, 1990) for the planetary boundary layer (PBL) scheme.

Figure 19: Simulated Footprints (ppb/(nmol/m^2/s)) at 1200 PST

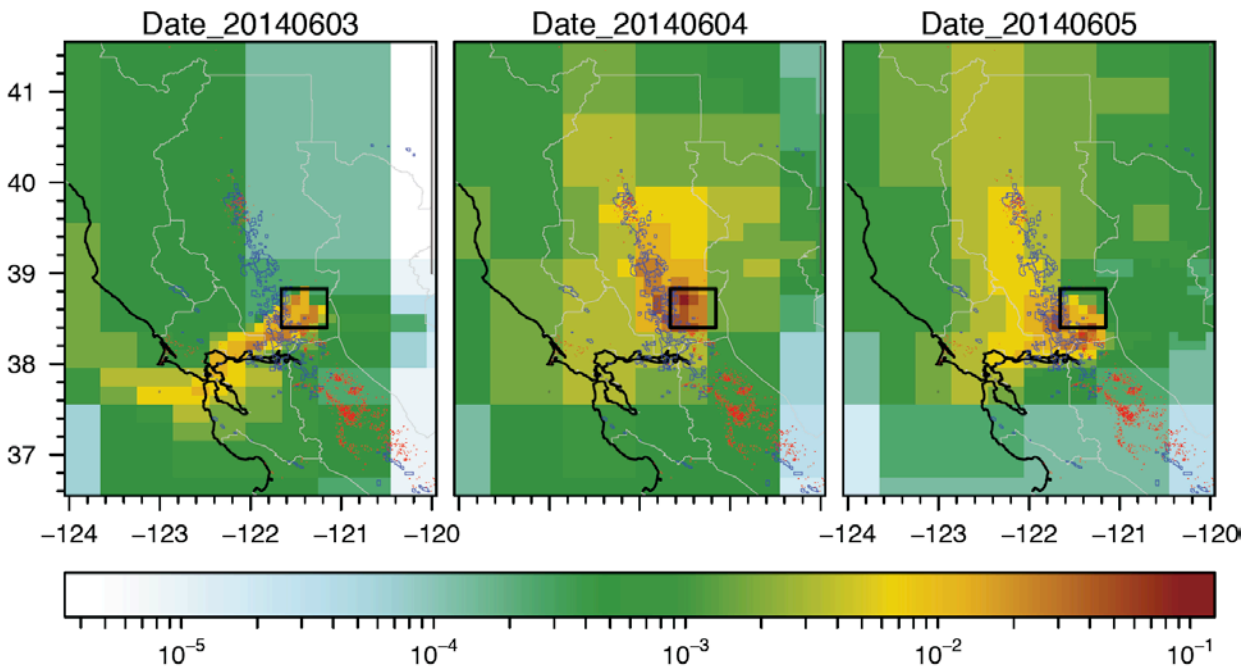

The light blue polygons represent the natural gas fields, the red polygons show dairy farms, and the white polygons indicate the air basin boundaries. The black box shows the measurement campaign area, and the Sacramento Valley Air Basin, which is the focus region of this study, includes the measurement area.

Estimates of VOC Ratios Relative to CH_4

Posterior VOC:CH_4 ratios (e.g., $f^*_{C_2H_6_NG}$) were estimated using hierarchical inverse optimization. As an illustration, Figure 20 shows the posterior C_2H_6:CH_4 ratios for the natural gas and petroleum sources estimated during the hierarchical inversion, simultaneously with other parameters that include the scaling factors. Recall that in HBI the prior information is provided as a probability distribution using hyper-parameters (e.g., mean 0.04 for $f^*_{C_2H_6_NG}$ in a normal distribution) instead of a fixed value. In the probability density plot for the VOC:CH_4 ratios, the median values and the 95% confidence intervals (CI) are presented, which are derived from posterior Markov chain Monte Carlo (MCMC) samples. For $f^*_{C_2H_6_NG}$, the median value from the posterior samples is similar to the prior assumption of 0.04. The posterior median estimate for $f^*_{C_2H_6_PL}$ is also similar to the prior assumption of 0.07 (i.e., C_2H_6:CH_4 = 0.07 for the petroleum sector). For other VOCs, the posterior values were also similar to those of the prior.

Figure 20: Estimated C_2H_6:CH_4 Ratios Using Hierarchical Inverse Optimization

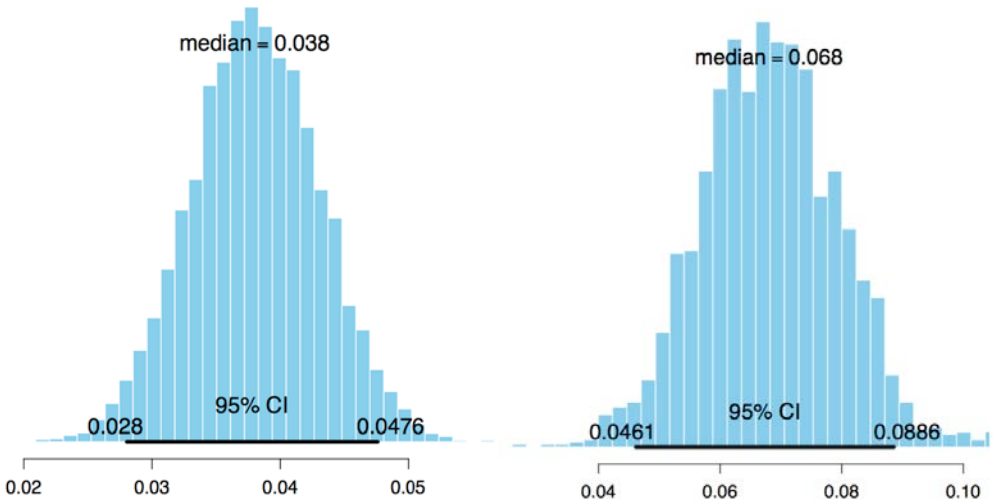

The median $f^*_{C_2H_6_NG}$ (left) from the posterior samples is similar to the prior assumption of 0.04 with the prior value well within the 95% confidence interval. The median value for the posterior $f^*_{C_2H_6_PL}$ (right) is also similar to the prior assumption of 0.07 (i.e., C_2H_6:CH_4 = 0.07 for the petroleum sector, see Table 2.1). The petroleum sector includes refinery and on-road emissions.

Estimates of Background Boundary Values

In this study, different methods for estimating upstream boundary values are used for CH_4 and VOCs. For predicted CH_4 upstream boundary values, researchers use a similar method to the one used in Jeong et al. (2012b, 2013). The details for estimating the background boundary values are described in Jeong et al. (2013) and only a summary is provided here. CH_4 boundary values were estimated using data from the Pacific coast aircraft network CH_4 profiles (http://www.esrl.noaa.gov/gmd/ccgg/aircraft/) and remote Pacific marine boundary layer sampling sites(http://www.esrl.noaa.gov/gmd/ccgg/flask.html) within the NOAA Earth System Research Laboratory (ESRL) Cooperative Air Sampling Network. The data were smoothed and interpolated to create a three-dimensional (3-D) curtain, varying with latitude, height and time. To quantify the errors associated with the 3-D curtain, a smooth curve was fit through the data and computed the seasonal cycle of the root mean square of the residuals from the curve. Predicted background values were computed for each hourly footprint simulation by sampling the curtain at each of the 500 particle trajectory endpoints (near the domain boundary at 130°W) and calculating the average value.

This HBI method directly estimates background boundary values for VOCs (Figure 21). Because the measurements were made during a short-term airborne campaign, a single value for the three-day average background was used. Overall, the estimated background values are similar to the low observations of each VOC species. The estimated ethane background indicates relatively larger local enhancements of ethane mixing ratios compared to the other VOC species. For toluene, the observations for the first day are somewhat different from those of the

following days during the three-day campaign period. This is likely due to the change in the source regions sensitive to the measurement locations as shown in the footprint.

Figure21: Estimated Background Values for VOCs During the Three-day Campaign Period Using Hierarchical Inverse Optimization

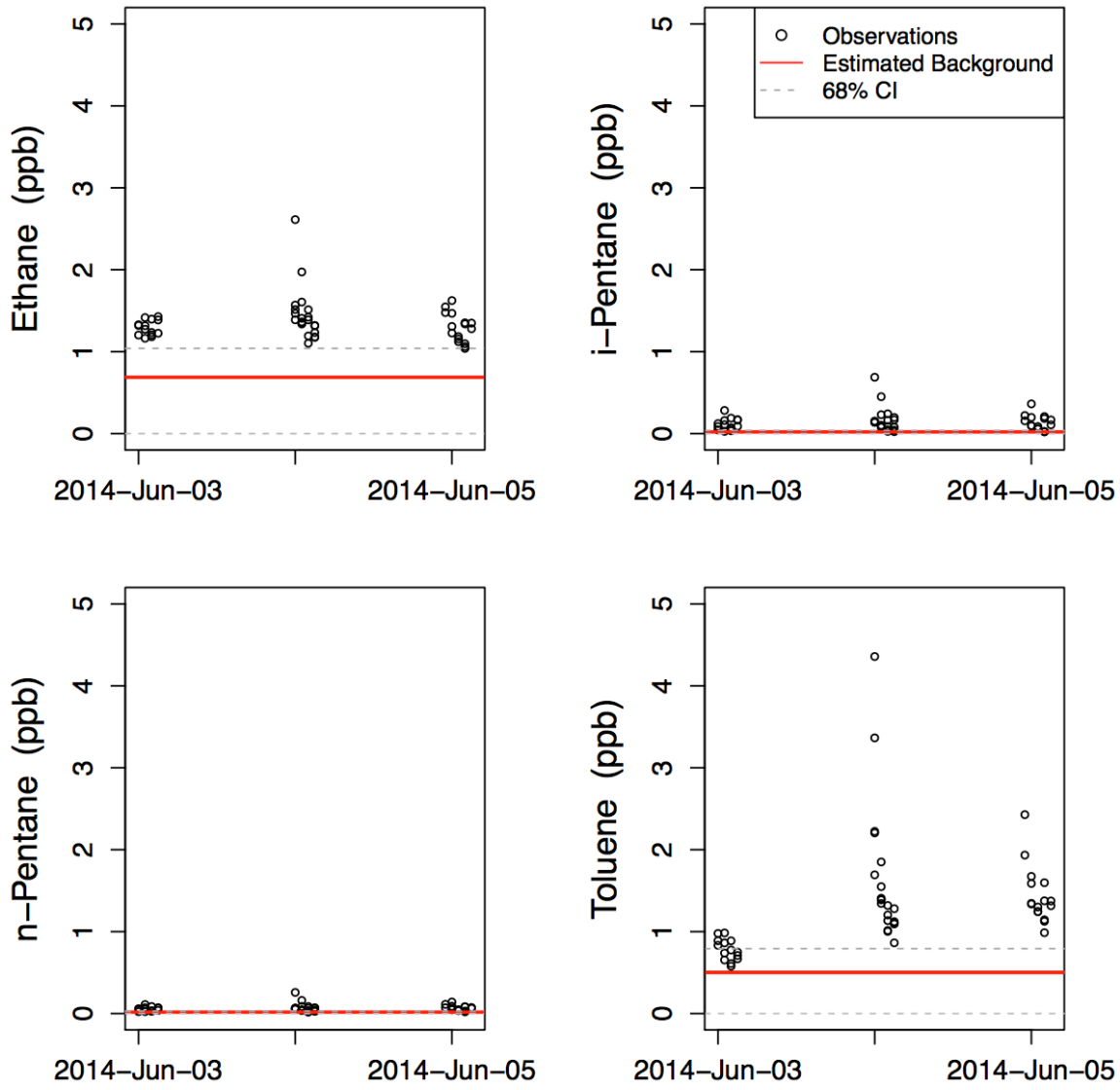

The horizontal red lines show the median estimates, and the grey dashed lines represent the upper and lower uncertainty bounds for the background estimates based on the 40000 posterior MCMC samples (at 68% confidence). These uncertainties for background values are fully incorporated in the inversion because these values are estimated simultaneously with other parameters including the VOC:CH_4 ratios and the scaling factors (**λ**).

2.3.3 Results and Discussion

Regional CH_4 Emissions

Using the short-period airborne observations during June 2014, researchers estimate CH_4 emissions in the Sacramento Valley Air Basin of California. In this section, t the inversion results using CH_4 only are present, and the results on source partitioning using CH_4 and VOCs are described.

The hierarchical Bayesian inversion analysis estimates that Sacramento Valley's CH_4 emissions are 312 - 479 Gg CH_4/yr (at 95% confidence), higher (1.3 – 1.9 times) than the prior for the summer season. The estimate for the Sacramento Valley agrees with the result from a recent inverse analysis study for this region (Jeong et al., 2013). Using 10-month-long measurements from a network of five towers in the Central Valley during 2010 – 2011, Jeong et al. (2013) estimated seasonal state and regional total CH_4 emissions. For the Sacramento Valley, Jeong et al. (2013) estimate the summer emissions are 361 – 450 Gg CH_4/yr (at 95% confidence). Jeong et al. (2013) estimated regional emissions solving for a single scaling factor for each sub-region of California (similar to California's air basins) whereas in this study the team solves the scaling factors for individual 0.3° pixels and aggregate pixel emissions for the region total. Also, in their analysis Jeong et al. (2013) used a prior emission model that is ~35% smaller in the total for the Sacramento Valley than the prior used in this study, calibrating their prior emissions to CARB's 2008 inventory (CARB, 2010). Although the two studies used different prior emissions, measurements and methods, they yield very similar emission estimates for the Sacramento Valley. The results from the two studies suggest that actual summer emissions for the Sacramento Valley are likely higher than the prior emissions used in this study.

Source Apportionment with CH_4 Measurements Only

In this section, possible source partitioning based on the spatial distribution of the spatially explicit emission maps are described with the source apportionment based on VOCs discussed in the following section. Figure 22 shows the posterior emissions after inversion by sector, adjusting the prior emissions for individual 0.3° pixels based on the corresponding posterior scaling factors (i.e., posterior $\boldsymbol{\lambda}$). Thus, source partitioning using this method depends on the accuracy of the relative source composition in the prior emission model and cannot be used as a completely independent one. As expected from the higher total posterior emission than the prior for the Sacramento Valley, which was shown in the previous section, the posterior median emissions for individual sectors are generally higher than those of the prior emission model. The crop agriculture sector (rice cultivation) shows a significantly higher posterior emission estimate than that in the prior model while the posterior emissions for the non-dairy livestock and landfill sectors are marginally higher than the prior estimates. The other sectors are similar to those of the prior model within error.

Figure 22: Summer CH_4 Emissions in the Sacramento Valley by Sector Using CH_4 Measurements Only

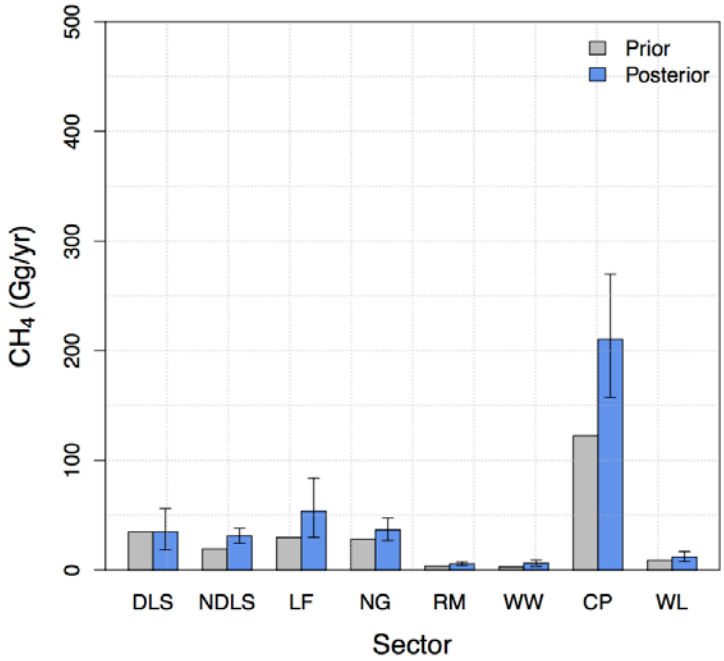

The sectors include dairy livestock (DLS), non-dairy livestock (NDLS), landfill (LF), natural gas (NG), petroleum refining and on-road mobile sources (RM), and wastewater (WW). For this result, researchers assume that the ratios of individual sector emissions to the total for each 0.3° pixel is known from the prior CH_4 emission map. Then they scaled each sector prior within each pixel by the corresponding posterior scaling factor to obtain posterior emissions. The error bars represent the 95% confidence intervals derived from the 40000 posterior MCMC samples.

For this summer period, the prior emission model and posterior analysis suggest the crop agriculture (mostly rice) sector is the dominant source of CH_4 emissions in the Sacramento Valley. The HBI analysis estimates that the CH_4 emission from rice cultivation is 157 - 270 Gg CH_4/yr (median = 210 Gg, at 95% confidence), which is higher than the prior. Applying the seasonality in the prior model, researchers estimate that the annual median emission for rice cultivation in the Sacramento Valley is 79 Gg CH_4/yr, which agree very well with those of recent studies (Jeong et al., 2013; Peischl et al., 2012). Note that in the prior model the rice emission total in the Sacramento Valley accounts for 97% of the state's total rice emissions. Using a tall tower in central California, Jeong et al. (2013) estimated annual CH_4 emissions from rice cultivation are 50 – 86 Gg CH_4/yr (at 95% confidence). Similarly, Peischl et al. (2012) estimated annual CH_4 emissions from rice cultivation to be 71 - 100 Gg CH_4 (at 95% confidence). This estimate by Peischl et al. (2012) is based on the rice emission study in a commercial rice field by McMillan et al. (2007) where they estimated annual CH_4 emissions of 26.1 - 31.0 g CH_4-C/m^2 during October 2001 to October 2002. As in the comparison for regional total emissions from the previous section, this good agreement between this analysis and previous work for the rice emission in the Sacramento Valley suggests reasonable inversion results.

Source Apportionment with CH_4 and VOCs

Incorporating both CH_4 and VOC measurements (C_2H_6, i-C_5H_{12}, n-C_5H_{12}, and C_7H_8) in the inversion, a more robust method is applied to separate CH_4 emissions into biological, natural gas (NG), and petroleum (PL, refinery and on-road mobile sources) sectors. The biological source sector includes all other source sectors except for NG and PL. As described in the previous section, VOC compositions relative to CH_4 are used to derive predicted concentrations of VOCs to be compared with VOC measurements. If more VOC measurements linked with other biological sources, such as dairy and landfill emissions, are available, the inversion system applied here can be used to distinguish those sources from other sources.

Figure 23 shows the estimated emissions by sector based on different sets of VOC measurements. The inversion was performed with CH_4 and C_2H_6 only, and d i-C_5H_{12} and n-C_5H_{12} was added to further constrain the petroleum sector. A third inversion was conducted combining CH_4 and all four VOCs. Although different inversion results are indistinguishable within error, the biological emissions (i.e., median estimates) tend to increase with addition of more VOCs while the median emission estimates for the natural gas and petroleum sectors decrease slightly. When all four VOCs were used, the petroleum median emission decreases by 7% relative to the one with C_2H_6 only.

Using CH_4 and all four VOC measurements it is estimated that CH_4 emissions for the Sacramento Valley are 334 - 460 Gg CH_4/yr (median = 398, at 95% confidence) and 1.3 – 1.8 times higher than the prior. This estimate for the regional total CH_4 emission is very similar to the one estimated using CH_4 measurements only (312 - 479 Gg CH_4/yr, see previous sections). Attributing the total CH_4 emissions to different sources, researchers estimate that the biological, natural gas, and petroleum emissions in the Sacramento Valley account for 90, 9, and 1% of the total posterior emission, respectively, showing the biological source CH_4 emissions are much higher than fossil-fuel-based emissions during this summer period. Similarly, the prior emission model suggests that the biological source was dominant (87%) in the Sacramento Valley. The HBI analysis estimates that the posterior emission for the biological source sector is 294 – 417 Gg CH_4/yr (at 95% confidence), higher than the prior (217 Gg CH_4/yr) by factors of 1.4 – 1.9. One of the reasons for this underestimate in the prior emissions is likely that the prior model for rice cultivation emissions was calibrated from Jeong et al. (2012a), which was originally taken from the denitrification and decomposition model (DNDC) output described by Salas et al. (2009), to match CARB's inventory for rice cultivation (CARB, 2014; 49 Gg CH_4/yr). This annual estimate is lower than those estimated by Jeong et al. (2013) (50 – 86 Gg CH_4/yr, at 95% confidence) or Peischl et al. (2012) (71 – 100 Gg).

Figure 23: Comparison of Posterior CH_4 Emissions (at 95% confidence) for the Sacramento Valley by Sector

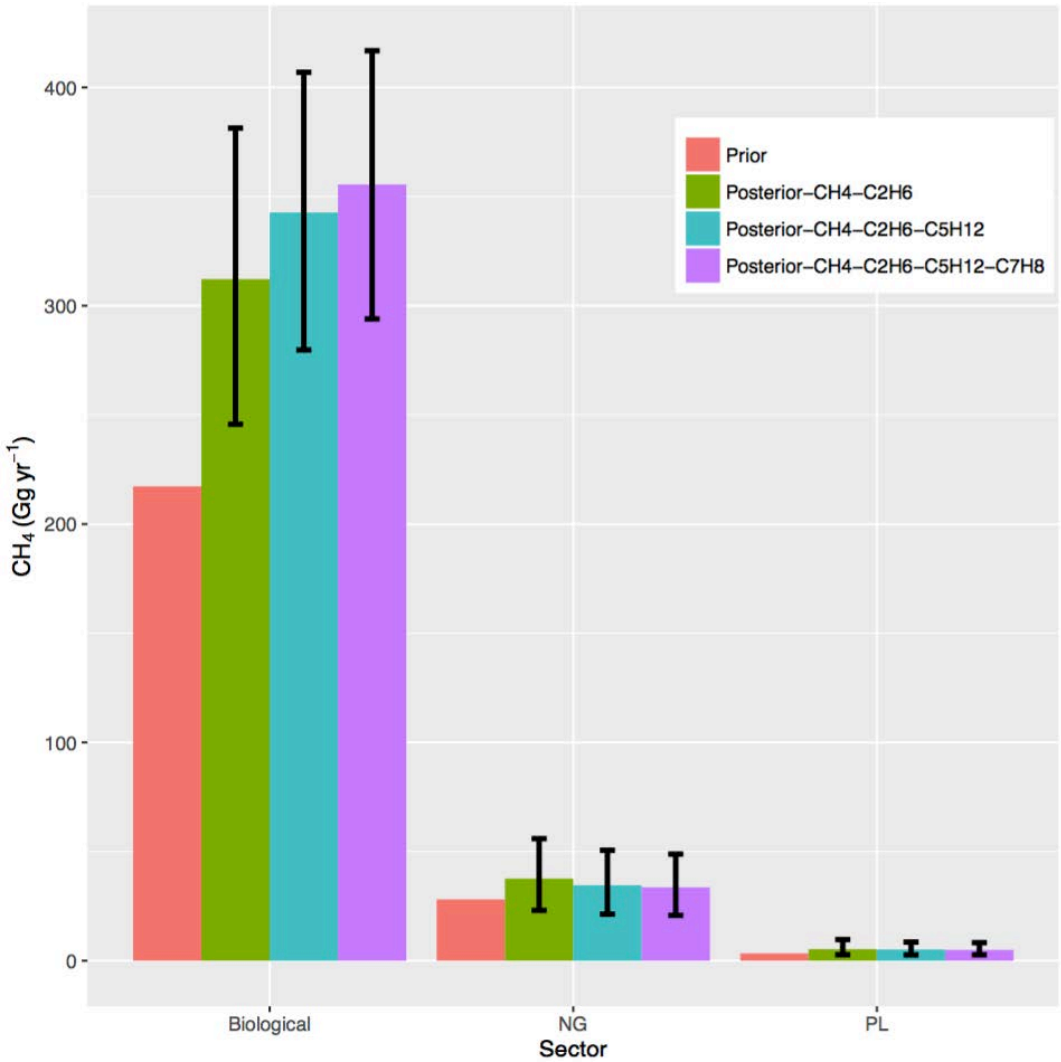

Inversions based on CH_4, C_2H_6 , i-C_5H_{12}, n-C_5H_{12} and C_7H_8 measurements are compared. The posterior emissions are estimated by solving for the scaling factors specific to the biological sources (livestock, wastewater, landfill, wetland), natural gas and petroleum (refinery and on-road mobile) emissions.

It is estimated total NG emissions for the Sacramento Valley are 21 – 49 Gg CH_4/yr (at 95% confidence), which is consistent with the prior (30 Gg CH_4/yr). Researchers estimate that the posterior petroleum (PL) emission is estimated at 3 – 8 Gg CH_4/yr (at 95% confidence), which is marginally consistent with the prior (3 Gg CH_4). Combining the NG and PL emissions, and the estimated fossil-fuel CH_4 emissions are 10±4% of the posterior total (i.e., median estimate) for this early summer period, which is comparable to the prior ratio (13%). The biological emission fraction relative to the total posterior median emission is 90±16%, much higher than that of the fossil-fuel sources for this early summer period. These estimates are based on measurements during an early summer period and do not represent the full annual sector-specific budget of CH_4 emissions in this region which has complex emission sources. More studies are required to

verify the regional total emissions and to further attribute emissions into different sources for effective mitigation planning.

Natural Gas Emissions

The emissions from the natural gas system in the Sacramento Valley Air Basin are further discussed, comparing this analysis results with recent spatially explicit emissions inventories for the natural gas system. In a recent study, Jeong et al. (2014) produced a spatially explicit emission inventory from the natural gas system and petroleum production across California. Following the approach of Jeong et al. (2014), researchers updated the emission maps for the natural gas system and petroleum production using more recent activity data and emission factors. For this update, researchers applied emission factors from the 2016 US EPA inventory (for 2014; US EPA (2016)) for production, transmission, processing and production. To be consistent with the campaign period, the 2014 oil and gas production activity data was used from California's Department of Conservation's Division of Oil, Gas, and Geothermal Resources[26] for the production sector. For processing the facility information for 2014 from US EIA was used[27]. For the transmission sector, the same activity data was used as those used in Jeong et al. (2014) except for the storage facilities for which researchers used the storage volume from the 2014 DOGGR database. As in Jeong et al. (2014), the distribution emission map was generated apportioning emissions in proportion to the population density.

Jeong et al. (2014) estimates a total of 34 Gg CH_4/yr for the Sacramento Valley from the natural gas sector, which is consistent with the study's posterior emissions (21 – 49 Gg CH_4/yr, median = 34 Gg CH_4) estimated from the HBI analysis. For comparison, the natural gas total emission for the region was estimated using emission factors for 2014 from the 2016 US EPA inventory (EPA, 2016). Note that Jeong et al. (2014) estimated natural gas emissions based on emission factors for 2010 from US EPA's 2012 inventory (EPA, 2012). The natural gas total emission for the region based on the 2016 EPA inventory (i.e., for 2014) is 1.4 times larger than that of Jeong et al. (2014) because the updated inventory revised up the emission factors for the production sector compared to the old 2012 inventory (for target year 2010), from which Jeong et al. (2014) derived emission factors. Figure 24 shows the comparison between the two spatially explicit inventories by subsector. Although both the spatial inventories estimate the natural gas emissions for the region that are consistent with the inverse analysis, the subsector-level emissions are different between the two inventories.

---

[26] DOGGR; http://www.conservation.ca.gov/dog/Pages/Index.aspx, accessed May 2016

[27] http://www.eia.gov/cfapps/ngqs/ngqs.cfm?f_report=RP9&f_sortby=&f_items=&f_year_start=&f_year_end=&f_show_compid=&f_fullscreen=, accessed May 2016

Figure 24: Ratios of 2014 to 2010 CH_4 Emissions for the Natural Gas System in Counties within the Sacramento Valley Air Basin (A) and Natural Gas Emission Comparison between 2010 and 2014 by Subsector (B)

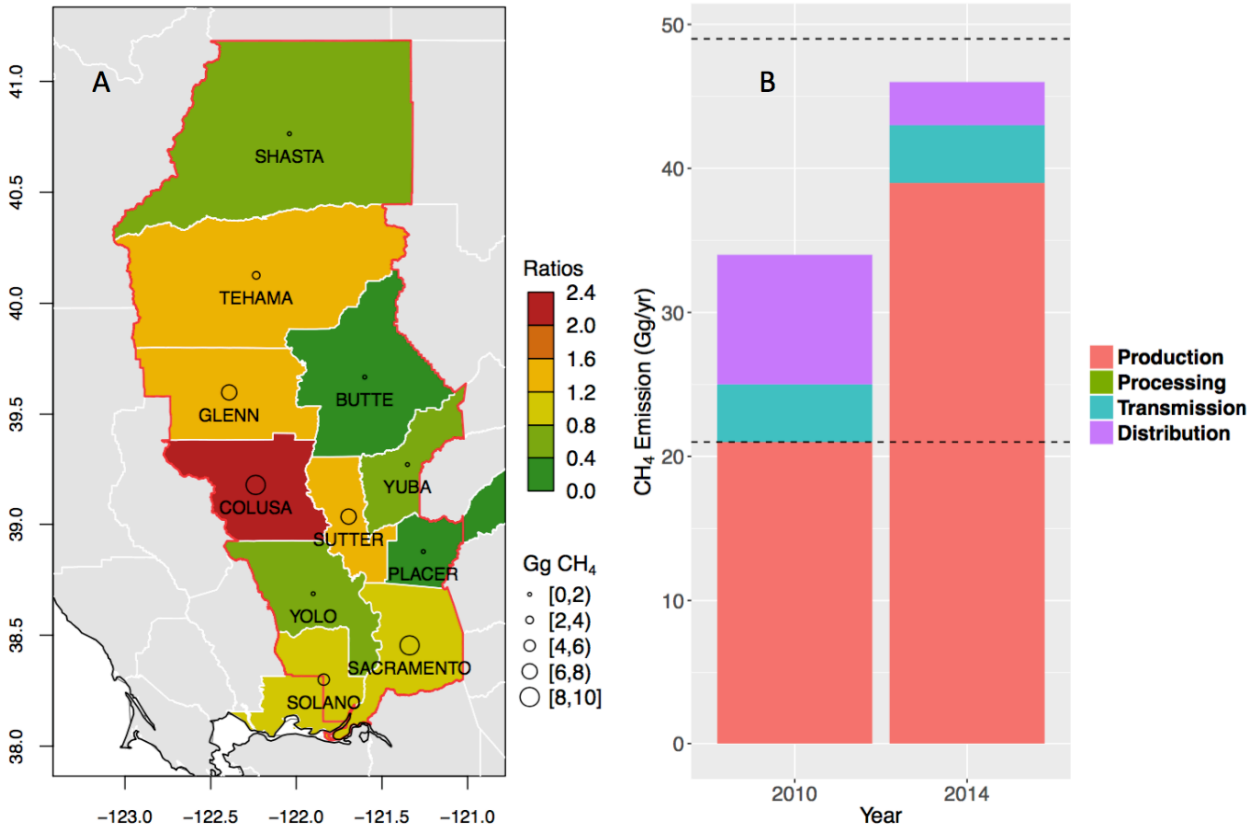

The red polygon in (A) represents the air basin boundary for the Sacramento Valley. The horizontal dashed lines in (B) shows the upper and lower bounds for the posterior emissions (at 95% confidence) estimated in this study. In (B), the 2010 and 2014 emission were estimated based on EPA's 2012 and 2016 inventories, respectively.

For the production sector, the updated inventory estimates a total of 39 Gg CH_4/yr, which is higher than that of Jeong et al. (2014) by a factor of 1.9. This increase in the production emission is reflected in the county-level ratios of the 2014 vs. 2010 (i.e., Jeong et al., 2014) emissions. For example, Colusa County shows an increase in the total emission by a factor of about two compared to the 2010 inventory because this county is one of the largest gas producing counties in California. For the natural gas distribution sector, however, the updated spatial inventory estimates the natural gas distribution emission total is only 3 Gg CH_4/yr for the region, which is only about 30% of the estimate by Jeong et al. (2014). This is because the distribution emission in the 2016 national inventory is also only 30% of that in the 2012 or 2013 inventory.

Although the possible CH_4 emissions from the natural gas system at the subsector level was indirectly examined by comparing the results with two spatial inventories, this study has not completely resolved the subsector-level source apportionment for the natural gas sector in the region. The comparison suggests that although the bottom-up inventories estimate total emissions for the natural gas system in the region that are comparable to the study's top-down

estimate, the subsector-level source emissions are sensitive to the emission factors applied. This further suggests that more studies, likely involving an array of VOC measurements, are required to partition CH_4 emissions into subsector sources. This study has shown the utility of a more sophisticated inverse method to incorporate VOC measurements for which additional information (e.g., VOC background values) is needed. Further development of more robust inverse methods would be useful to fully utilize more atmospheric measurement (e.g., VOCs) and more detailed spatially explicit inventories.

CHAPTER 3:
Facility Scale Natural Gas Production and Processing Emissions

3.1 Overview of Non-Electricity California Natural Gas Facilities

In this part of the study, the team attempts to quantify CH_4 emissions from storage facilities, petroleum refineries (which use NG for chemical processing), oil production fields, and power generation facilities located in oil and gas fields. This motivated the use of airborne measurement technology to examine the methane emissions from these large natural gas facilities at daily timescales to examine variability over time. Measurement methods and results are described from a series of airborne campaigns that quantify CH_4 emissions from individual facilities in California using a closed loop flight pattern and estimating a source rate using Gauss's Theorem. The benefit of using closed loops is that emissions from outside the loop do not influence the estimation of emissions from within the loop to first order allowing sufficiently isolated sources (e.g., well pads, gas storage facilities, and refineries) to be accurately quantified without being strongly conflated with neighboring sources. By targeting individual sites, a better estimation of the total contribution of CH_4 to the total GHG budget can be established and, even more importantly, leaks can be identified and remediated.

3.2 Measurement Sites and Method

3.2.1 Measurements Sites

Twenty-four facilities were measured during this airborne study on 34 individual days spanning during two years from June 2014 to September 2016 (Table 13). Eight storage facilities, three refineries, and seven compressor stations were measured for methane, and ethane (after September 2014). Ethane measurements provide not only an unambiguous marker of fossil fuel sources, but further establish a quantitative measure of the ratio of ethane to methane that can be compared with pipeline gas supplied by utilities for regional source apportionment. McDonald storage, Rodeo refinery, and Kirby storage which were measured (11, seven, and seven times respectively), have enough data sets that the team can begin to estimate variations over time. These facilities use (storage facilities may use gas to power compressor engines) and emit natural gas during their operation, making them of key interest when attempting to quantify GHG emissions from California's natural gas infrastructure. The facilities were sampled on randomly chosen days (during favorable meteorological conditions), without communication with facility operators. As such, the research team is not aware of site status or operations conditions at the time of sampling. In addition, researchers measured the Elk Hills power plant and the Belridge South petroleum production field in the Southern San Joaquin valley. Although Belridge South was sampled three times, two samples were considered incomplete due to cloud cover limiting the ability to climb (11/3/15) and light and highly variable winds (6/17/14). Belridge South and Elk Hills power station had only one reported sampling which prevented any assessment of variability in emissions for those sites.

Table 13: Location and Facility Type Targeted during the Field Campaign

Site Name	Facility Type	Latitude	Longitude	Number of Visits
Gill Ranch	Storage	36.7914	-120.2529	3
Honor Rancho	Production Field & Storage	34.4561	-118.5942	1
Kirby	Storage	38.1607	-121.9166	7
La Goleta	Storage	34.4209	-119.8321	1
Los Medanos	Power Plant & Storage	38.0286	-122.0071	3
McDonald	Storage	37.9900	-121.4772	11
Princeton	Storage	39.3842	-122.0307	1
Pleasant Creek	Storage	38.5499	-122.0020	4
Wild Goose	Storage	39.3238	-121.8833	4
Benicia	Refinery	38.0674	-122.1357	7
Martinez	Refinery	38.0267	-122.0654	3
Rodeo	Refinery	38.0447	-122.2512	5
Belridge	Production & Power	35.4681	-119.7275	1
Blythe	Compressor/Processing Station	33.6055	-114.6419	1
Burney	Compressor/Processing Station	40.8966	-121.6361	1
Elk Hills Power	Gas Processing & Power	35.2778	-119.4755	2
Hanford	Compressor/Processing Station	36.0717	-120.0908	1
Mettler	Compressor/Processing Station	35.0611	-119.0283	1
Moreno	Compressor/Processing Station	33.9094	-117.1200	1
Needles	Compressor/Processing Station	34.6966	-114.6101	1
Newberry	Compressor/Processing Station	34.7803	-116.5962	1
Panoche Energy	Power Plant	36.6507	-120.5805	1
Wild Goose	Compressor/Processing Station	39.9499	-121.8575	1

3.2.2 Aircraft Instrumentation

The aircraft and instrumentation used for this study is a Mooney TLS M20 high performance single engine aircraft modified for air sampling. The primary instruments used for this campaign were the Picarro methane and carbon dioxide cavity ring down spectrometer and an Aerodyne ethane gas analyzer. The Picarro samples the air every 0.55 seconds and has a lag time of nine to 12 seconds, where the Aerodyne samples the air every 0.81 seconds and has a lag time of five to nine seconds. The lag time depends primarily on the size of the inlet lines and the sampling flow rate of the air. This was verified routinely by performing "breathe tests," where a person would abruptly blow into the inlet and the delay in instrument response would be timed. The tubes were modified once during the campaign which altered the lag time and was considered when making estimates. Data from the gas analyzers were interpolated onto a GPS

time stamp for analysis. Wind speed in the meridional and zonal directions were also computed by taking the difference between the GPS speed of the aircraft which measures the speed over ground, and the true airspeed of the aircraft (Conley et al., 2014).

3.2.3 Airborne Estimation of Facility-scale Emissions.

To quantify facility emissions a cylindrical flight pattern was employed to measure gas concentration gradients and wind velocities and then calculated facility emissions as the divergence of mass flux within the flight cylinder using Gauss's Theorem as described by Conley et al. (2017). Using this mass balance (or conservative scalar budget) approach, the emissions from a site, E, is expressed as:

$$E = \int_{z_{min}}^{z_{max}} \oint c' \boldsymbol{u_h} \cdot \hat{\boldsymbol{n}} dl\, dz \tag{3.1}$$

where the outer integral represents the height of the cylindrical flight pattern which extends from the lowest safe altitude, z_{min}, to the maximum flight altitude, z_{max}, where there is no indication of a plume crossing. Due to Federal Air Administration regulations, the minimum safe altitude the aircraft can be flown is 500 feet above ground level (AGL) or approximately 150 m. As of October 2015, special permission was granted to Scientific Aviation, Inc. by the FAA to fly as low as 200 feet (60 m) AGL over unpopulated areas. This lower limit allows a greater altitude range of measurements which improves accuracy and reduces error. The integrand in Equation 3.1 is the path integral representing the dot product of the horizontal advective flux, $c'\boldsymbol{u_h}$, and the vector normal of the flight path, $\hat{\boldsymbol{n}}$. Here c' represents the fluctuating methane or ethane density multiplied by $\boldsymbol{u_h}$, the horizontal wind vector. Details of the method are explicated in [Conley et al., 2017]. The benefit of using closed loops as opposed to traditional horizontal transects is that emissions can be assumed to be coming from a confined regional source, therefore individual wells, refineries, and storage facilities can be accurately quantified in a manner that minimizes confusion with other surrounding sources.

When calculating emissions, a flux divergence profile is generated from altitude binned averages of each flight loop around the source, and the total emission rate is calculated as the integral under this curve (Equation 1). To average each loop's flux divergence over natural turbulent variability, the measurements are first averaged in altitude bins of approximately 100 m depth. The orange diamonds shown in Figure 25 represent each loop flown and the blue circles represent a binned average that consists of loops in a specified altitude segment. The bottom altitude bin is then extrapolated to the ground with a vertical line, which is shown to be accurate by Conley et al. (2017) in a certain range of distances downwind of the source.

Figure 25: Flux Divergence Profiles

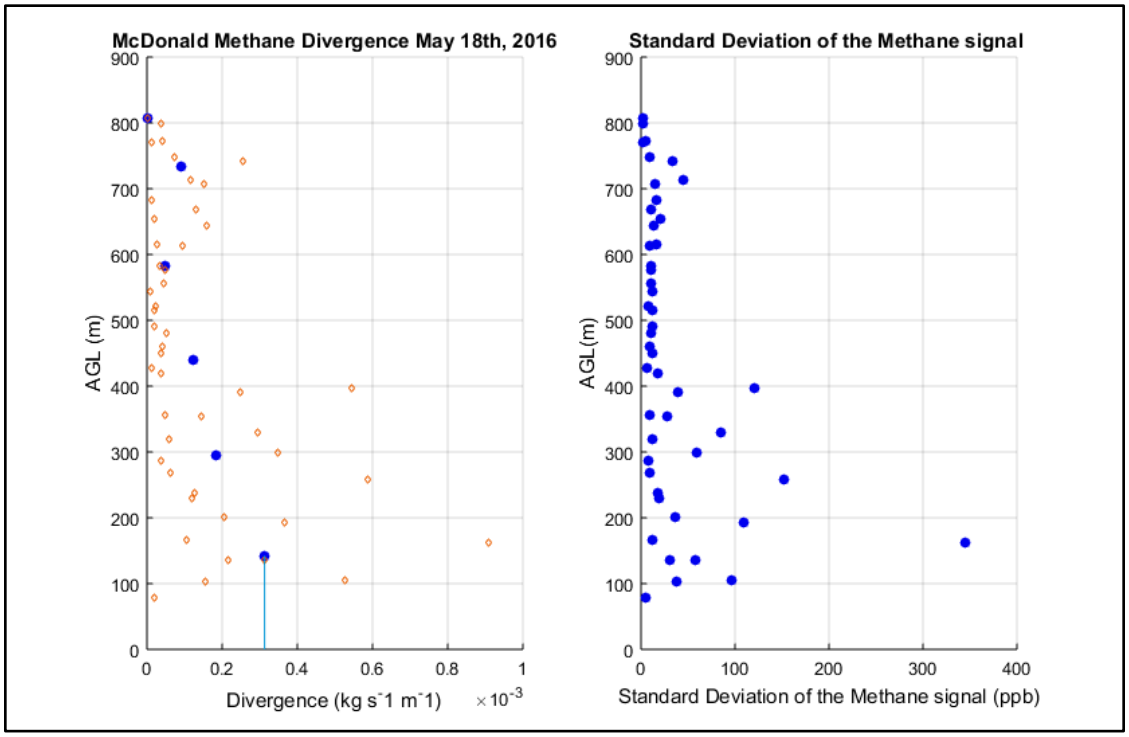

Each loop's flight data (orange diamonds) to estimate the total emission strength and its associated error. Solid blue circles are the binned averages, and the light blue line extending down from the lowest point is the extrapolated flux divergence representing the "ground contribution term", which is assumed based on LES simulations. (right) The standard deviation measured on each loop around the source. The data is from the McDonald Storage Facility May 18, 2016.

3.2.4 Error Analysis

To verify the accuracy of the cylindrical mass balance method, controlled releases of known source strength were sampled on several occasions and the analysis is reported by Conley et. al. (2017). From those tests accuracies of the measurements are thought to be 15% or better with an average error of 6%. The controlled release experiments were generally sampled under optimal conditions, and took place over the course of the field results discussed here while continual improvements were being made to the sampling technique. The average error representative of the estimates reported in this study are likely greater than the results of the controlled releases and reported in Conley et al. (2017). In this paper, the uncertainty under less ideal flight conditions is estimated, including contributions from four main sources. A "quality factor" is defined that considers factors that are inherently unique to each sampling such as the number of loops, the proximity to the source, and the wind conditions during sampling. Next to estimate the total uncertainty the binning error term (BE) was added, in quadrature, which is present even with "ideal" sampling. This term is due to varying the number of bins, which represents the average divergence for a subset of loops, and is subject to variations due to the nature of turbulence.

The uncertainty is considered from not capturing horizontal efflux below the lowest leg of the aircraft profile. In their detailed explanation of the airborne measurement method, Conley et al. (2017) show theoretical flux divergence profiles from LES simulations that indicate a nearly constant flux divergence below the lowest altitude leg but only when the distance at which the plume is sampled (in terms of advection time, x/U, distance divided by mean horizontal wind speed) is approximately one-half a large eddy turnover time (z_i/w_*), where z_i is the ABL depth and w_* is the convective velocity scale, an estimate of vertical wind vigor in turbulent ABL's dominated by convective forcing based on the surface buoyancy flux.) A non-dimensional distance (X) is derived to normalize the physical distance from the source with the mean wind speed encountered while sampling. This allows a more accurate determination of the fraction of the plume that slipped under the lowest flight leg.

$$X = \frac{xw_*}{Uz_i} \tag{3.2}$$

While the theoretical treatment in Conley et al. (2017) shows variations in the slopes of the near surface flux divergence profiles, no deviations are incorporated from the constant vertical extrapolation based on the sampling distance downwind of the source in these error estimates here because the difference appears to be usually less than ~15%, and the average non-dimension downwind distance of 0.56 +/- 0.36 is close to 0.45, the downwind distance where vertical extrapolation is considered ideal. Nevertheless, the fraction of the plume that has to be inferred below the minimum flight altitude is a function of how close the downwind leg is to the source, and has some bearing on the uncertainty of the emission estimate. This source of error is parameterized by a fraction of the emission rate that is below the lowest leg, scaled by the complement of a normal distribution centered at the optimal non-dimensional distance downwind of the source (X≈0.45), where the vertical extrapolation to the surface is found to be most accurate (Conley et al., 2017). In short, the fraction below can be estimated with a high degree of certainty if the non-dimensional distance is close to 0.45, but this was not explicitly understood throughout the period of this study and the parameterization is a simple attempt to conservatively estimate this sampling shortcoming.

Second, how the error varies is considered with the number of loops flown around each facility. Based on the analysis of flight data around controlled releases and large eddy simulations Conley et al., 2017 show that estimates asymptotically approach actual values and are within 15-20% after approximately 20 sampling flight loops. To capture the general behavior of this sampling limitation a simple logistic curve is used that approximates the diminishing variability of the estimates as the number of loops increases, saturating after 25-30 flight loops, as additional loops do not appear to improve the error estimate significantly. The parameters in the logistic function such as the offset of eight loops and the multiplier of 0.15 were determined 'by eye' from the controlled release data and were chosen to generate a conservative estimate of the error variance associated with this under sampling of the source.

The third source of uncertainty included is due to the lack of consistency of the wind velocity during the observations. A dimensionless wind consistency parameter is defined, WC, as the ratio of the vector mean wind speed to the average wind speed during the flight sampling.

(3.3) $$WC = \frac{\sqrt{(u_i)^2+(v_i)^2}}{\sqrt{u_i^2+v_i^2}}$$

where, u_i and v_i are the instantaneous meridional and zonal winds speeds respectively

This indicates the degree of variability in the wind direction as described by Stewart et. al (2002). Ideal winds are considered to blow consistently from the same direction during the sampling (which would yield a wind consistency value of 1.) It is generally seen that stronger winds yield a higher wind consistency and this, in principle, leads to greater precision in the emission estimates. For most cases the wind consistency parameter was above 0.8 and thus the research team does not expect that this was a dominant source of error in the measurements presented herein.

Taking these three terms together, researchers estimate a generic quality factor for each emission estimate based on the sampling conditions:

(3.4) $$Q = \sqrt{\frac{1}{3}((1-FB)*(e^{-|x-0.45|}))^2 + \frac{1}{3}\left(\frac{1}{1+e^{(-0.15*(LN-8))}}\right)^2 + \frac{1}{3}WC^2}$$

where,

Q = Quality Factor

WC = Wind consistency

FB = Fraction Below (fraction of estimate measured when extrapolating to the surface)

X = mean non-dimensional distance from the source

LN = complete loops flown around the site

Beyond the sampling characteristics, there is an inherent variability in the method that arises from the arbitrary number of altitude bins into which loops are averaged before evaluating the flux integral of Equation 1. Emission estimates vary 11% on average, depending on the exact number of altitude bins, and this variability is included the error estimates. This was determined by taking the standard deviation of the emission estimates when varying the number of altitude bins from two to the number of loops flown for all of the data gathered for each facility during this campaign. The BE is then averaged to derive the mean emission estimate and the relative standard deviation of this mean is added in quadrature with (1-Q), an approximate measure of the relative error induced by inadequacies of sampling, to determine the overall relative error estimate.

(3.5) $$TC = \left(\sqrt{\frac{1}{2}(BE)^2 + \frac{1}{2}(1-Q)^2}\right) \times |E|$$

where,

TC = total uncertainty

E = emission estimate

3.3 Aircraft Mass Balance Emission Estimates

Emission estimates for all of the facility observations are reported in Appendix M and reported by facility types in the next sections. In general, these spot measurements obtained methane emissions that varied between facilities and over time at individual facilities. For some facilities, the spot measurements were similar to bottom-up or industry reporting, while at others emitted more during the observation periods than the average annual rates reported in the US EPA Greenhouse Gas Reporting Program (US-EPA GHGRP, 2017) and the California Air Resources Board (2017) industry reporting.

3.3.1 Storage Facilities.

Overall the results indicated a great amount of variability in emissions relative to documented estimates. Unfortunately, agencies estimates were only available for half of the facilities and coverage from ARB and the US EPA inventories was limited to three facilities (Table 14). Geographically isolated, McDonald Island was visited 11 times, the largest storage facility of the campaign (82 Bcf working capacity), McDonald Island displayed irregular statically significant variance in emissions. On May 12, 2015 McDonald was emitting 22 +/- 10 kg/hr then a few hours later it was measured at 93 +/- 24 kg/hr, the next day the team measured 187 +/- 34 kg/hr. Despite the high levels of variance observed across all the samples, the average was 223 +/- 36 kg/hr, 2.6 times higher than ARB inventories. Kirby, which was visited seven times, had an emission range from essentially 0 kg/hr to 150 kg/hr with an average of 55 +/- 16 kg/hr which is nine times higher than what is in the ARB inventories. Honor Rancho which was sampled twice measured at 835 +/- 152 kg/hour and -20 +/- 26 kg/hr in June and September, 2016 respectively. Wild Goose was sampled four times and on one occasion was not emitting any detectable CH_4 (< ~5 kg/hr), though one of the observations was made of the compressor station which was physically separated from the storage field and observed to emit 160 kg/hr on that day. Due to highly variable temporal changes in emissions for storage facilities, numerous samples such as from the McDonald Island facility are required for all the facilities to better understand the role of temporal variability in the overall annual emissions. Statistical analysis as well as an in-depth look at the temporal variability for McDonald will be discussed in the following section.

Table 14: Storage Facility Characteristics, Measured and Reported Emissions (kg CH_4/hr)

Facility Name	Start Year	Working Storage (Bcf)	Min	Max	Avg (Std. Dev)	US-EPA	CARB
Gill Ranch	2010	20	5	59	33 (27)	NA	NA
Honor Rancho	1975	24	-21	835	407 (605)	75	76
Kirby	1975	15	-10	150	55 (54)	NA	6
La Goleta	1941	22	NA	NA	215	NA	242
Lodi	2001	9	NA	NA	-90	NA	1
Los Medanos	1979	18	24	38	33 (7)	2	3
McDonald	1976	82	22	461	223 (127)	NA	86

Facility Name	Start Year	Working Storage (Bcf)	Min	Max	Avg (Std. Dev)	US-EPA	CARB
Pleasant Creek	1979	2	8	24	16 (9)	NA	NA
Princeton	2010	11	NA	NA	43	NA	NA
Wild Goose*	1997	75	-3	105	35 (61)	31	88

* Excludes measurement of compressor near Wild Goose storage field

3.3.2 Refineries.

The greatest discrepancies were found for the three refineries that were sampled a total of 15 times (Table 15). For example, average methane emissions in excess of 300 kg CH_4 hr^{-1} where detected from Rodeo refinery during the four samplings as compared with the EPA's GHGRP value of 16. The three refineries emitted, on average, 14 times as much methane verses what was report to the US EPA. Rodeo, which reports a CH_4 emission rate of 16 kg/hr, was visited five times and had an average estimated emission of 306 +/-102 kg/hr, this ranged from 22 to 527 kg/hr (Figure 26). Benicia which reports 42 and 119 kg/hr to US EPA and ARB respectively, had an average measured emission rate of 382 kg/hr with a range of 220 to 700 kg/hr during the seven visits. Martinez refinery, sampled thrice, emitted more than four times its reported value of 64 kg/hr. The three samples gave approximately the same source strength of ~260 kg/hr, however this is not necessarily conclusive that the emissions are constant due to a limited number of visits. Unlike storage facilities, the refineries were consistently measured to emit significantly more than the annual average emission rate reported to the US EPA and ARB.

Table 15: Measured and Reported Emissions from Refineries (kg CH_4/hr)

Facility Name	Min	Max	Average (Std. Dev)	US-EPA	CARB
Benicia	220	700	382 (185)	42	119
Martinez	239	283	260 (22)	190	102
Rodeo	23	527	306 (206)	16	15

Figure 26: Observed CH_4 Mixing Ratios for Loops Surrounding Rodeo Refinery (May 23, 2016)

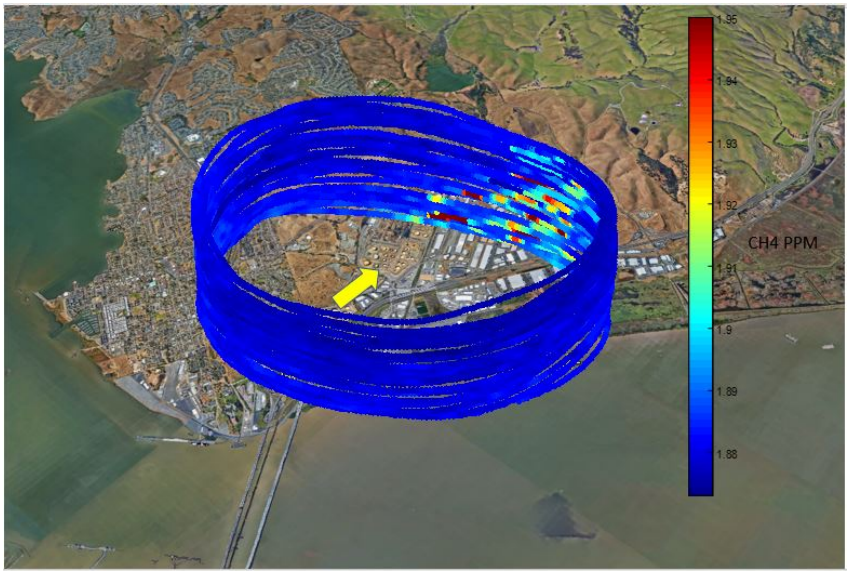

Downwind CH_4 of the flight pattern show clear enhancements relative to the upwind. The mean wind direction is shown by the yellow arrow.

3.3.3 Power Plants, Production Fields, and Processing/Compressor Stations.

Belridge South, a production and processing field, was sampled just once, and Elk hills was sampled twice. When sampling Belridge, 15 minutes was required to loop the entire facility once - at least a two-hour flight to get a reasonably accurate estimate. Since the field is large and the multiple emission sources are simplified as a single source, a large radius loop is flown. This means the sources were likely sampled at a large, less than ideal downwind distance. Despite these caveats of measuring emissions from a large production field, a final CH_4 estimate of 1,953 kg/hr was obtained, considerably higher than reporting to US EPA and ARB, but roughly consistent with a bottom-up estimate of production and processing emissions[Jeong et al., 2014].

Table 16: Measured and Reported Emissions from Production, Compressor and Power Stations (kg CH_4/hr)

Facility Name	Facility Type	Min	Max	Avg (Std. Dev)	US EPA (2015)	CARB (2014)
Belridge South	Production Field	63	1953	827 (996)	8.1	379
Blythe	Compressor	NA	NA	234.9	80.8	49
Burney	Compressor	NA	NA	73	7.9	7
Elk Hills	Gas Processing & Power Plant	334	533	433 (141)	21.6	231

Facility Name	Facility Type	Min	Max	Avg (Std. Dev)	US EPA (2015)	CARB (2014)
Hanford	Compressor	NA	NA	3	0.0	0
Mettler	Compressor	NA	NA	93	18.2	15
Moreno	Compressor	NA	NA	43	13.5	16
Needles	Compressor	NA	NA	12	60.7	30
Newberry	Compressor	NA	NA	72	0.0	0
Panoche	Power Plant	NA	NA	158	1.3	1
Wild Goose	Compressor	NA	NA	167	0.0	121

Source: USEPA 2015 inventory, CARB 2014 inventory.

Because the majority of natural gas used in California is transported from out of state, during the summer of 2016, seven compressor stations were sampled along the main transmission lines to survey the import infrastructure. Methane emission varied greatly from no emissions at the Hanford compressor to more than 230 kg/hr measured at the Blythe compressor station. In total the seven compressor stations emitted four times more than inventories reported.

Section 3.3.4 Analysis of Variability.

The significance of observed temporal variability was examined for the four facilities which were measured five or more times (Table 17). Under the assumption that the observations were normally distributed and the average of estimated uncertainties captures the measurement related variation in the observations, the F statistics were evaluated as the ratio of observed variance in emissions to the average of the estimated uncertainties. The corresponding probabilities, p were computed that one would exceed the observed values of F, given the number of samples collected for N-1 degrees of freedom. As shown in Table 18, the F-statistics and p-values of exceeding F is significant at the $p < 0.05$ for two (McDonald and Kirby).

Table 17: F-Test Results for Facilities Sampled More Than Once

Facility Name	# Samples	Facility Type	Average Estimate (kg/hr)	Variance $(kg/hr)^2$	Average Uncertainty squared $(kg/hr)^2$	Average F ratio (-)	prob (-)
Benicia	7	Refinery	382	34328	9435	3.64	0.07
Kirby	7	Storage	55.4	2916	666	4.38	0.05**
McDonald	11	Storage	223	20787	2159	9.63	0.00***
Rodeo	5	Refinery	306	47193	11244	4.20	0.10

Based on the F-test results it was clear that Kirby and McDonald had highly variable emissions well outside any uncertainties that were computed from the error estimation method. McDonald Island was sampled 11 times and was observed to have the largest and most variable emissions observed during this two-year campaign. The range of emissions varied from 21 kg/hour to 461 kg/hour with an average of 223 +/- 137 kg/hour. The cause of such a high variance is uncertain at the time, but is likely due to intentional venting during maintenance operations reported for the site (PG&E private communication).

Section 3.3.5 Discussion

This work quantifies methane emissions from a sampling of California natural gas facilities. A total of 23 unique sites were sampled, with 10 being storage facilities, three being refineries, seven compressor stations, two oil production field and the combination of a power plant and nearby compressor and processing facilities.

Three petroleum refineries were found to be the largest methane emitters, with emissions up about an order of magnitude larger than that reported to the EPA or ARB. These observations are similar to those reported previously, suggesting the need for additional measurements (Lavoie et al., 2015).

The storage facilities measured during this study emitted less than the refineries, and only differed by a factor of 1.7 from ARB bottom reporting. One exception was the McDonald Island storage facility that exhibited large and variable emissions, likely associated with maintenance operations at the site.

Emissions measured at seven compressor stations were in the same general range as storage facilities. While compressor emissions were not separated from subsurface leakage, this raises the likelihood that a significant fraction of methane emitted from storage facilities may be associated with above compression activities. As mentioned, the compressor station servicing the Wild Goose subsurface storage facility appeared to be physically separated from gas storage

field. On the day it was measured, the compressor station emitted about 160 kg CH_4/ hr, considerably more than observed during three measurements centered on the Wild Goose storage field, and roughly consistent with the annual average reporting to ARB.

While compressor stations are expected to emit variable amounts of methane depending on the equipment type maintenance operations, this suggests a value in coordinating some fraction of measurements with site operators. Since compressor stations are used to maintain pressure in transmission pipelines may be a significant source of natural gas related methane. The compressors at Wild Goose and likely other facilities in California are likely powered at least in part by natural gas fired reciprocating internal combustion engine compressors (California Public Utilities Commission, 2010). Previous measurement of five compressors at five facilities in Texas showed methane emissions ranged from about 8 to 25 kg CH_4/hr (Johnson et al., 2015). However, even about 25 kg CH_4/hr is less than the median of about 90 kg CH_4/hr observed at eight facilities, consistent with the reporting estimates for total facility emissions that likely include other component-level methane emissions (e.g., vent valves, etc.).

To improve annual average emission estimates and capture variations due to either accidental releases or operational activities, additional measurements of California natural gas facilities are clearly necessary. As part of this sampling, it will be important to sample facilities during different times of the year, and perhaps during both week days and weekends and/or at different hours of day to identify the importance of seasonal, weekly, and diurnal variations.

CHAPTER 4: Mobile Measurements of Distribution and Small Facility System Leakage

4.1 Introduction to Mobile Plume Measurements

With a few exceptions, methane emissions from natural gas distribution and end use in urban residential and commercial areas of California have not been separately quantified from biogenic sources and remain substantially uncertain. As an initial survey of methane emissions from natural gas infrastructure in California, conducted ground based mobile measurements of methane emissions were conducted and the initial results of ground based mobile plume integration surveys are described.

4.2 Methods for Plume Integration Measurements

The Lawrence Berkeley National Laboratory (LBNL) Mobile Plume Integrator (MPI) facility was developed to provide continuous roadway measurement of the vertical distribution of CH_4 plumes and associated meteorological variables. These measurements were necessary to integrate the wind-borne advective flux of CH_4 across the path of motion to estimate total emissions within multiple plumes over large travel distances. The MPI draws air streams from 12 inlets on the mast. The 12 inlets are evenly spaced across the 4m mast and aggregated into three streams taking air from inlets at 0.25-1.5 m, 1.5-2.75 m, and 2.75-4 m above the road. The three air streams are continuously measured by the three gas analyzers (Picarro G2301 or similar), with flow rates adjusted to provide approximately 0.5 Hz time response. In addition, the vehicles location, speed and heading data are measured with a GPS (Garmin 18x), while wind velocity is measured with a sonic anemometer (RM Young 81000). All data are synchronized and recorded at 1 Hz on a data logger (Campbell CR1000). For some earlier MPI tests, the air system was configured with different inlets. Bakersfield tests were conducted with three distinct inlets on the mast and Sacramento tests were conducted with three lengths of perforated tubing to draw air in from the same three regions as the 12-inlet setup.

Background levels were estimated based on a smoothed time series of methane mixing ratios with peaks removed. The peaks were then selected from the time series of mixing ratios and filtered for peaks above a threshold for methane enhancement above background within 1.5 minutes. Any plume wider than 1.5 minutes was deemed impossible to calculate due to uncertain background levels and based on diffusion plume dispersion, probable distant source. A threshold of 0.1ppm was selected to be above the noise in the background mixing ratios and give real plumes. Emission for an individual plume, Q, is calculated as sum of area integral of flux elements calculated as the product of the normal component of the wind with respect to the motion of the vehicle and the concentration enhancements above background at each height along the height of the mast,

$$Q = \int v * (C_i - C_b)\, \delta L * \delta z\,, \qquad (4.1)$$

where v (m s^{-1}) is the normal component of the wind velocity, C_i and C_b (kg m^{-3}) are mass densities of CH_4 in the plume and background respectively, the integral is computed over the horizontal δl and vertical δz extent of the plume.

Tests of the MPI system were conducted in a wide, open paved area with known releases of CH4 in Argon and Air to determine measurement error of the system. The team drove past the leak with the MPI at a distance of 10-30m. The tests showed that individual runs vary by up to 40%. With repeated passes, the measurement error was greatly reduced. Estimates for 17 passes where the plume was well captured by the 4m height resulted in an average estimate of 102 +/- 11% of the actual release. MPI surveys in the field include some plumes with multiple passes and some where only a single measurement was taken. For single pass measurements, a measurement error of 40% is used. For those sources with multiple measurements, variation in measurements is used as an estimate of measurement error.A schamtic diagram of the MPI is shown in figure 26, and figure 27 shows an example of measurement from MPI.

Figure 26:: Diagram of MPI System from Above Showing CH_4 Source and Plume (top) and from Side Showing Possible Measurements Taken from Three Levels by Driving through Plume (bottom)

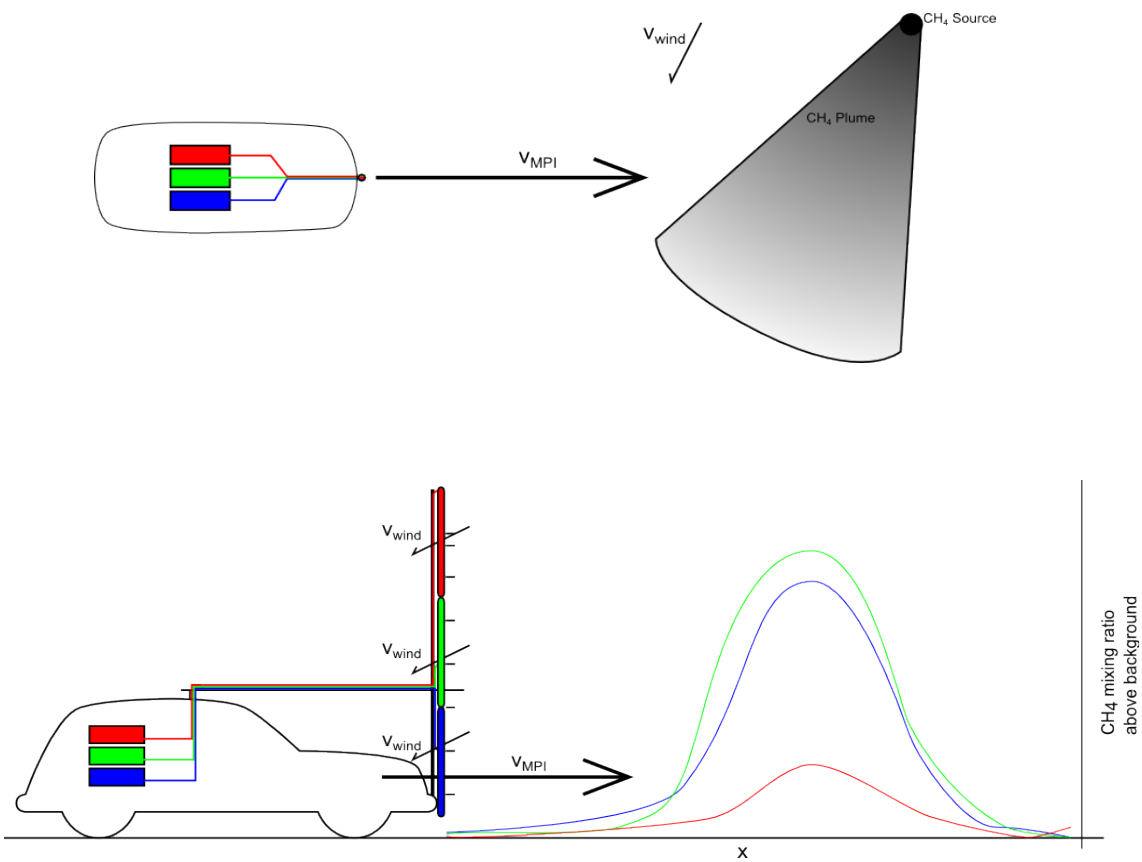

Figure 27: Example Cross Section Views of Measured Plumes by Mixing Ratio above Background

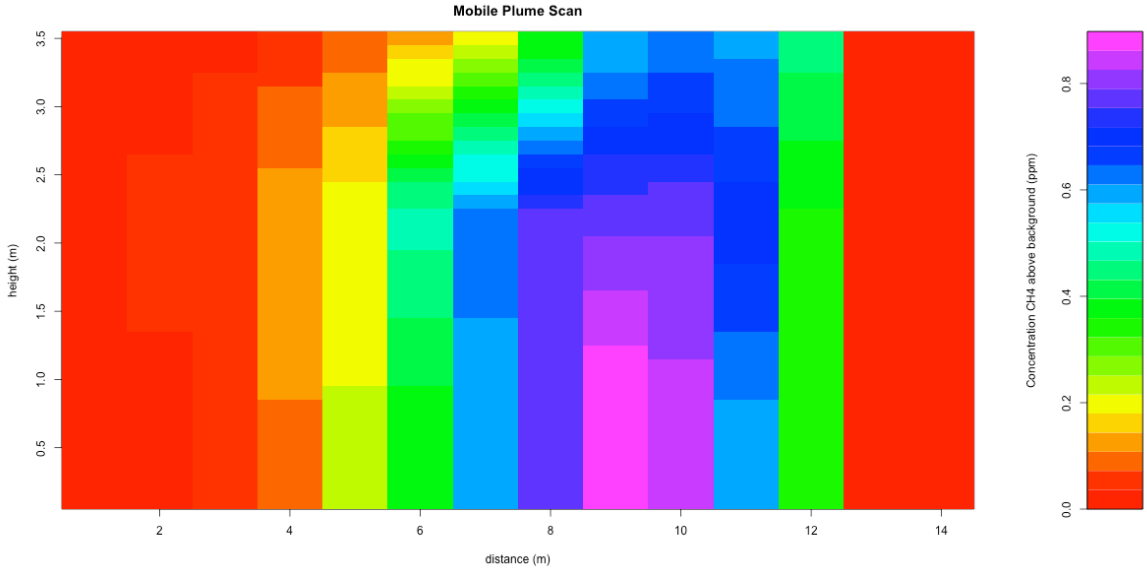

Top plume considered well captured in 4-m mast, bottom plume goes over mast.

4.3 Mobile Plume Integration Results and Disussion

4.3.1 Bakersfield Production, Distribution, and Consumption Leakage

Selecting plumes at >0.3ppm enhancement yielded 17 plumes. Emissions from these plumes totaled 7.04 +/- 2.82 L/min. Assuming the observed leak rate per unit distance applies to all 670 miles of paved roads in the Bakersfield metropolitan area, the total emissions from the area would be approximately 102.7 +/- 35.9 kg/hr of methane to the atmosphere (Figure 28).

Estimates of background levels include a bias that leads to an underestimation of emissions of up to 5%. In addition, for at least four of the 17 measured plumes, the plumes were not fully captured by the plume detection because of a much higher vertical extent than the 4.2-m mast, resulting in underestimation of those plumes.

Figure 28: Histogram of Plumes Observed in Bakersfield Area

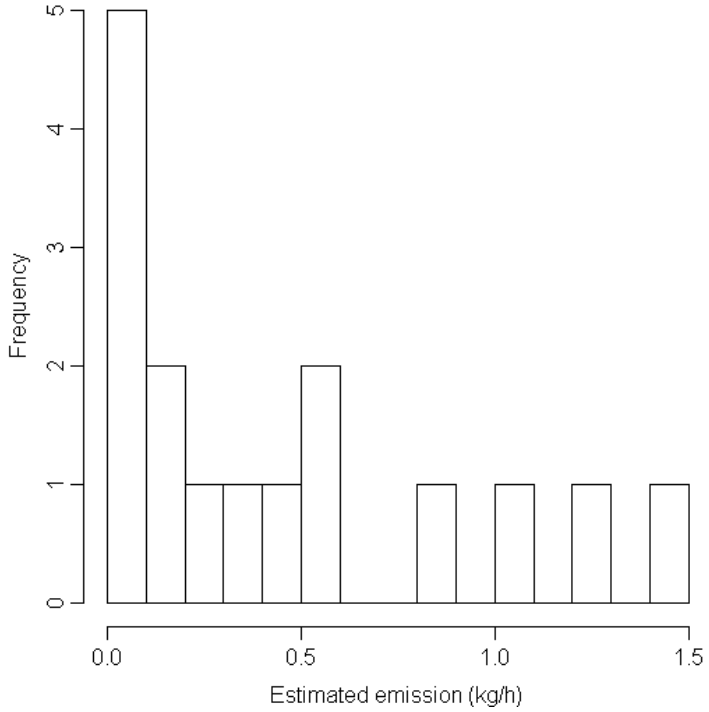

4.3.2 Sacramento Distribution and Consumption Leakage

In the Sacramento area, measurements were taken of integrated methane leakage from roadway plumes obtained from about 2.8 km^2 near non-highway roads from 5 AM to 9:30 AM local time on June 3, 4, and 6, 2014 shown in Figure 29. After selecting plumes registering as > 0.1 ppm enhancements the detection algorithm found 152 distinct plumes. The mixing ratio enhancement above background is shown for an example plume as a function of vertical and position perpendicular to the mean wind. However, some measured plumes were not fully captured by the research team's plume detection because the observed mixing ratio did not decrease significantly from the 2 m sampling height to the 4 m sampling height, and hence the emissions for those plumes must be considered a lower limit. In addition, some areas of elevated readings above the otherwise steady background levels were not identified as plumes because they were elevated for long enough to temporarily define higher background level.

Figure 29: Map of Mobile Survey Driving Route (Blue) of the Sacramento Area

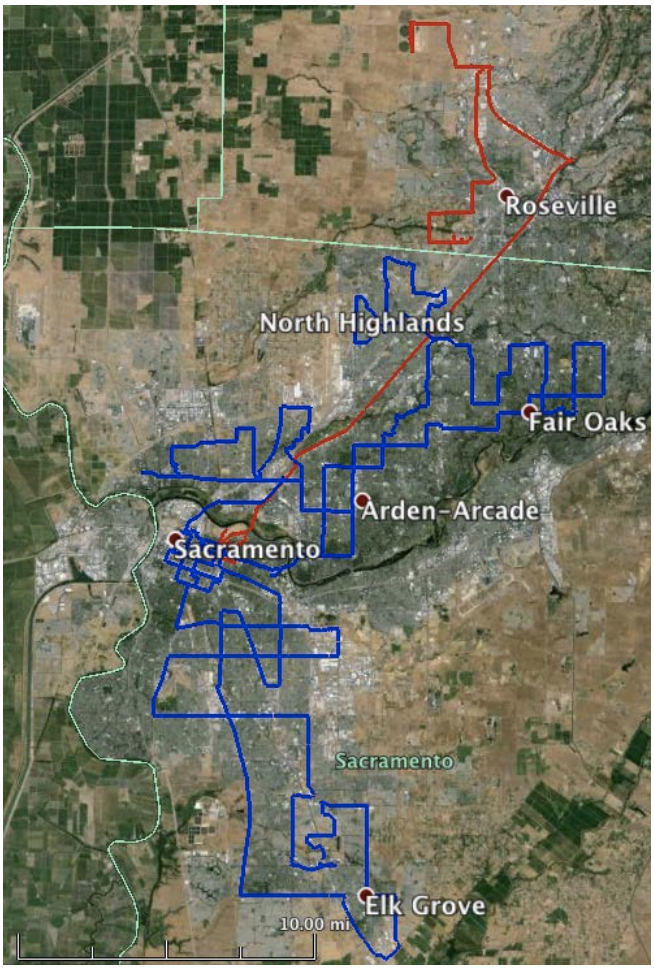

One such "plume" spanned about 3 km on Watt Avenue, with a clear, steady background at the ends of the street. Since this plume was unusually large, the carbon-13 delta values were analyzed to look for evidence of a fossil fuel source (Figure 30). This street was also a few miles downwind of a former landfill, so the carbon-13 delta values for a landfill were also used as a comparison. This analysis suggests that the source was not from a landfill and possibly fossil fuel based. By integrating this large plume, it was found that the source emits methane at about 0.3 kg/h. However it should be noted that the integration was done using an average wind speed for the entire length of the plume although the wind varied throughout. Additionally, the measured mixing ratios were similar at all heights for the entire plume, which suggests that much of the plume was not detected. With those caveats, summing emissions from the detected plumes yields total emissions of 1.86 +/- 0.74 kg/h without the plume on Watt Avenue., and 2.16 kg/h with the plume on Watt Avenue (Figure 31). When scaling to the entire area of the greater Sacramento area, this translates to 222.3 +/- 77.8 kg/h and 297.5 kg/h respectively.

Figure 30: Isotope Ratio Comparisons for Large Plume near Watt Avenue (Sacramento, CA)

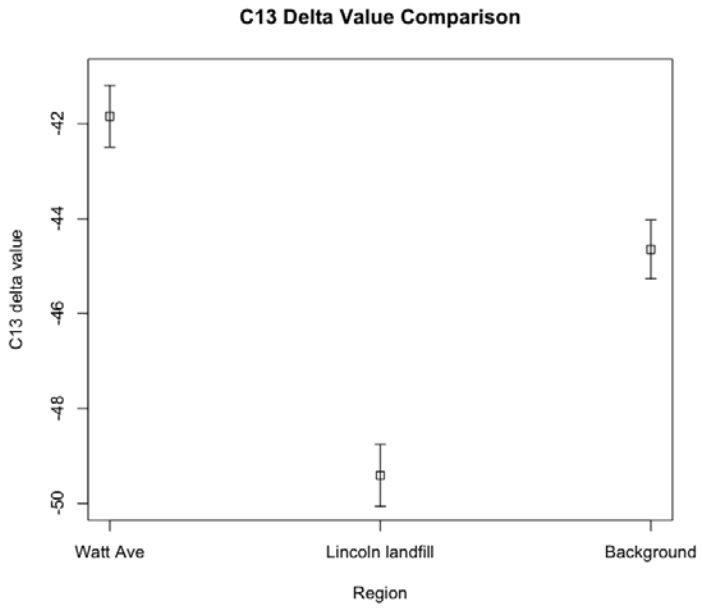

Figure 31: Histogram of Estimated Plume Emissions Measured in the Sacramento Area

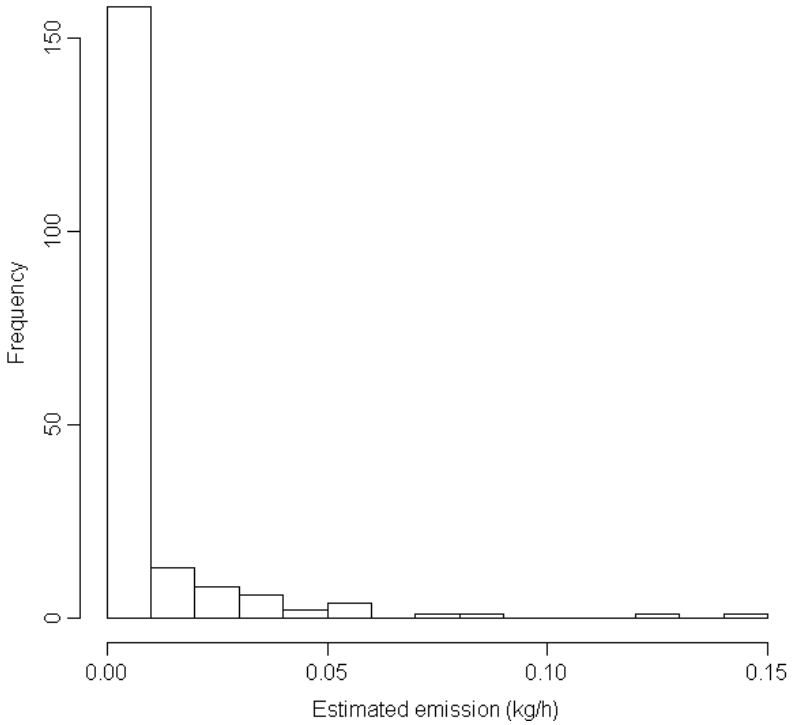

4.3.3 Berkeley and Oakland Distribution and Consumption Leakage

Selecting plumes with a threshold of 0.02 ppm, 141 plumes were measured (Figures 32 and 33). The sum of emissions estimated from these plumes was 0.38 +/- 0.15 kg/h. These measurements do not include leaks from CNG filling stations in the area summarized as those surveys were not part of a representative sampling of roads.

Figure 32: Map of Drives in Oakland and Berkeley, CA with Height Representing Measured CH_4 Concentrations

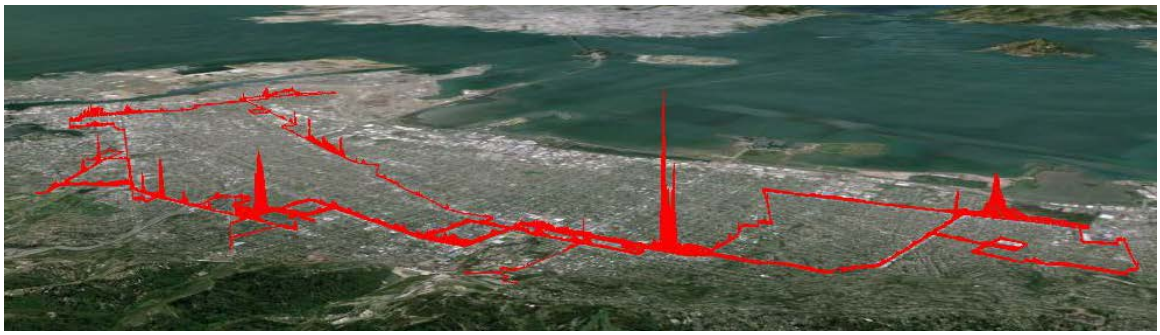

Figure 33: Histogram of Estimated CH_4 Emissions from Drives in Oakland and Berkeley, CA

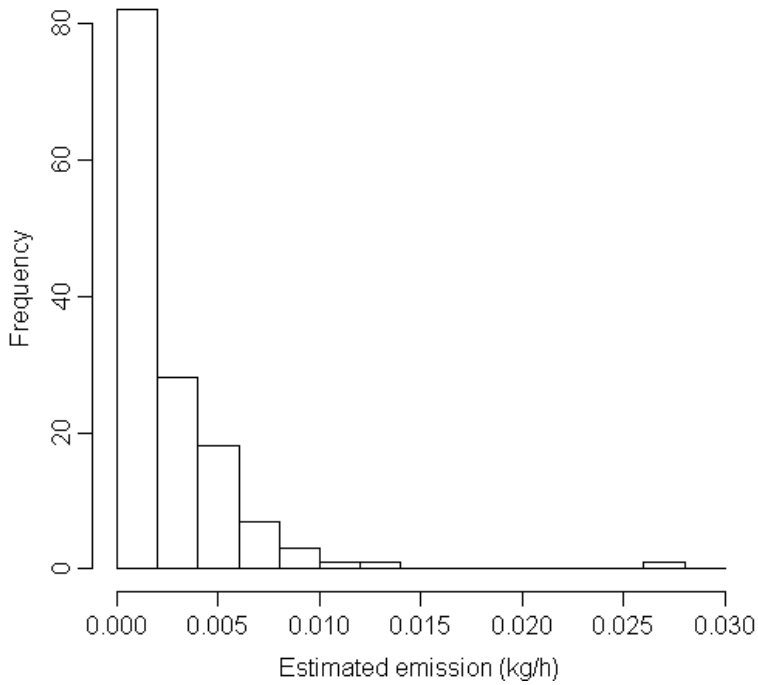

4.3.4 Compressed Natural Gas (CNG) Fueling Stations

As part of the MPI surveys, methane emissions from nine CNG filling stations in the Sacramento and San Francisco Bay Areas were measured. The measurements were made without interacting with facility operators without assessing the level of activity at each station.

Of the 9 CNG facilities, only four showed distinct CH_4 enhancements (peaks) above the local CH_4 background at the time of the observations. Of the four that showed peaks, the team collected data passing through the plume multiple times to estimate the variability of the measurements. An example of driving path for one station is shown in Figure 34.

Figure 34: Driving Path of an Example CNG Filling Station Showing Multiple Passes

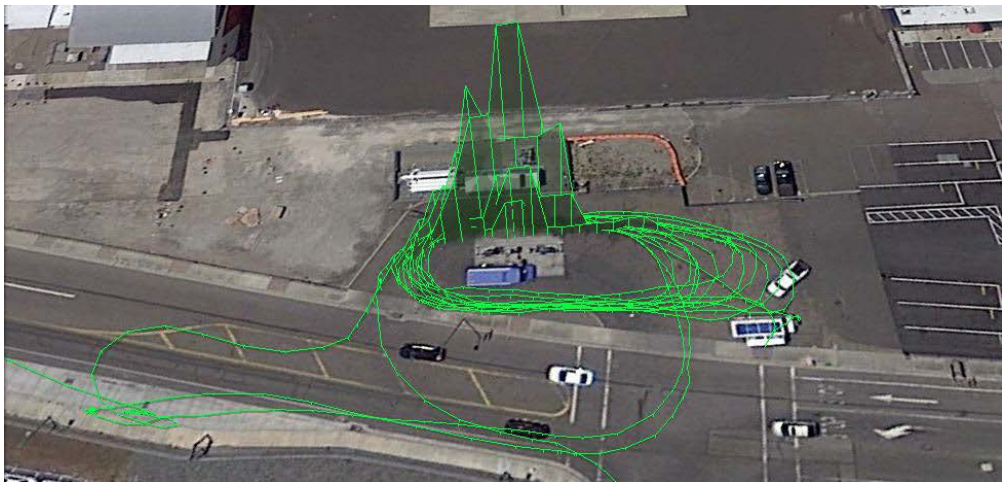

Three of sites with detections were measured on January 13, 2015 in the San Francisco Bay Area. The first site was measured 14 times, with nine of the passes resulting in measurements that had significantly higher values at the two lower levels on the sampling mast. For this subset, the plume integration leak rate was 0.077+/-0.017 kg/h. A second site was measured to have smaller leakage of 0.0086+/-0.004 kg/h during 4 of 6 passes when the plumes were captured by the 4-m mast. The third site measured appeared to be coming from gas pipes near the filling station. Despite being 5-20 meters from any probable source, most of the plumes produced were observed to have concentrations with larger values at the highest sampling level, suggesting the plume was largely blown over the top of the mast. This is likely because a fence and vegetation obstructed the airflow. The integrated estimate is 0.15 +/- 0.03 kg/h from three passes where the car moved at a constant velocity through the plume. Because this data was gathered under conditions where a large but unknown fraction of the plume was not captured by the sampling lines, it must be treated as a lower limit on emission rate. The fourth filling station with clear plume detection was measured on January 23, 2015, with emissions estimated at 0.19+/-0.05 kg/h from 11 passes. This filling station was not readily accessible at the time of observation so measurement were made from a road about 15 m from the station with a high wall between, many of these measurements saw high concentrations on the upper inlets, indicating that this estimate should be treated as a lower limit. Taking the arithmetic mean of the leakage from the nine stations yields ~ 0.05 kg CH_4/hr.

Although these measurements are unlikely to accurately reflect the annual average emissions from California CNG filling stations, an order of magnitude comparison between the observed

leakage and CNG delivered to retail stations. Total CNG consumption and the number of stations in 2012 were obtained from the Energy Commission transportation fuel web page (http://energyalmanac.ca.gov/gasoline/piira_retail_survey.html). The 32 retail CNG stations in California provided 6.6 million gallons gasoline equivalent (gge) of CNG in 2012, or 202,000 gge/station/yr. Assuming 5.7 lb/gge for CNG, and leaks occurring 24 hours each day, this is about 60 kg CNG/hr/station average dispensing rate . Assuming CNG is 100% CH_4 (the error is likely ~ 5%), an average fractional leak rate is estimated at about 0.1%. If leaks only occur during hours when CNG filling occurs (e.g., eight hours) then the estimate would be about three times lower, or around 0.03%. For comparison, these leaks are extremely small compared to the average leakage rate assumed for production and transmission of 1.15% assumed in the CNG vehicle life-cycle assessment (V. Perisnova, private communication).

4.3.5 Abandoned Natural Gas Wells

As part of the MPI surveys, spot measurements of methane emissions were made from 13 abandoned (plugged or buried) dry natural gas in the Rio Vista field area. Attempts to measure six of the 13 wells were successful, though seven others did not have public road access downwind of the wells. Of the six wells measured, two wells did not produce measurable CH_4 enhancements. Of the four wells with clearly measurable CH_4 enhancements, emissions were quantified for one as 5 +/- 1.7 g CH_4 /hr with five passes (Figure 35). Three others were also measured with one pass for each, with resulting emissions ranging from 1.6 to 14 g CH_4 /hr.

Using the measured leak rates, an order-of-magnitude for CH_4 emissions was estimated from the roughly 1,000 abandoned wells in the Rio Vista field as 2 to 20 kg CH_4 / hr. Even in total, this estimate is small compared to that observed for the storage facilties previously described. However, if wells leak with a fat-tailed distribution such that a small fraction of wells leak at a high rate that contributes most of the total emissions as described in Lyon et al. (2015), then this average is likely an underestimate of emissions from the entire population of abandoned wells.

Figure 35: Driving Path of an Example Abandoned Well Showing CH_4 Enhancements for Multiple Passes

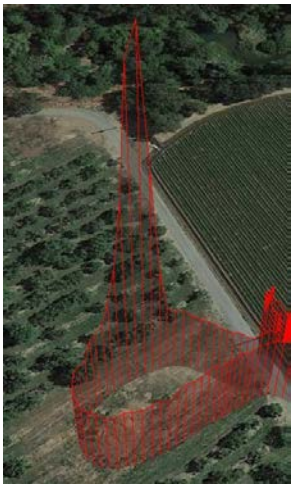

CHAPTER 5:
Residential Building Leakage

5.1 Introduction to Residential Building Leakage

Residential CH_4 usage in the United States totals nearly 150 billion m^3 (~ 5 trillion cubic feet) of natural gas per year. Even if a small percentage of this gas is leaking, residential natural gas leakage could contribute around 10^9 m^3 of CH_4 to the atmosphere. However, due to the large number of other CH_4 sources that need to be measured, there have not been any studies to look at levels of CH_4 leakage in residential applications, the gas lines, fittings and appliances such as those for heating homes, hot water, cooking and clothes drying. For example, tankless or instantaneous water heaters, are a relatively new and growing part of residential natural gas (California Statewide Codes and Standards Team, 2011).

Motivated by these concerns, the California Energy Commission began a series of investigations to quantify methane emissions from different sub-sectors of California's natural gas infrastructure. This chapter discusses the methods to measure methane leakage from single family residences, results from initial measurements of total interior CH_4 leaks during quiescent periods (when combustion appliances are idle) from 10 California single family homes, additional measurements of externally vented CH_4 emissions from gas appliances, and the implications for total residential leakage if these initial results are directly extrapolated to the California residential housing stock.

5.2 Building Measurement Methods

5.2.1 Building Methane Leakage Measurements

Methane emissions from interior leaks and idle appliances were measured by depressurizing the building and measuring the enhancement of indoor CH_4 relative to outdoor "background" air at a measured total exhaust flow rate as (Figure 36).

Figure 36: Diagram of the Total House Methane Leak Measurement Method

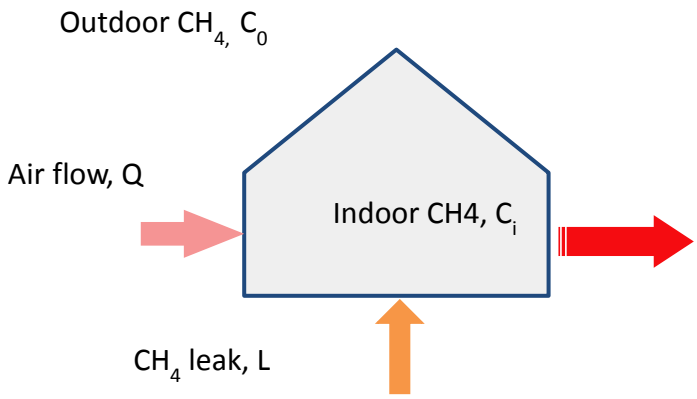

Schematic shows outdoor air with methane concentration Co drawn through a house at flow rate Q, methane added by indoor leak, L, and resulting indoor air methane concentration, Ci.

Considering the building shell as a well-mixed control volume, the time rate of change of CH_4 concentration in the indoor air can be expressed as the difference of inflow minus outflow of CH_4 normalized by the building volume,

$$dC_i/dt = Q/V\,(C_o - C_i) + L/V, \qquad (5.1)$$

where Ci and Co (μg m^{-3}) are the indoor and outdoor concentrations, Q is the total air flow rate, and V is the building volume, and L is the interior CH_4 leak rate. In the simple case that the methane is increased from zero to L at time t=0, this first order linear differential equation has a solution of the form,

$$C_i(t) = C_o + L/Q\,(1 - \exp(-t/\tau)), \text{ where } \tau = V/Q, \qquad (5.2)$$

which at long times yields a steady state solution (when $t \gg \tau$) for L as,

$$L = Q\,(C_i - C_o) \qquad (5.3)$$

After allowing a building to reach steady state it is possible to directly estimate L from building measurements to within an uncertainty that depends on the validity of the well-mixed assumption, and uncertainty in the measurements of Ci, Co, and Q. For typical residential U.S. buildings subjected to a 50 Pa depressurization using a blower door, one may expect a total air flow infiltration rate on the order of 10 air changes per hour (ACH), and hence a near-steady-state condition ($t = 3\tau$) after ~ 18 minutes. However, because a 50 Pa depressurization will likely also reverse venting, it is advisable not to operate combustion appliances under these conditions and tests of hence this test should be performed with appliances in a quiescent state.

To distinguish contribution to observed methane enhancements from thermogenic CH_4 (natural gas) from biogenic CH_4 (e.g., sewer gas) sources, researchers measured the stable isotope $^{13}C/^{12}C$

ratios of indoor CH_4, δ_{in}, and outdoor air, δ_{out}. and applied a two-component mass balance model

$$Q\, C_{in}\, \delta_{in} = Q\, C_{out}\, \delta_{out} + L\, \delta_L, \qquad (5.4)$$

to estimate the $^{13}C/^{12}C$ ratio of the added indoor CH_4 as

$$\delta_L = Q/L\, (C_{in}\, \delta_{in} - C_{out}\, \delta_{out}) = (C_{in}\, \delta_{in} - C_{out}\, \delta_{out}) / (C_i - C_o). \qquad (5.5)$$

Last, the research team estimated methane emissions from partial combustion in gas appliances as,

$$E = N\, R, \qquad (5.6)$$

where the methane consumption rate, N (mol s^{-1}), was estimated from using the time rate of change of utility gas meter reading, and R (mol CH_4 / mol CO_2) is the ratio of CH_4 to CO_2 in the appliance exhaust gas, under the assumption that the majority (~ 99%) of the gas is combusted to CO_2.

5.2.2 Measurements at Residences

As an initial sample, methane emissions were measured from 10 single-family residences the San Francisco Bay Area. These residences include a range of building ages and floor areas (Table 18) but are not meant to be representative of the Bay Area or State as a whole.

Table 18: Building Characteristics for 10 Homes Measured in the San Francisco Bay Area*

Building Age (approx.)	Building Volume (m^3)	CH_4 Enhancement (Ci – Co) (ppb)	Air Flow Rate, Q ($m^3\ hr^{-1}$)	Quiescent Methane Leak Rate, L (sccm)
1910	490	177	5470	16.1 (0.8)
1910	420	137	4360	10.0 (1.0)
1910	690	27	8015	3.6 (3.2)
1920	270	99	3420	5.6 (2.2)
1920	410	35	4719	2.8 (0.3)
1930	720	8	7230	1.0 (0.4)
1930	222	8	2730	7.2 (1.0)
1940	290	67	4430	4.9 (1.6)
1980	480	161	4083	11.0 (2.0)
1990	390	68	2796	3.2 (0.4)

*The CH_4 enhancement, air flow rate, and quiescent leakage for each test are also shown with estimated uncertainty in leakage rate shown in parentheses.

For four of the residences, the average natural gas consumption from the past year's gas utility bills were estimated with a median value of 1.8 l pm (liters per min., 1.2 therms day^{-1}),

fortuitously close to the state average residential consumption 1.2 therms day^{-1} in 2012.[28] Throughout this work methane leakage rates are normalized to gas at standard temperature and pressure.

For the leakage measurements a commercial blower door and manometer (The Energy Conservatory Inc.) was used, adjusted to depressurize the house, producing an inflow of outdoor air with a turnover time of between six and 10 minutes. The house was operated as near to a single well mixed space as possible by keeping all interior doors open and placing a mixing fan in each room and any long hallways. The precision differential manometer is used to continuously monitor the pressure difference between indoor and outdoor air and the pressure across the blower door. Total methane and the 13/12C stable isotope ratio of methane were measured with a cavity ring-down spectrometer (Picarro G2132-*i*), which provided absolute accuracy and precision for CH_4 of about 2 and 0.05 ppb for 100 s integrations, respectively. Similarly, CO_2 could be measured with accuracy and 100s precision near 0.2 ppm and 0.05 ppm, respectively, while the stable isotope $^{13}C/^{12}C$ ratio of ambient air could be measured with a precision near 0.3 per mil based measured variations of gas cylinder measurements, sufficient to detect the changes in $^{13}CH_4$ content of indoor relative to outdoor air. Controlled releases of known CH_4 into residences were conducted in one house by metering commercial mixture 2.5% CH_4 in air from a compressed gas cylinder (Praxair Inc.) through a regulator and volumetric flow meter.

During the quiescent house leakage testing, air supplied to the gas analyzer was alternated every five minutes between the indoor air at the blower door and outdoor background air sampled far from the location of the blower door exhaust. To minimize the residence time of the house, the highest flow rate available from the blower door was used such that the outdoor-indoor pressure difference was no more than 60 Pa, to maintain about 5% accuracy in measuring the exhaust flow. The uncertainty in methane leak rate for each house was measured as the standard deviation in the difference between adjacent indoor and outdoor methane mixing ratios, assuming that the errors in indoor-outdoor differences were uncorrelated over each 10 minute switching cycle. In an initial test, a calibrated flow of 16.5 +/- 0.3 standard cm^3 min^{-1} (sccm defined at T = 0 C, P = 101.3 kPa) CH_4 was released into a large single room laboratory building with volume of 410 m^3, containing no natural gas infrastructure. Using an exhaust flow rate of 4500 m^3 hr^{-1} the estimated emission rate was within 2% of the calibrated leak rate.

To measure the combustion appliance methane emissions, CH_4 emitted was estimated from incomplete combustion during operation of individual appliances using the ratio of CH_4 to CO_2 enhancements measured with a $CO_2/CH_4/H_2O$ analyzer (Picarro G2301) with accuracy better than 0.5 ppm CO_2 and 2 ppb CH_4 as determined with NOAA primary gas standards. Measurements of appliance exhaust gas were diluted with zero air (ultra-high-purity N_2) to maintain CO_2 enhancements within the measurement range of the analyzer (30,000 ppm). Total

[28] http://energyalmanac.ca.gov/naturalgas/residential_natural_gas_consumption.html.

appliance methane usage was estimated by recording the utility gas meter to within 10% and the known (95-97%) methane composition of utility natural gas.[29]

5.3 Building Leakage Results and Discussion

5.3.1 Observed CH_4 Enhancements and Leak Rates

Across the houses, indoor CH_4 enhancements (100-300 ppb) were obtained relative to outdoor air so that leakage rates could be estimated, though some showed more or less variability in outdoor CH_4 sometimes generating large uncertainty in the estimated leak rate. Combining the enhancements with the measured flow rate of the blower door, the estimated CH_4 leak rates varied from 1 to 16 sccm CH_4, with an roughly log-normal distribution with median = 5.0 sccm CH_4 (3.3-9.8 sccm 25-75% quartiles). Comparing with no significant correlation with building volume or age.

As part of the house tests, a calibrated flow rate of CH_4 was released into one of the residences (Figure37). The building volume was approximately 300 m^3 and flow tests were conducted with a flow rate of 3200 $m^3 hr^{-1}$ obtained at 50 Pa depressurization. Using a calibrated CH_4 release flow of 10 +/- 0.3 sccm, the errors in estimated leak rates for releases in four rooms of the house ranged from -4 to -30%, depending on the distance to the blower door exhaust. The underestimate of the release is attributed to incomplete coupling of air from the release location to the blower door. This suggests the need to open doors within buildings under test to increase the coupling between different rooms, to use fans to actively mix air, and to verify depressurization (e.g., 4-5 Pa) in different building zones (e.g., crawl space, attic, garage, utility/laundry room) containing natural gas infrastructure.

As described, the source of methane enhancements were also evaluated by measuring the stable isotope $^{13}C/^{12}C$ ratio of indoor CH_4 enhancement. In all cases with significant indoor enhancement, the indoor air contained measurably (0.4-1.6 per mil) higher $^{13}C/^{12}C$ CH_4 ratio than of the outdoor air, in amounts consistent with an amount expected for the estimated leak rate of CH_4 being dominated by ^{13}C rich (~ 40 per mil) natural gas (Townsend-Small et al., 2012).

[29] (PG&E, http://www.pge.com/pipeline/operations/gas_quality/index.shtml)

Figure 37: Time Series of Indoor (white background) and Outdoor (grey shaded) CH_4 Mixing Ratio During a Residential Measurement

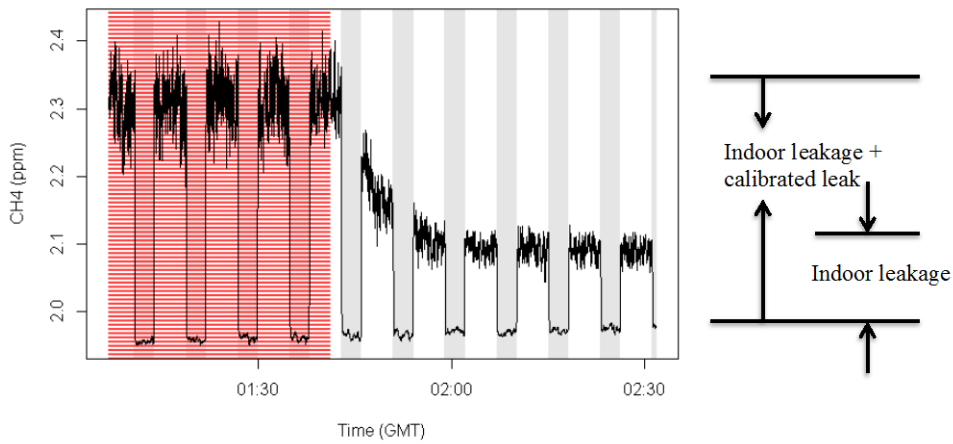

Initial measurements (shaded red) show enhancements relative to outdoor background with a calibrated CH_4 leak applied. The exponential decay of indoor CH_4 toward a steady state enhancement due to quiescent indoor leakage was obtained when the calibrated leak was removed.

Although not operated during the quiescent measurements, three houses used on-demand (tank-less) water heaters. To estimate emissions from incomplete combustion, CH_4:CO_2 ratios for combustion air relative to background air at the appliance inlet were made with the heaters running. Combining the measured enhancement ratios with the measured supply flow of natural gas and publicly reported gas composition[30], showed that CH_4 emitted in the flue gas during operation ranged from 80 to 500 sccm CH_4, 15-100 times that of the mean quiescent leakage rate (Figure 38). In addition, the mean emission rate estimated for a cycle from ratio measurement of two clothes driers was ~ 10 cm^3 min^{-1}. Last, measurements of flue gas from two modern high efficiency (95% efficient) forced air furnaces showed that CH_4 was reduced relative to the outdoor air, suggesting CH_4 was consumed in the combustion process.

Methane emissions from residential natural gas leakage represent an ignored source of greenhouse gas emissions that have not been previously considered. At the level of individual houses, leakage was clearly observed in nearly every case. All measurements were taken while natural gas appliances were not being used, so the leak is likely to be a consistent source of CH_4. If these results are extrapolated to the approximately 10 million residential buildings in California, statewide methane emissions from residential structures would equal approximately 28 (18-54) x 10^6 m^3 yr^{-1} (or ~ 20 Gg CH_4/yr). This is roughly 0.2% of reported residential natural gas consumption (13.3 m^3 yr^{-1})).[31] For comparison, this would represent a small (~10%), but as

[30] PG&E, http://www.pge.com/pipeline/operations/gas_quality/index.shtml

[31] http://energyalmanac.ca.gov/naturalgas/residential_natural_gas_consumption.htm

yet unaccounted for, additional source of oil and gas related methane emissions from California (ARB, 2014).

Figure 38: Time Series Plot of CO_2 and CH_4 Concentrations in the Exhaust of an On-demand Water Heater in Operation

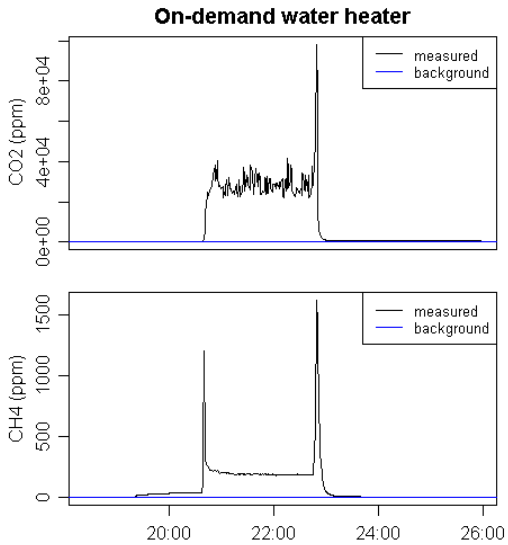

Interestingly, this work suggests that on-demand water heaters are a potentially significant source of natural gas leakage. For two houses studied, the leak rate from the on-demand heaters when they were running was 16-40 times greater than the mean leak rate. This suggests that wide-spread adoption of on-demand heaters could increase residential methane leakage. At present more than 24% of new water heaters are on-demand water heaters, with that fraction growing approximately 10% per year (California Statewide Codes and Standards Team, 2011). In sum, this preliminary work from 10 houses, suggests that methane leakage from residential buildings, quiescent and operating gas appliances may constitute a small but non-zero fraction of natural gas related methane leakage to the atmosphere. This suggests that measurements of a larger sample of residential and commercial buildings would be valuable to accurately evaluate the magnitude of methane emissions in the post-utility-meter consumption sector of the natural gas system in California.

CHAPTER 6:
Summary of Natural Gas Emissions and Mitigation Costs

In this chapter the likely range of CH_4 emissions from specific NG subsectors (i.e., production, processing, storage, distribution, and consumption) of natural gas infrastructure is summarized and the existing information on the likely options and costs for mitigating NG CH_4 emissions is discussed.

6.1 Summary of California Natural Gas Emissions

To cover the large spatial area of California, sub-sector totals were estimated over air basin regions that often contain mixtures of contributions from different NG subsectors. These estimates cover, at most, seasonal averages with some estimates obtained from observations covering only a few days.

With the above caveats, the top-down estimates of emissions from distribution and consumption subsectors are derived from the combination of regional inversions in the SFBA, Sacramento, SoCAB using results from previous work. Table 20 shows a summary of top-down results of NG CH_4 emissions for comparison with the regional estimates derived from bottom-up mapping in Chapter 1 that use the 2012 and 2016 US-EPA emissions totals for US NG CH_4 emissions by sub-sector. The season specific estimates of CH_4 emissions from distribution and consumption are corrected to the first order assuming emissions are proportional to seasonal gas consumption in SoCAB and the SFBA. One exception is Sacramento, where emissions from the dry gas production dominate and are assumed to be constant with time. Using the estimated uncertainties in the various estimates, researchers also include 95% confidence lower and upper estimates of emissions for comparison with the bottom-up estimates.

First, the top-down estimates of CH_4 emissions from production and processing are available at the regional scale only for associated gas in SoCAB and for dry gas near Sacramento. In both cases top-down estimates bound the 2012 and 2016 US-EPA estimates scaled to those regions, suggesting that production emissions are only approximately known but do not obviously differ from the range of existing bottom-up estimates. These limited results from airborne observations of the Belridge South production field described in Chapter 3 for the San Joaquin Valley show a similar result of approximately matching the bottom-up estimates for that field.

Second, the lower limits of the top-down estimates for distribution and consumption subsectors in SoCAB and SFBA are marginally consistent with the scaling of the bottom-up 2012 US-EPA inventory to California but the 2016 US-EPA inventory is substantially smaller and not consistent with the top-down estimates. Part of this discrepancy may be that California imports a majority of gas distributed and consumed and so the fraction of CH_4 emissions from distribution and consumption would likely be higher than in the continental US where production systems constitute a larger fraction of total gas activities. It is important to note that the emissions from distribution and consumption appear roughly similar to those from

production and processing at the state total level. This suggests that additional work is required to verify the top-down estimates of emissions from distribution and consumption (that primarily occur in urban areas) and that mitigation activities that address NG CH_4 emissions need to include effort across all NG subsectors. These points will be touched on in the Section 6.2 on mitigation options.

It should be emphasized that CH_4 emissions from production occurring outside California that support California consumption have not been explicitly measured in this study. Because California imports the majority of NG consumed, California's climate commitment might arguably include CH_4 emissions occurring in the production fields and transmission pipelines that feed California consumption. In rough numbers, California imports 90% of gas consumed. If that gas is produced and transmitted with a rough average leakage of around 1.5% as suggested by other studies (e.g. Brandt et al., 2014), then these emissions would likely be larger than total in-state CH_4 emissions estimated in this study.

Table 19 Estimated Regional NG CH_4 Emissions

Emissions (gG CH4/yr)	Season-specific Top-down Central Estimate	Top-down uncertainty*	Seasonal Correction	Annual-mean Top Down Central Estimate	Annual-mean Top Down Uncertainty*	Annual Mean Top-Down Lower Limit*	Annual Mean Top-Down Upper Limit*	2010 Emissions based on 2012 US-EPA Inventory	2014 Emissions based on 2016 US-EPA Inventory
SoCAB (see note1)									
Production								24	18
Processing								0.4	0.2
Subtotal	32	14	1.0	32	14	18	46	26	21
Transmission								3	3
Distribution								54	16
Subtotal	131	108	1.3	170	140	30	311	57	19
Total	163			202		35	314	83	40
SFBA (see note2)									
Production									
Processing									
Subtotal									
Transmission									
Distribution								26	8
Subtotal	34	8	0.9	31	7	23	38	26	8
Total	34			31		23	38	26	8
Sacramento (see note3)									
Production								21	39
Processing								0	0
Subtotal								21	39
Transmission								4	4
Distribution								9	3
Subtotal								13	7
Total	35	14	1	35	14	21	49	34	46
Other region (see note 4)									
Production									
Processing									
Subtotal	192	84	1	192	84	108	276	141	169
Transmission									
Distribution									
Subtotal	152	125	1	152	125	27	277	47	23
Total	344			344		111	391	188	192
CA Total (see note 5)									
Production								168	215
Processing								12	7
Subtotal	224	82	1	224	82	142	306	188	229
Transmission								13	17
Distribution								130	39
Subtotal	317	276	1.3	412	359	53	771	143	57
Total	541			636		152	829	331	286

*	uncertatinties esimated at 95% confidence. Due to rounding errors, the subtotal/total may not match the individual sums
note 1	scaled from 2010 emissions based on the 2012 US EPA inventory using results from Peischl et al described in Chapter 1 after subtraction of 61 Gg CH4/yr tar pit emissions
note 2	follows results of Chapter 2 for SFBA assuming no production emissions
note 3	follows Chapter 2 for Sacramento estimating sum of dry gas production and distributioion; assumes seasonality in the distribution sector is small given production is a dominant
note 4	difference between CA total below and sum of above regions for reference to show majority of production from San Joaquin Valley not directly observed in this study
note 5	emissions scaled from 2010 US EPA inventory using results from SoCAB as per note 1

6.2 Assessment of Mitigation Options

Detailed assessment of the leak detection and repair (LDAR) and component level replacement costs necessary to mitigate CH_4 emissions from the upstream portion of the US natural gas system has been reported in studies by ICF (2014 & 2016). Because the majority of California's gas is imported, this work can be expected to provide an approximate cost estimates to mitigate the production, processing, and transmission related subsectors providing California's total gas consumption. These results from the 2016 ICF study are applied. Because California gas usage constitutes roughly 10% of total US natural gas consumption[32], and the total annualized cost to save 88 Bcft across US (equivalent to $3.35/Mcf of methane reduced) is about $300 million (ICF, 2016), the approximate cost to mitigate California's share of US NG CH_4 related emissions (~ 8.8 Bcft or ~ 200Gg CH_4 yr^{-1}) is about $30 million yr^{-1} for the upstream sectors not including distribution and end-use consumption.

To extend this work to include mitigation of distribution and consumption sectors it was assumed the relative proportion of in-state emissions from distribution and consumption are roughly equal to those from production and processing, however the costs to mitigate distribution and consumption emissions are poorly known at this time. The previous ICF studies did not estimate costs to mitigate CH_4 emissions from the distribution and consumption. Lacking more information, an order of magnitude estimate can be made assuming mitigation costs per unit of gas mitigated are similar for the combination of distribution and consumption as for the upstream sub-sectors. Since these estimates for emissions from the distribution and consumption subsectors from are also roughly similar to those from in-state production, it might be expected the cost to mitigate in-state consumption and distribution leakage might be another about $30 million yr^{-1}. This would suggest a total cost of about $60 million yr^{-1} in total to mitigate CH_4 in-state emissions from wells to burners.

Finally, a more carefully considered estimate of the costs to mitigate emissions from the distribution and consumption sectors would benefit from information on the details of what portions of those sub-sectors are responsible for the emissions and identification of the costs for leak detection and repair. For the distribution sub-sector, it is suggested consultation with gas utilities would be helpful. The consumption sub-sector includes costs to mitigate post-meter leaks in gas plumbing that supplies appliances in residential and commercial settings, and then costs to develop, purchase, and install modern appliances that emit less CH_4 in their combustion processes.

[32] https://www.eia.gov/tools/faqs/faq.cfm?id=46&t=8

REFERENCES

Allen, D. T., Torres, V. M., Thomas, J., Sullivan, D. W., Harrison, M., Hendler, A., Herndon, S. C., Kolb, C. E., Fraser, M. P., Hill, A. D., Lamb, B. K., Miskimins, J., Sawyer, R. F., Seinfeld, J. H (2013), Measurements of methane emissions at natural gas production sites in the United States. Proc. Nat'l. Acad. Sci. doi: 10.1073/pnas.1304880110.

Alvarez, R. A., Pacala, S. W., Winebrake, J. J., Chameides, W. L., Hamburg, S. P. (2012), Greater focus needed on methane leakage from natural gas infrastructure. Proc. Nat'l. Acad. Sci. doi/10.1073/pnas.1202407109.

BAAQMD (2015), Bay Area Emissions Inventory Summary Report: Greenhouse Gases Base Year 2011 (http://www.baaqmd.gov/~/media/files/planning-and-research/emission-inventory/by2011_ghgsummary.pdf, updated January 2015; accessed March 2016).

BAAQMD (2016), 2015 Air Monitoring Network Plan (http://www.baaqmd.gov/~/media/files/technical-services/2015_network_plan-pdf.pdf?la=en; accessed May 2016).

Beaulieu, N. C., Abu-Dayya, A. A., McLane, P. J. (1995), Estimating the distribution of a sum of independent lognormal random variables. IEEE Trans. Commun., *43* (12), 2869 – 2873.

Brandt, A. R., et al. (2014), Methane leaks from North American natural gas systems. Science, 343 (6172), 733 – 735. DOI: 10.1126/science.1247045.

Brioude, J., et al. (2013), Top-down estimate of surface flux in the Los Angeles Basin using a mesoscale inverse modeling technique: assessing anthropogenic emissions of CO, NOx and CO_2, Atmospheric Chemistry and Physics, 13, 3661-3677. doi:10.5194/acp-13-3661-2013.

Burnham, A., Han, J., Clark, C. E., Wang, M., Dunn, J. B., Rivera, I. P. (2011), Life-cycle greenhouse gas emissions of shale gas, natural gas, coal, and petroleum. Environ. Sci. Technol. DOI: 10.1021/es201942m.

California Air Resources Board (2013). California Greenhouse Gas Emissions Inventory. California Air Resources Board Staff Report (August 2013 version, http://www.arb.ca.gov/cc/inventory/inventory.htm, accessed April 2014).

California Air Resources Board (2013), Oil and Gas Industry Survey Results, Final Report (Revised). Stationary Source Division (http://www.arb.ca.gov/cc/oil-gas/FinalReportRevised.pdf, accessed April 2014).

California Air Resources Board (2014), California Greenhouse Gas Emissions Inventory. California Air Resources Board Staff Report, Accessed January 2015 (http://www.arb.ca.gov/cc/inventory/inventory.htm, version March 2014).

California Air Resources Board (2015), California Greenhouse Gas Emissions Inventory. California Air Resources Board Staff Report, Accessed September 2015 (http://www.arb.ca.gov/cc/inventory/inventory.htm, version April 2015).

California Air Resources Board (2016), California Greenhouse Gas Emissions Inventory. California Air Resources Board Staff Report, Accessed June 2016 (http://www.arb.ca.gov/cc/inventory/inventory.htm, version June 2016).

California Air Resources Board (2017), California Industry Reporting. https://www.arb.ca.gov/ei/tools/ievt/#mapTab.

California Dept. of Conservation, Division of Oil, Gas, and Geothermal Resources (DOGGR) (2010), 2009 Report of California Oil and Gas Production Statistics, PR03. (ftp://ftp.consrv.ca.gov/pub/oil/annual_reports/2010/PR03_PreAnnual_2010.pdf, accessed April 2014).

California Dept. of Conservation, Division of Oil, Gas, and Geothermal Resources (DOGGR) (2011), 2010 Preliminary Report of California Oil and Gas Production Statistics, PR03 (ftp://ftp.consrv.ca.gov/pub/oil/annual_reports/2010/PR03_PreAnnual_2010.pdf, accessed April 2014).

California Public Utilities Commission (2010), Permit applications for Wild Goose and Kirby Hills gas storage facilities. (http://www.cpuc.ca.gov/environment/info/ene/wild%20goose_phase%203/fseir/fseir_appendix.pdf, http://www.cpuc.ca.gov/environment/info/dudek/sngs/sectiond2airquality.pdf).

California Statewide Codes and Standards Team (2011), High-efficiency Water Heater Ready: 2013 California building energy efficiency standards California Utilities, California Public Utilities Commission Report (http://www.energy.ca.gov/title24/2013standards/prerulemaking/documents/current/Reports/Residential/Water_Heating/2013_CASE_WH2.WH5_WaterHeaterReady-10.28.2011.pdf).

Chen, F., and J. Dudhia (2001), Coupling an advanced land surface hydrology model with the Penn State NCAR MM5 modeling system. Part 1: model implementation and sensitivity, Mon. Weather Rev., 129, 569–585.

Colman, J. J., A. L. Swanson, S. Meinardi, B. C. Sive, D. R. Blake, and F. S. Rowland (2001), Description of the analysis of a wide range of volatile organic compounds in whole air samples collected during PEM-tropics A and B, Anal. Chem., 73, 3723–3731, doi:10.1021/ac010027g.

Conley, S. A., I. C. Faloona, D. H. Lenschow, A. Karion, and C. Sweeney (2014), A low-cost system for measuring horizontal winds from single-engine aircraft, J. Atmos. Oceanic Technol., 31, 1312–1320.

Conley, S., G. Franco, I. Faloona, D. R. Blake, J. Peischl, and T. B. Ryerson (2016), Methane emissions from the 2015 Aliso Canyon blowout in Los Angeles, CA, Science, 10.1126/science.aaf2348.

Conley, et al., (2017), Application of Gauss's Theorem to quantify localized surface emissions from airborne measurements of wind and trace gases. Atmospheric Measurement Techniques Discussion (submitted).

Cui, Y. Y., J. Brioude, S. A. McKeen, W. M. Angevine, S.-W. Kim, G. J. Frost, R. Ahmadov, J. Peischl, N. Bousserez, Z. Liu, T. B. Ryerson, S. C. Wofsy, G. W. Santoni, E. A. Kort, M. L. Fischer, and M. Trainer (2015), Top-down estimate of methane emissions in California using a mesoscale inverse modeling technique: The South Coast Air Basin. J. Geophys. Res. Atmos., 120, 6698–6711. doi: 10.1002/2014JD023002.

DOE (2015) http://energy.gov/energysaver/tankless-or-demand-type-water-heaters

Fairley, D., and M. L. Fischer (2015). Top-down methane emissions estimates for the San Francisco Bay Area from 1990 to 2012, Atmospheric Environment, doi:10.1016/j.atmosenv.2015.01.065.

Farrell, P., Culling, D., Leifer, I. (2013), Transcontinental methane measurements: Part 1. A mobile surface platform for source investigations. Atmos. Environ., 74, 422 – 431. doi:10.1016/j.atmosenv.2013.02.014.

Gelman, A. and J. Hill (2007), Data analysis using regression and multilevel/hierarchical models, Cambridge University Press, New York, NY, USA.

Gelman A., J. B. Carlin, H. S. Stern, D. B. Dunson, A. Vehtari, and D. B. Rubin (2014), Bayesian data analysis (3rd Ed.), Chapman & Hall/CRC.

Ganesan, A. L. et al. (2014), Characterization of uncertainties in atmospheric trace gas inversions using hierarchical Bayesian methods. Atmos. Chem. Phys., 14, 3855–3864, doi:10.5194/acp-14-3855-2014.

Gentner, D.R., et al. (2014), Emissions of organic carbon and methane from petroleum and dairy operations in California's San Joaquin Valley, Atmos. Chem. Phys. 13, 28225–28278.

Gerbig, C, J. Lin, S. Wofsy, B. Daube, A. E. Andrews, B. Stephens, P. S. Bakwin and C. Grainger (2003), Toward constraining regional-scale fluxes of CO_2 with atmospheric observations over a continent: 2. Analysis of COBRA data using a receptor-oriented framework. J. Geophys. Res., 108(D24), doi:10.1029/2003JD003770.

Guha, A., D.R. Gentner, R.J. Weber, R. Provencal, A. Gardner, and A.H. Goldstein (2015), Source apportionment of methane and nitrous oxide in California's San Joaquin Valley at CalNex 2010 via positive matrix factorization, Atmos. Chem. Phys., 15, 12043–12063, doi:10.5194/acp-15-12043-2015.

Hopkins, F. M., E. A. Kort, S. E. Bush, J. R. Ehleringer, C.-T. Lai, D. R. Blake, and J. T. Randerson (2016), Spatial patterns and source attribution of urban methane in the Los Angeles Basin, J. Geophys. Res. Atmos., 121, doi:10.1002/2015JD024429.

Howarth, R. W., Santoro, R., Ingraffea, A. (2011), Methane and the greenhouse-gas footprint of natural gas from shale formations. Climatic Change. DOI 10.1007/s10584-011-0061-5.

Hsu, Y.-K., T. VanCuren, S. Park, C. Jakober, J. Herner, M. FitzGibbon, D. R. Blake, and D. D. Parrish (2010), Methane emissions inventory verification in southern California, Atmos. Environ., 44, 1 – 7, doi:10.1016/j.atmosenv.2009.10.002.

ICF (2014). Methane Abatement Costs for US. https://www.edf.org/sites/default/files/methane_cost_curve_report.pdf

ICF (2016). Economic Analysis of Methane Emission Reduction Potential from Natural Gas Systems. Report for OneFuture. http://www.onefuture.us/wp-content/uploads/2016/06/ONE-Future-MAC-Final-6-1.pdf

Interstate Natural Gas Association of America (INGAA) (2005), Greenhouse gas emission estimation guidelines for natural gas transmission and storage. Volume 1 – GHG emission estimation methodologies and procedures, E-2005-01 (http://www.ingaa.org/File.aspx?id=5485, accessed April 2014).

IPCC (2013) Myhre, G., D. Shindell, F.-M. Bréon, W. Collins, J. Fuglestvedt, J. Huang, D. Koch, J.-F. Lamarque, D. Lee, B. Mendoza, T. Nakajima, A. Robock, G. Stephens, T. Takemura and H. Zhang, 2013: Anthropogenic and Natural Radiative Forcing. In: Climate Change 2013: The Physical Science Basis. Contribution of Working Group I to the Fifth Assessment Report of the Intergovernmental Panel on Climate Change [Stocker, T.F., D. Qin, G.-K. Plattner, M. Tignor, S.K. Allen, J. Boschung, A. Nauels, Y. Xia, V. Bex and P.M. Midgley (eds.)]. Cambridge University Press, Cambridge, United Kingdom and New York, NY, USA. http://www.ipcc.ch/pdf/assessment-report/ar5/wg1/WG1AR5_Chapter08_FINAL.pdf

Jeong, S., C. Zhao, A. E. Andrews, L. Bianco, J. M. Wilczak, and M. L. Fischer (2012a), Seasonal variation of CH4 emissions from central California. J. Geophys. Res., 117, D11306, doi:10.1029/2011JD016896.

Jeong, S., C. Zhao, A. E. Andrews, E. J. Dlugokencky, C. Sweeney, L. Bianco, J. M. Wilczak, and M. L. Fischer (2012b), Seasonal variations in N_2O emissions from central California. Geophys. Res. Lett., 39, L16805, doi:10.1029/2012GL052307.

Jeong, S., Y.-K. Hsu, A. E. Andrews, L. Bianco, P. Vaca, J. M. Wilczak, and M. L. Fischer (2013), A multitower measurement network estimate of California's methane emissions, J. Geophys. Res. Atmos., 118, 11,339–11,351, doi:10.1002/jgrd.50854.

Jeong, S., D. Millstein, and M. L. Fischer (2014), Spatially explicit methane emissions from petroleum production and the natural gas system in California, Environ. Sci. Technol., 48, 5982–5990.

Jeong, S., X. Cui, D. R. Blake, B. Miller, S. A. Montzka, A. Andrews, A. Guha, P. Martien, R. P. Bambha, B. LaFranchi, H. A. Michelsen, C. Clements, P. Glaize and M. L. Fischer (2016). Estimating methane emissions from biological and fossil-fuel sources in the San Francisco Bay Area. Geophysical Research Letters, 43, DOI: 10.1002/2016GL071794.

Johnson, M. S., E. L. Yates, L. Iraci, M. Loewenstein, J. Tadić, K. J. Wecht, S. Jeong, and M. L. Fischer (2014), Analyzing source apportioned methane in northern California during Discover-AQ-CA using airborne measurements and model simulations, Atmos. Environ., 99, 248-256, doi:10.1016/j.atmosenv.2014.09.068.

Johnson, D. R., A. N. Covington and N. N. Clark (2015). Methane Emissions from Leak and Loss Audits of Natural Gas Compressor Stations and Storage Facilities. Environmental Science & Technology **49**(13): 8132-8138. DOI: 10.1021/es506163m.

Karion, A., et al. (2013), Methane emissions estimate from airborne measurements over a western Uited States natural gas field. Geophys. Res. Lett., 40, 4393–4397. doi:10.1002/grl.50811.

Kirchstetter, T. W., B. C. Singer, R. A. Harley, G. R. Kendall, and W. Chan (1996), Impact of oxygenated gasoline use on California light-duty vehicle emissions, Environ. Sci. Technol., 30, 661–670.

Kirchstetter, T. W., B. C. Singer, and R. A. Harley (1999), Impact of California reformulated gasoline on motor vehicle emissions. 2. Volatile organic compound speciation and reactivity, Environ. Sci. Technol., 33(2), 329 – 336, 10.1021/es980374g.

Kort, E. A., J. Eluszkiewicz, B. B. Stephens, J. B. Miller, C. Gerbig, T. Nehrkorn, B. C. Daube, J. O. Kaplan, S. Houweling, and S. C. Wofsy (2008), Emissions of CH_4 and N_2O over the United States and Canada based on a receptor-oriented modeling framework and COBRA-NA atmospheric observations, Geophy. Res. Lett., 35, L18808, doi:10.1029/2008GL034031.

Korner-Nievergelt, F, T. Roth, S. von Felten, J. Guélat, B. Almasi, and P. Korner-Nievergelt (2015), Bayesian Data Analysis in Ecology Using Linear Models with R, BUGS, and Stan: Including Comparisons to Frequentist Statistics, Elsevier Science.

Kruschke, J. K. (2015), Doing Bayesian data analysis (2nd Ed.), Academic Press, 759 pp.

Lamb, B. K., S. L. Edburg, T. W. Ferrara, T. Howard, M. R. Harrison, C. E. Kolb, A. Townsend-Small, W. Dyck, A. Possolo and J. R. Whetstone (2015). Direct Measurements Show Decreasing Methane Emissions from Natural Gas Local Distribution Systems in the United States, Environmental Science & Technology **49**(8): 5161-5169, DOI: 10.1021/es505116p.

Lavoie, T. N., P. B. Shepson, C. A. Gore, B. H. Stirm, R. Kaeser, B. Wulle, D. Lyon and J. Rudek (2017). Assessing the Methane Emissions from Natural Gas-Fired Power Plants and Oil Refineries. Environmental Science & Technology **51**(6): 3373-3381. DOI: 10.1021/acs.est.6b05531.

Lelieveld, J., Lechtenböhmer, S., Assonov, S. S., Brenninkmeijer, C. A. M., Dienst, C., Fischedick, M., Hanke, T. (2005), Low methane leakage from gas pipelines. Nature., 434, 841-842.

Lin, J. C., C. Gerbig, S. C. Wofsy, A. E. Andrews, B. C. Daube, K. J. Davis, and C. A. Grainger (2003), A near-field tool for simulating the upstream influence of atmospheric observations: The Stochastic Time-Inverted Lagrangian Transport (STILT) model. J. Geophys. Res., 108(D16), 4493, doi:10.1029/2002JD003161.

Lyon, D. R., D. Zavala-Araiza, R. A. Alvarez, R. Harriss, V. Palacios, X. Lan, R. Talbot, T. Lavoie, P. Shepson, T. I. Yacovitch, S. C. Herndon, A. J. Marchese, D. Zimmerle, A. L. Robinson and S. P. Hamburg (2015). Constructing a Spatially Resolved Methane Emission Inventory for the Barnett Shale Region. Environmental Science & Technology **49**(13): 8147-8157. DOI: 10.1021/es506359c.

McKain K., et al., (2015), Methane emissions from natural gas infrastructure and use in the urban region of Boston, Massachusetts, Proc. Nat'l. Aca. Sci., 112 (7), www.pnas.org/cgi/doi/10.1073/pnas.1416261112.

McMillan, A. M. S., M. L. Goulden, and S. C. Tyler (2007), Stoichiometry of CH_4 and CO_2 flux in a California rice paddy, J. Geophys. Res., 112, G01008, doi:10.1029/2006JG000198.

Mesinger, F., G. DiMego, E. Kalnay, K. Mitchell, P. C. Shafran, W. Ebisuzaki, D. Jovic, J. Woollen, E. Rogers, E. H. Berbery, M. B. Ek, Y. Fan, R. Grumbine, W. Higgins, H. Li, Y. Lin, G. Manikin, D. Parrish, and W. Shi (2006), North American Regional Reanalysis. Bull. Amer. Meteor. Soc., 87 (3), 343-360.

Michalak, A. M., A. Hirsch, L. Bruhwiler, K. R. Gurney, W. Peters, and P. P. Tans (2005), Maximum likelihood estimation of covariance parameters for Bayesian atmospheric trace gas surface flux inversions, J. Geophys. Res., 110, D24107, doi:10.1029/2005JD005970.

Michalak, A. M. (2008), A Gibbs sampler for inequality-constrained geostatistical interpolation and inverse modeling, Water Resource. Res., 44, W09437, doi:10.1029/2007WR006645.

Miller, S. M., et al. (2013), Anthropogenic emissions of methane in the United States, Proc. Natl. Acad. Sci. U.S.A, 110 (50): 20018 - 20022.

Miller, S. M., A. M. Michalak, and P. J. Levi (2014), Atmospheric inverse modeling with known physical bounds: an example from trace gas emissions, Geosci. Model Dev., 7, 303–315, doi:10.5194/gmd-7-303-2014.

Nakanishi, M. and H. Niino (2006), An improved Mellor Yamada level-3 model: its numerical stability and application to a regional prediction of advection fog, Bound. Layer Meteorol., 119, 397– 407.

Nehrkorn, T., J. Eluszkiewicz, S. C. Wofsy, J. C. Lin, C. Gerbig, M. Longo, and S. Freitas (2010), Coupled weather research and forecasting - stochastic time-inverted lagrangian

transport (WRF-STILT) model. Meteor. Atmos. Phys., 107 (1), 51-64, doi:10.1007/s00703-010-0068-x.

Newman, S., S. Jeong, M. L. Fischer, X. Xu, C. L. Haman, B. Lefer, S. Alvarez, B. Rappenglueck, E. A. Kort, A. E. Andrews, J. Peischl, K. R. Gurney, C. E. Miller, and Y. L. Yung (2013), Diurnal tracking of anthropogenic CO_2 emissions in the Los Angeles basin megacity during spring 2010, Atmos. Chem. Phys., 13, 4359–4372, doi:10.5194/acp-13-4359-2013.

Peischl, J., et al. (2012), Airborne observations of methane emissions from rice cultivation in the Sacramento Valley of California, J. Geophys. Res., 117, D00V25, doi:10.1029/2012JD017994.

Peischl, J., et al. (2013), Quantifying sources of methane using light alkanes in the Los Angeles basin, California, J. Geophys. Res. Atmos., 118, doi:10.1002/jgrd.50413.

Pétron, G., et al. (2012), Hydrocarbon emissions characterization in the Colorado Front Range: A pilot study. J. Geophys. Res., 117, D04304, doi:10.1029/2011JD016360.

PG&E (2015) Online reporting of natural gas composition. http://www.pge.com/pipeline/operations/gas_quality/index.page; accessed Jan-Dec, 2015.

Pfister, G., P. G. Hess, L. K. Emmons, J. F. Lamarque, C. Wiedinmyer, D. P. Edwards, G. Pétron, J. C. Gille, and G. W. Sachse (2005), Quantifying CO emissions from the 2004 Alaskan wildfires using MOPITT CO data, Geophys. Res. Let., 32(11), L11809, doi:10.1029/2005GL022995.

Plummer, M. (2003), JAGS: A program for analysis of Bayesian graphical models using Gibbs sampling, Proceedings of the 3rd International Workshop on Distributed Statistical Computing (DSC 2003), March 20–22, Vienna, Austria. ISSN 1609-395X.

Rasmussen, C. E., and C. K. I. Williams (2006), Gaussian Processes for Machine Learning, MIT Press, Cambridge, Massachusetts.

Salas, W., C. Li, F. Mitloehner, and J. Pisano (2009), Developing and applying process-based models for estimating greenhouse gas and air emissions from California dairies, Rep. CEC-500-2008-093, Public Interest Energy Res. Program, Calif. Energy Comm., Sacramento, Calif.

Shorter, J. H., McManus, J. B., Kolb, C. E., Allwine, E. J., Siverson, R., Lamb, B., Byard, M. W., Harriss, R. C., Howard, T., Lott, R. A (1997), Collection of leakage statistics in the natural gas system by tracer methods, Environ. Sci. Technol., 31, 2012-2019.

Skamarock, W.C., J. B. Klemp, J. Dudhia, D.O. Gill, D. M. Barker, X. Z. Huang, W. Wang, and J. G. Powers (2008), A description of the advanced research WRF version 3. Technical Note 475+STR. Mesoscale and Microscale Meteorology Division, NCAR, Boulder, Colorado.

Stan Development Team (2015), Stan Modeling Language: User's Guide and Reference Manual (Version 2.9.0.; http://mc-stan.org/documentation/).

Subramanian, R., L. L. Williams, T. L. Vaughn, D. Zimmerle, J. R. Roscioli, S. C. Herndon, T. I. Yacovitch, C. Floerchinger, D. S. Tkacik, A. L. Mitchell, M. R. Sullivan, T. R. Dallmann and A. L. Robinson (2015). Methane emissions from natural gas compressor stations in the transmission and storage sector: measurements and comparisons with the EPA Greenhouse Gas Reporting Program Protocol., Environmental Science & Technology 49(5): 3252-3261. DOI: 10.1021/es5060258.

Townsend-Small, A., S. C. Tyler, D. E. Pataki, X. Xu, and L. E. Christensen (2012), Isotopic measurements of atmospheric methane in Los Angeles, California, USA: Influence of "fugitive" fossil fuel emissions, J. Geophys. Res., 117, D07308, doi:10.1029/2011JD016826.

US Energy Information Administration (EIA) (2013), Annual Energy Outlook 2013 with Projections to 2040. DOE/EIA-0383(2013) (http://www.eia.gov/forecasts/aeo/pdf/0383(2013).pdf, accessed April 2014).

US EIA (2016), Energy Consumption Overview: Estimates by Energy Source and End-Use Sector, 2013, http://www.eia.gov/state/seds/data.cfm?incfile=/state/seds/sep_sum/html/sum_btu_1.html&sid=US (accessed April 2016).

US EPA (2004), Inventory of U.S. Greenhouse Gas Emissions and Sinks: 1990 – 2002 (http://www.epa.gov/climatechange/Downloads/ghgemissions/04CR.pdf, accessed April 2014).

US EPA (1997), Methane emissions from the natural gas industry: Project summary. EPA/600/SR-96/080 (http://psb.vermont.gov/sites/psb/files/docket/7970addison/CLF/CLF-EAS-05%20-%20EPA%20Report.pdf, accessed April 2014).

US EPA (2012), Inventory of U.S. Greenhouse Gas Emissions and Sinks: 1990 – 2010. EPA 430-R-12-001 (http://www.epa.gov/climatechange/ghgemissions/usinventoryreport/archive.html, accessed April 2014).

US EPA (2013), Inventory of U.S. Greenhouse Gas Emissions and Sinks: 1990 – 2011. EPA 430-R-13-001 (http://www.epa.gov/climatechange/ghgemissions/usinventoryreport.html, accessed April 2014).

US EPA (2016), Inventory of U.S. Greenhouse Gas Emissions and Sinks: 1990 – 2014. EPA 430-R-16-002 (http://www.epa.gov/climatechange/ghgemissions/usinventoryreport.html, accessed May 2016).

US EPA (2017), Greenhouse Gas Facility Reporting. https://ghgdata.epa.gov/ghgp

Wecht, K. J., Jacob, D. J., Sulprizio, M. P., Santoni, G. W., Wofsy, S. C., Parker, R., Bösch, H., and Worden, J. (2014), Spatially resolving methane emissions in California: constraints from the CalNex aircraft campaign and from present (GOSAT, TES) and future (TROPOMI,

geostationary) satellite observations, Atmos. Chem. Phys., 14, 8173-8184, doi:10.5194/acp-14-8173-2014.

Wennberg, P. O., W. Mui, D Wunch, E. A. Kort, D. R. Blake, E. L. Atlas, G. W. Santoni, S. C. Wofsy, G. S. Diskin, S. Jeong, and M. L. Fischer (2012), On the Sources of Methane to the Los Angeles Atmosphere. Environ. Sci. Technol., 46 (17), 9282 - 9289, doi:10.1021/es301138y.

Willis, G.E., and J. W. Deardorff (1976), A laboratory model of diffusion into the convective planetary boundary layer. Q. J. Roy Meteorol. Soc. 102:427–445.

Wong, K. W., Fu, D., Pongetti, T. J., Newman, S., Kort, E. A., Duren, R., Hsu, Y.-K., Miller, C. E., Yung, Y. L., and Sander, S. P. (2015), Mapping CH_4 : CO_2 ratios in Los Angeles with CLARS-FTS from Mount Wilson, California, Atmos. Chem. Phys., 15, 241-252, doi:10.5194/acp-15-241-2015.

Wunch, D., P. O. Wennberg, G. C. Toon, G. Keppel-Aleks, and Y. G. Yavin (2009), Emissions of greenhouse gases from a North American megacity, Geophys. Res. Lett., 36, L15810, doi:10.1029/2009GL039825.

Wunch, D., G. C. Toon, J. Hedelius, N. Vizenor, C. M. Roehl, K. M. Saad, J.-F. L. Blavier, D. R. Blake, and P. O. Wennberg (2016), Quantifying the loss of processed natural gas within California's South Coast Air Basin using long-term measurements of ethane and methane, Atmos. Chem. Phys. Discuss., doi:10.5194/acp-2016-359.

Yacovitch, T. I., et al. (2014), Demonstration of an Ethane Spectrometer for Methane Source Identification, Environ. Sci. Technol., 48 (14): 8028–8034, DOI: 10.1021/es501475q.

Zavala-Araiza, D., D. R. Lyon, R. A. Alvarez, K. J. Davis, R. Harriss, S. C. Herndon, A. Karion, E. A. Kort, B. K. Lamb, X. Lan, A. J. Marchese, S. W. Pacala, A. L. Robinson, P. B. Shepson, C. Sweeney, R. Talbot, A. Townsend-Small, T. I. Yacovitch, D. J. Zimmerle and S. P. Hamburg (2015). Reconciling divergent estimates of oil and gas methane emissions. Proceedings of the National Academy of Sciences **112**(51): 15597-15602. DOI: 10.1073/pnas.1522126112.

Zhao, C., A. E. Andrews, L. Bianco, J. Eluszkiewicz, A. Hirsch, C. MacDonald, T. Nehrkorn, and M. L. Fischer (2009), Atmospheric inverse estimates of methane emissions from Central California. J. Geophys. Res., 114, D16302, doi:10.1029/2008JD011671.

GLOSSARY

Term	Definition
AB-32	Assembly Bill 32
ACH	air changes per hour
AGL	above ground level
ANGA	America's Natural Gas Alliance
API	American Petroleum Institute
BAAQMD	Bay Area Air Quality Management District
Bcf	billion cubic feet
BWT	Designation given by the research team to a two-story home with a 5-m mast
CALGEM	California Greenhouse Gas Emission Measurements
ARB	California Air Resources Board
CARB-OGS	California Air Resources Board - Oil and Gas Survey
Energy Commission	California Energy Commission
CEIDARS	California Emission Inventory Development and Reporting System
cf	cubic feet
CI	confidence interval
CIAT	Centro Internacional de Agricultura Tropical
CIESIN	Center for International Earth Science Information Network
CNG	Compressed Natural Gas
CO	carbon monoxide
CH_4	methane
DNDC	De-nitrification and de-composition
DOGGR	Department of Conservation, Division of Oil, Gas, and Geothermal Resources
EDGAR	Emission Database for Global Atmospheric Research
EIA	Energy Information Administration
EPA	Environmental Protection Agency
FAA	Federal Aviation Administration
GC-MS	gas chromatography mass spectrometry
gge	gallons gasoline equivalent
GHG	greenhouse gas
Gg	gigagram (10^9 g)
GIS	Geographic Information System
Gj	gigajoule
HBI	hierarchical Bayesian inversion
INGAA	Interstate Natural Gas Association of America
IPCC	Intergovernmental Panel on Climate Change
LBNL	Lawrence Berkeley National Laboratory

LES	large eddy simulation
LSM	land surface model
Mcf	1000 cubic feet
MCMC	Markov chain Monte Carlo
Mg	megagram (10^6 gram)
μmol	micromole (10^{-6} mole)
Mj	megajoule
MPI	Mobile Plume Integrator
MYJ	Mellor–Yamada- Janjić scheme
MYNN2	Mellor–Yamada Nakanishi Niino Level 2.5 scheme
NARR	North American Regional Reanalysis
NG	natural gas
NOAA-ESRL	National Oceanic and Atmospheric Administration Earth System Research Laboratory
PBL	planetary boundary layer
per mil	parts per thousand
PL	petroleum
ppb	parts per billion
ppm	parts per million
PST	Pacific Standard Time
Scfd	standard cubic feet per day
SFBA	San Francisco Bay Area
SJV	San Joaquin Valley
SNL	Sandia National Laboratory
SoCAB	South Coast Air Basin
STILT	Stochastic Time-Inverted Lagrangian Transport
Tg	tera gram, 10^{12} g
UCI	University of California, Irvine
USDA	United States Department of Agriculture
VOC	volatile organic compound
WRF-STILT	Weather Research and Forecasting and Stochastic Time-Inverted Lagrangian Transport

APPENDIX A:
Natural Gas Processing Facilities in California

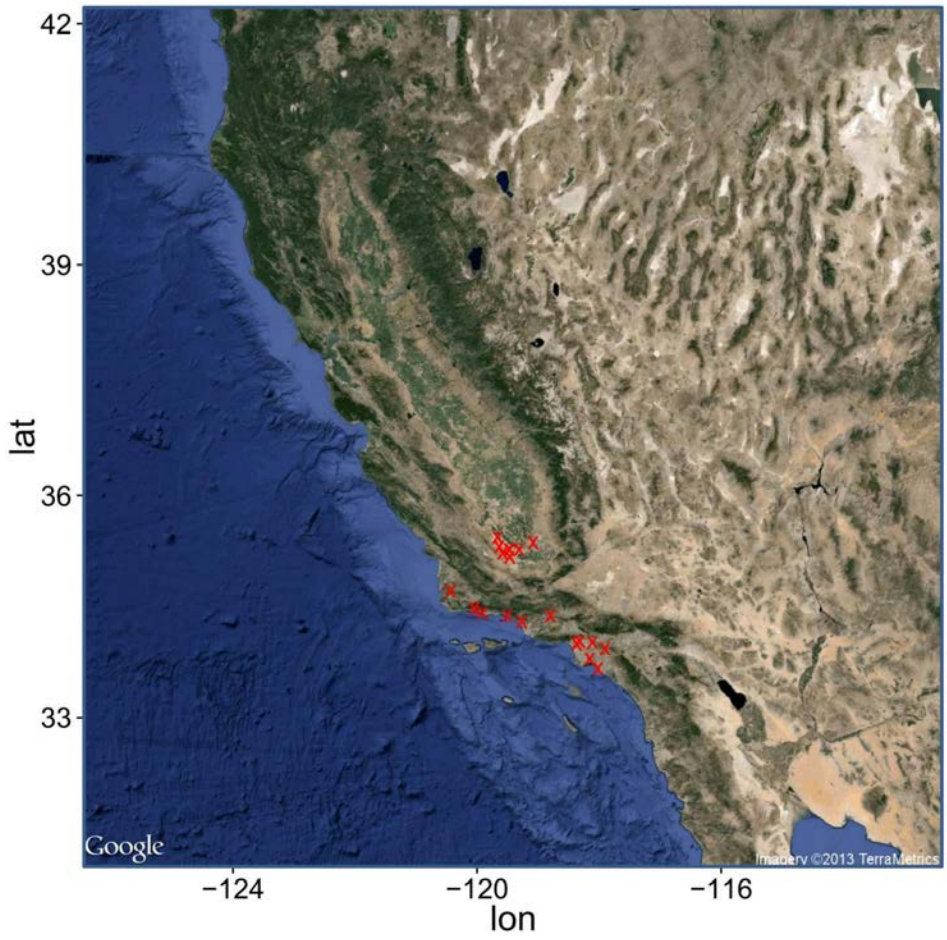

APPENDIX B:
Population Density Map (persons per 0.1°×0.1° pixel) in California Based on CIESIN and CIAT

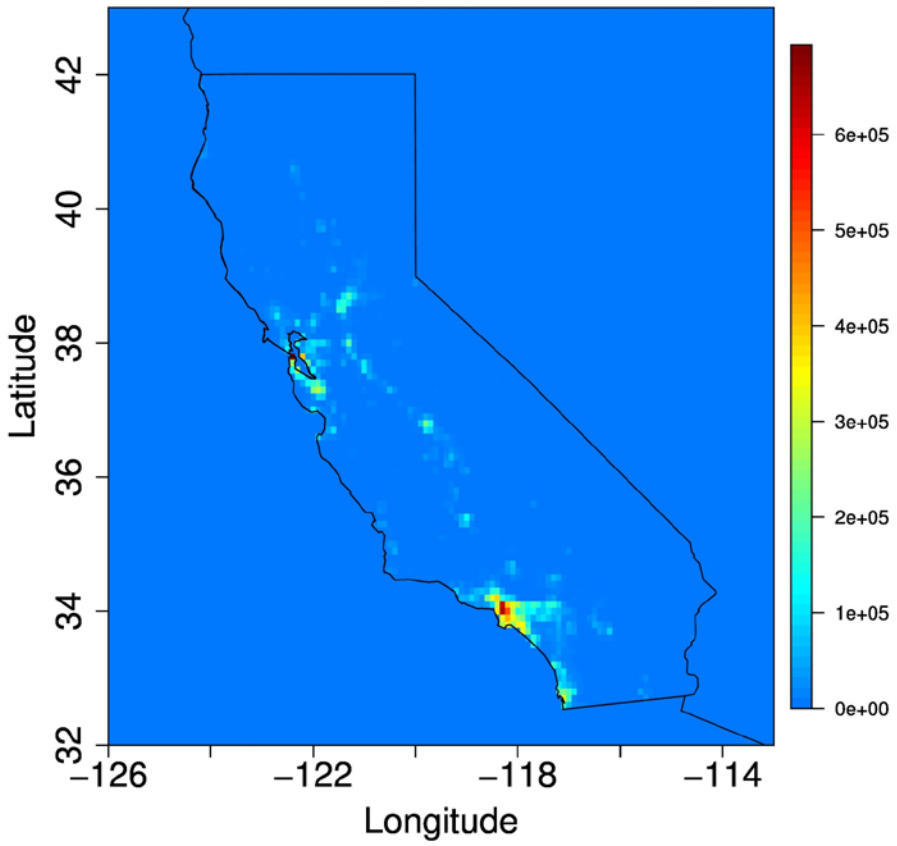

APPENDIX C:
Uncertainty Estimates for the Initial Bottom-up Emissions

We use EPA's uncertainty estimates for the natural gas and petroleum systems because uncertainty estimates for emission factors or activity data are not readily available (US EPA, 2012; US EPA, 2013). EPA's uncertainty for each sector (e.g., natural gas system) is provided as the percentage deviation above and below the mean emission estimate. Because we applied EPA emission factors to estimate California CH_4 emissions for most of the sectors, we also use EPA's uncertainty estimates for the natural gas and petroleum systems as the basis of uncertainty estimates for our initial bottom-up inventory. EPA estimates the percentage deviations below and above the mean emission estimate for the natural gas system are 19% and 30% (95% confidence interval), respectively (US EPA, 2012; US EPA, 2013). For the petroleum system, the percentage deviations below and above the mean estimate are 24% and 149%, respectively (US EPA, 2012; US EPA, 2013). Because this asymmetric property in uncertainty we assume a lognormal distribution in emission estimates for both natural gas and petroleum systems among the five different distributions EPA used. Given our initial bottom-up estimates (i.e., mean estimates) and the percentage deviations (from the mean) provided by EPA, we can characterize the lognormal distribution by estimating the standard deviation. The estimated standard deviations are 0.14 and 0.48 Gg (in log-scale) for the natural gas and petroleum systems, respectively. Note that since we only have the overall uncertainty for the entire natural gas and petroleum systems (one for each), we separated our state total initial bottom-up estimate (330.9 Gg/year) into two: associated production emissions (140.2 Gg/year) and the other emissions from the natural gas system (190.7 Gg/year). In order to estimate the total uncertainty for the natural gas system and petroleum production, we need to combine the two lognormal distributions we defined above. However, there is no closed-form solution to combining two lognormal distributions (Beaulieu et al, 1995). Therefore, we use a simple numerical method to estimate the combined uncertainty for petroleum production the natural gas system using our initial bottom-up estimates and the estimated standard deviations (0.14 and 0.48 Gg (in log-scale) for the natural gas and petroleum systems, respectively). Assuming uncorrelated errors between the natural gas and petroleum systems, we generated random samples (100000 samples) based on the lognormal distributions that we characterized. Then we used bootstrapping (resampling with replacement and 1000 replicates) to estimate the lower and upper bounds of the combined emission from petroleum production and the natural gas system with estimation errors. We find that the state total initial bottom-up emissions range from 222 (standard error = 0.3) to 518 (standard error = 1.2) Gg/year. This estimate is presented in Table 1.5 of Chapter 1.

APPENDIX D:
Sensitivity Analysis

Sensitivity to Liquid Unloading Emission Factor

Liquid unloading is one of the most significant emission sources for non-associated gas production (not applicable to associated wells). In this sensitivity analysis, we compare estimated emissions based on two different emission factors from the 2010 (US EPA, 2012) and 2011 (US EPA, 2013) EPA inventories. The 2011 EPA inventory updated the methodology for liquid unloading based on a recent survey conducted by American Petroleum Institute and America's Natural Gas Alliance (API/ANGA; API/ANGA, 2012) (2011 inventory includes updated emissions for 2010). For 2010, the updated emission for liquid unloading is 5.42 Tg CH_4, which is only 6.3% of the previous estimate (85.6 Tg CH_4). In this study, we use the updated emission factor for liquid unloading, which can be directly applied to well activity data (many other emission factors from the 2011 inventory cannot be directly used because they are for potential emissions). When two different emission factors for liquid unloading were applied, the estimated state CH_4 emissions from liquid unloading were 22.0 and 1.5 Gg/year for the old and new emission factors, respectively. Although the difference is significant (factor of 15) and exceeds the uncertainty range for the natural gas system (~30%) suggested by EPA, we lack data (e.g., atmospheric measurements) to consolidate the difference as described in the main report.

Sensitivity to Well Completion Activity Data

We performed sensitivity analysis of activity data for well completion. The 2010 EPA inventory (US EPA, 2012) reports only 2 well completions for non-associated wells in the West Coast Region while we identified 71 well completions for from the DOGGR well data (DOGGR, http://www.conservation.ca.gov/dog/Pages/Index.aspx, accessed April 2014). Note that we compare (region-specific) well completion data for non-associated gas only because petroleum system emission data are national averages. For non-associated wells, EPA estimates 0.04 Mg CH_4 for well completion in California (assuming the 2 completions are all in California because gas production in Oregon is negligible compared to that of California). On the other hand, when we apply the same emission factor to the 71 completions we identified based on DOGGR well data, we estimate a state total emission of 1.4 Mg CH_4/year from well completion. We note that although the estimated emissions from different well completion activity data are different by more than an order of magnitude (significantly larger than 30% uncertainty for the natural gas system from EPA), the total state emission from well completion is a small fraction of the total emission from the production sector.

Sensitivity to Processing Emission Factor

The emission factor for the processing sector is estimated by calculating the ratio of the 2010 national total emission for the processing sector from EPA (US EPA, 2012) to the total natural

gas processed. This simple emission factor can vary depending on the volume of processed natural gas. EIA reports 51,289 and 44,368 million cf/day for 2008[33] and 2012[34], respectively (2010 data are not available). This difference in processed natural gas volumes yields a 16% difference in estimated state total emissions (10.5 vs. 12.1 Gg/year). This uncertainty falls within the 95% confidence interval uncertainty range (30% at the upper bound) for the natural gas system (see Appendix C above). For the purpose of spatial explicit emission mapping, we used the 2012 dataset where gas flow information from individual processing facilities are available.

Sensitivity to Emission Rate for the Distribution Sector

Although the emission rate for the distribution sector is highly uncertain, separate emission rates for the distribution sector are not readily available. As described in the main report, the US EPA 1997 study estimates an emission rate (total distribution emission / total consumed natural gas) of 0.38% (US EPA, 1997). Lelieveld et al. (2005) report the amount of natural gas lost from pipes in the US to be 1.5±0.5% based on the EPA 2002 Inventory (US EPA, 2004). Wennberg et al. (2012) estimate an emission rate of 3.5% based on the ratio of total CH_4 emissions from the natural gas system to the amount of natural gas delivered to customers. Although this 3.5% emission rate is for the total emissions from the natural gas system (not from the distribution), Wennberg et al. (2012) suggest that most of the leakage occur post consumer metering. These studies show that emission rates for the distribution sector can differ by an order of magnitude. This suggests that estimated emissions are much more sensitive to the uncertainty in the emission rate than that of driving data (e.g., natural gas consumption). Because these emission rates are either national averages or cannot be uniquely distinguishable from those of the other sectors, we used emission rates from Peischl et al. (2013) to adjust our initial bottom-up estimates in the main report.

Sensitivity of the State Total CH_4 Emission Estimates to Scaling Individual Subsectors

In the main report we make the assumption that the difference between the observed (Peischl et al., 2013) Category 1 and Category 2 emissions and our initial bottom-up estimates of those categories can be attributed in equal proportion to each of the subsectors within the category. For example we scale our initial estimates of both transmission and distribution by a factor of 2.2 in order to match Category 2 estimates from Peischl et al. (2013). Later (as shown below), we relax the assumption of equal attribution in order to examine how sensitive our adjusted state

---

[33] Natural Gas Processing Plants in the United States: 2010 Update, http://www.eia.gov/pub/oil_gas/natural_gas/feature_articles/2010/ngpps2009/table_2.cfm (accessed April 2014).

[34] US EIA Natural Gas Annual Respondent Query System, http://www.eia.gov/cfapps/ngqs/ngqs.cfm?f_report=RP9 (accessed April 2014).

total estimate is to the equal attribution assumption. For example, in the column labeled "Distribution" we assume equal attribution for Category 1 sources (multiplying each by 1.2 to match Peischl et al. (2013)) but for Category 2 we assume that our initial estimate of emissions from transmission is correct and that the full difference between the initial bottom-up and the observations is due to higher emissions (relative to the initial bottom-up) from the distribution sector. For the distribution column, we keep our initial transmission estimate at 13 Gg CH_4 yr^{-1} but scale our distribution emissions up so that the total Category 2 emissions match the observations (see below for equations). We note that the adjusted State total emissions vary by -4% to +5% based on relaxing the equal attribution assumption across the major category 1 subsectors (onshore production and offshore production) and the major category 2 subsectors (transmission and distribution).

The second column ('Even Scaling') is described by the equations:

$$PRD_{b_state_n} = PRD_{b_state_i} \times \frac{[PRD + PRC + STR]_{Peischl}}{[PRD + PRC + STR]_{b_SoCAB_i}}$$

$$PRC_{b_state_n} = PRC_{b_state_i} \times \frac{[PRD + PRC + STR]_{Peischl}}{[PRD + PRC + STR]_{b_SoCAB_i}}$$

$$STR_{b_state_n} = STR_{b_state_i} \times \frac{[PRD + PRC + STR]_{Peischl}}{[PRD + PRC + STR]_{b_SoCAB_i}}$$

$$TRN_{b_state_n} = TRN_{b_state_i} \times \frac{[TRN + DST]_{Peischl}}{[TRN + DST]_{b_SoCAB_i}}$$

$$DST_{b_state_n} = DST_{b_state_i} \times \frac{[TRN + DST]_{Peischl}}{[TRN + DST]_{b_SoCAB_i}}$$

where, PRD are emissions from associated onshore and offshore production, PRD_ONS is onshore production only, PRD_OFFS is offshore production only, PRC are emissions from processing, STR are emissions from storage, TRN are emissions from transmission, and DST are emissions from distribution. The subscript b_state_i indicates state total from the initial bottom-up estimate, b_SoCAB_i indicates SoCAB total from the initial bottom-up estimate, Peischl indicates the total reported by Peischl et al. (2013), and b_state_n indicates the new statewide estimates.

Column 3, ('Onshore') in Table A.D1 maintains the even scaling for Category 2 emissions, but scales only the on-shore production sector within Category 1 so that the total Category 1 estimate is consistent with Peischl et al. (2013). The third column is described by the equations:

$$PRD_{b_state_n} = PRD_{b_state_i} \times \frac{[PRD + PRC + STR]_{Peischl} - [PRC + STR]_{b_SoCAB_i}}{PRD_{b_SoCAB_i}}$$

$$TRN_{b_state_n} = TRN_{b_state_i} \times \frac{[TRN + DST]_{Peischl} - DST_{b_SoCAB_i}}{TRN_{b_SoCAB_i}}$$

where all other Category 1 sectors are unchanged and Category 2 sectors are scaled under the equal attribution assumption as in Column 2. In the other columns we have followed the methods described for Column 3, but have picked different major subsectors to which to attribute the emission differences.

Table A.D1: Sensitivity of the State Total CH_4 Emission Estimates*

Category	Sector	Initial bottom-up	Even Scaling	Onshore	Offshore	Transmission	Distribution
Category 1	Production (associated on-shore)	103	127	169	103	127	127
	Production (associated off-shore)	37	46	37	53	46	46
	Production (non-associated)	28	28	28	28	28	28
	Processing	12	15	12	12	15	15
	Storage	8	9	8	8	9	9
	Sub-total	***188***	***224***	***254***	***203***	***224***	***224***
Category 2	Transmission	13	30	30	30	208	13
	Distribution	130	288	288	288	130	302
	Sub-total	***143***	***317***	***317***	***317***	***338***	***315***
	Total	***331***	***541***	***571***	***520***	***562***	***540***
Percent change from even scaling				5%	-4%	4%	0%

*Sensitivity of the state total CH_4 emission estimates (Gg CH_4 yr^{-1}) from California's natural gas system and petroleum production constrained by Peischl et al. (2013) to scaling individual subsectors.

Attribution of Emissions

Finally, from a climate policy perspective, it may be appropriate to consider CH_4 emissions from a given energy production activity relative to the total energy content of all fuel produced. For this purpose, a simple calculation of the total energy produced from natural gas associated with petroleum production (~75% of total natural gas production in California) can be estimated by multiplying the associated gas volume (~5.1 Gm^3 in 2011 from a recent DOGGR report (DOGGR, 2011) by its approximate energy content (~39 Mj m^{-3}) and comparing it to the energy content of petroleum estimated from petroleum production (197 million barrels in 2011; DOGGR, 2011) multiplied by the energy content of petroleum (~5.7 Gj / barrel). This calculation results in only ~15% of CH_4 emitted from gas associated with petroleum production in California being attributable to the energy derived from natural gas, with the remaining 85% of CH_4 emitted attributable to energy derived from petroleum. Alternatively, if one considers attributing CH_4 emissions in relation to the economic value of the natural gas and petroleum, then the burden shifts even further to petroleum. Based on these estimates, the full climate consequences of natural gas and petroleum production significantly outweigh the component due to direct natural gas CH_4 emissions to the atmosphere.

APPENDIX E:
Estimated Background Biases for SFBA Sites*

Site/Gas	Sep - Oct Period			Nov - Dec Period		
	Median	Lower	Upper	Median	Lower	Upper
BWT.CH4	1.49	-5.47	8.27	7.81	-0.63	16.17
LVR.CH4	4.64	-3.76	12.60	12.55	4.42	20.85
OAK.CH4	1.61	-5.69	8.55	4.46	-5.60	13.83
SJSU.CH4	7.31	-2.45	16.86	2.75	-6.24	11.65
STR.CH4	-4.34	-9.90	0.93	-0.13	-7.47	6.77
WGC.CH4	3.48	-5.40	12.52	1.01	-8.42	10.63
BWT.C2H6	1.35	1.08	1.62	1.92	1.57	2.26
LVR.C2H6	1.97	1.60	2.33	2.98	2.66	3.30
OAK.C2H6	0.92	0.63	1.20	1.61	0.89	2.37
SJSU.C2H6	1.06	0.76	1.36	0.96	0.67	1.25
STR.C2H6	-0.06	-0.15	0.03	0.41	0.17	0.66
WGC.C2H6	-0.01	-0.24	0.21	0.33	0.02	0.60
BWT.iC5H12	0.21	0.07	0.34	0.14	0.04	0.23
LVR.iC5H12	1.63	1.31	1.93	2.66	2.13	3.19
OAK.iC5H12	0.53	0.37	0.70	0.43	0.22	0.64
SJSU.iC5H12	0.70	-0.01	1.44	0.30	0.12	0.48
STR.iC5H12	0.00	-0.06	0.04	0.07	0.00	0.13
WGC.iC5H12	0.03	-0.03	0.07	0.11	0.03	0.18
BWT.nC5H12	0.10	0.04	0.15	0.09	0.02	0.13
LVR.nC5H12	0.58	0.47	0.68	1.00	0.83	1.16
OAK.nC5H12	0.17	0.10	0.24	0.16	0.08	0.24
SJSU.nC5H12	0.26	0.00	0.52	0.21	0.07	0.36
STR.nC5H12	0.00	-0.05	0.03	0.06	-0.01	0.10
WGC.nC5H12	0.01	-0.04	0.04	0.06	0.00	0.10
BWT.C7H8	0.28	0.03	0.53	0.15	0.06	0.23
LVR.C7H8	1.14	0.84	1.44	1.41	1.01	1.81
OAK.C7H8	0.31	0.23	0.38	0.30	0.13	0.46
SJSU.C7H8	0.68	0.36	1.00	0.45	0.08	0.82
STR.C7H8	-0.03	-0.08	0.00	-0.01	-0.06	0.03
WGC.C7H8	-0.04	-0.09	-0.01	-0.01	-0.07	0.02

*The positive value in the bias estimate indicates that the local measured mixing ratio after background subtraction was systematically higher (i.e., estimated background was lower) than predictions.

APPENDIX F:
Comparison of Bottom-up Inventories between SFBA and SoCAB

Sector	SFBA		SoCAB**	
	Emission (Gg CH_4/yr)	Source Emission Ratio Relative to Total (%)	Emission (Gg CH_4/yr)	Source Emission Ratio Relative to Total (%)
DLS	9.2	8%	37.9	11%
LF	61.5	51%	157	45%
NDLS	9.0	8%	5.8	2%
NG	17.5	15%	112.2	32%
PL	4.1	3%	12	3%
WW	7.0	6%	23.6	7%
WL	3.7	3%	0.9	0%
OTHER	8.1*	7%	0	0%
Total	120.1		349.4	

*BAAQMD's estimates for miscellaneous emissions including emissions from solid fuel (wood) combustion, other stationary combustion, ships, aircraft, and off-highway mobile sources.

**CALGEM emissions (Jeong et al., 2013; 2014) matching CARB's 2012 CH_4 inventory (see Section 2.2.2 in Chapter 2).

APPENDIX G:
VOC Measurements at the THD Background Site

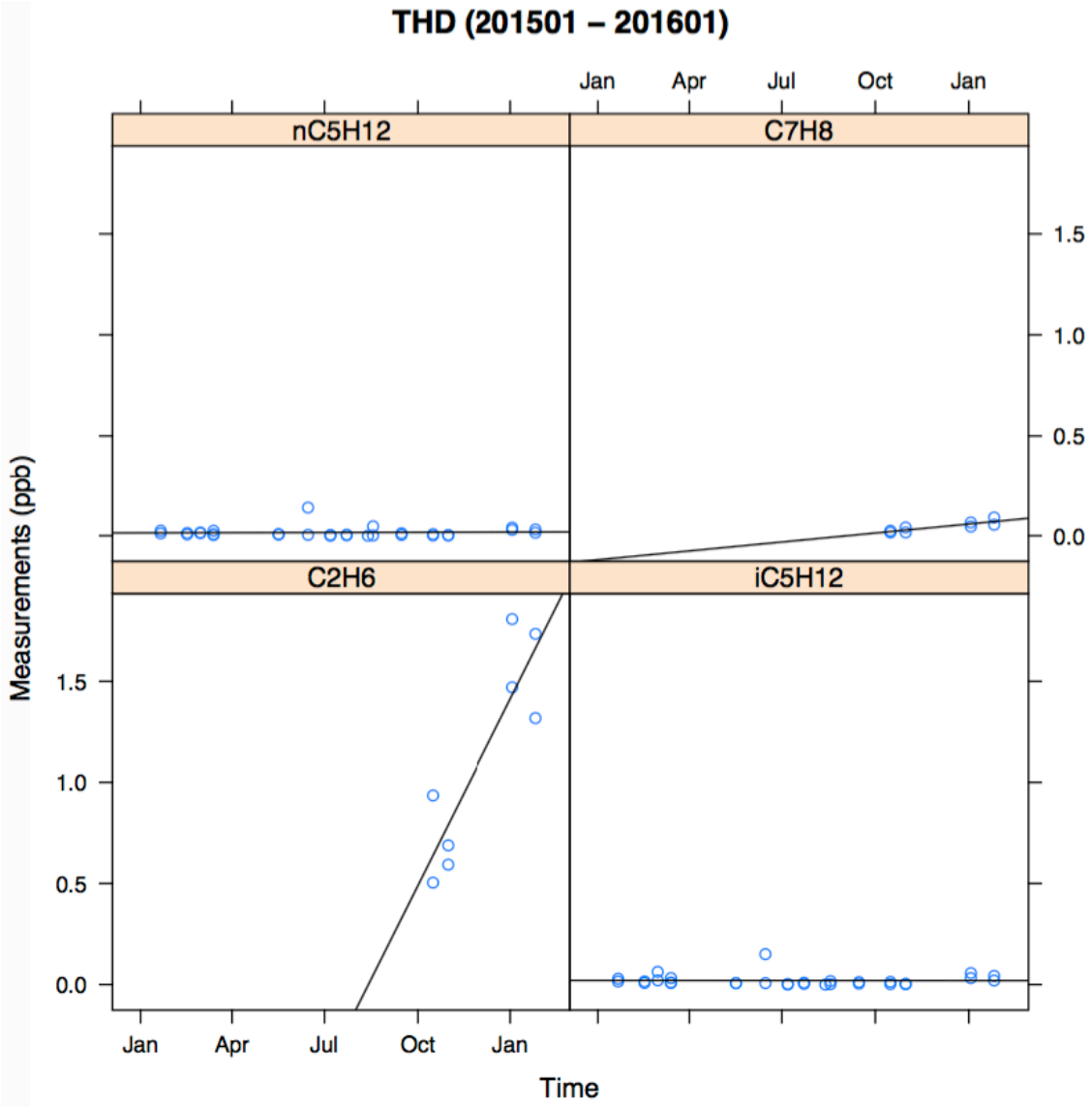

APPENDIX H:
Comparison of Measured and Predicted CH_4 Mixing Ratios and Estimated CH_4 Background for SFBA Analysis

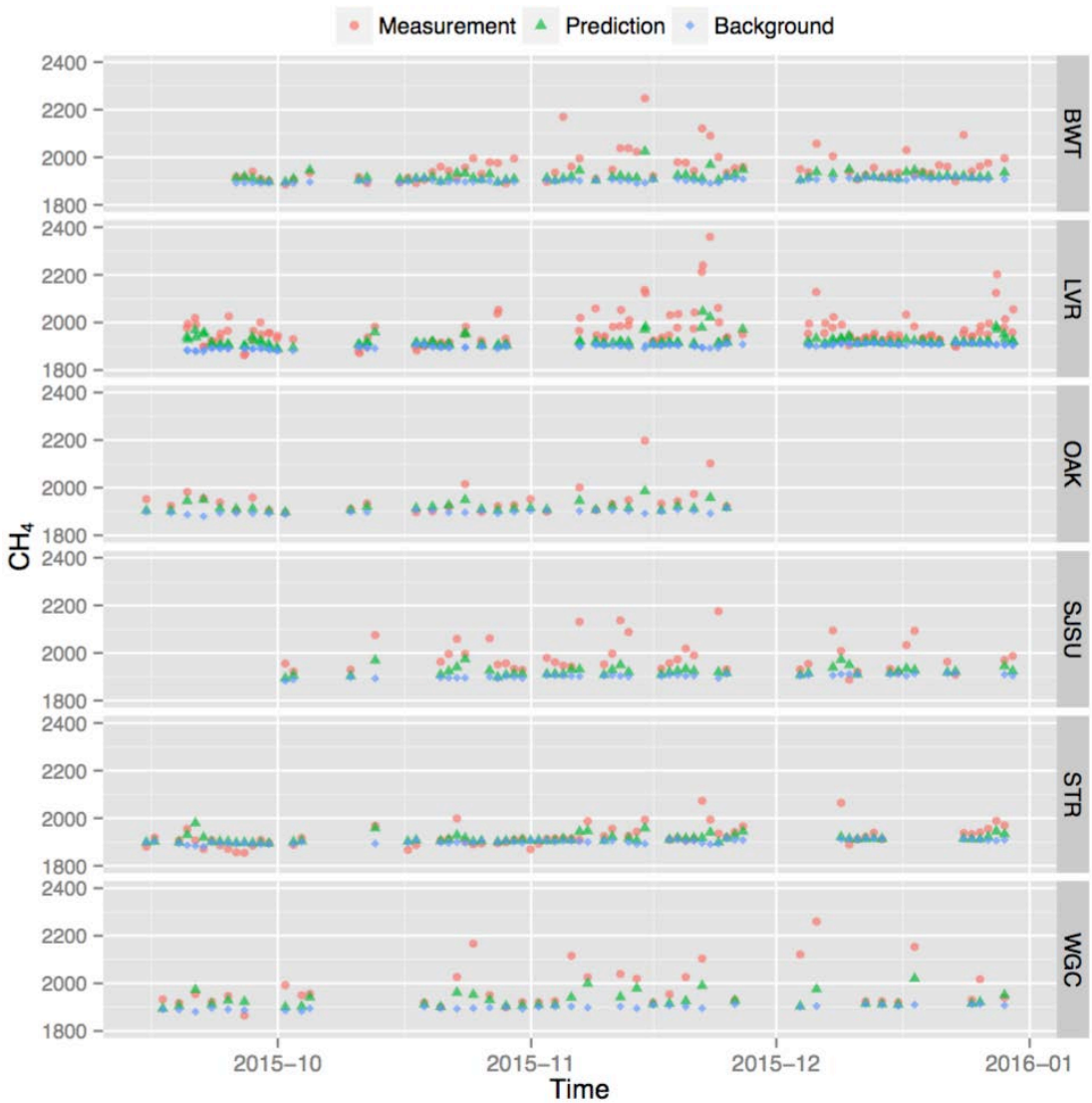

WRF-STILT model predictions are obtained using high-resolution (1 km) prior emission maps and footprints (i.e., surface influence). The estimated CH_4 background was added to the prediction for comparison. Each panel of the figure (top to bottom) shows the comparison for each site with the site information shown on the right. Overall, the predicted CH_4 mixing ratios are lower than the measurements, suggesting actual CH_4 emissions in SFBA are higher than the prior estimate.

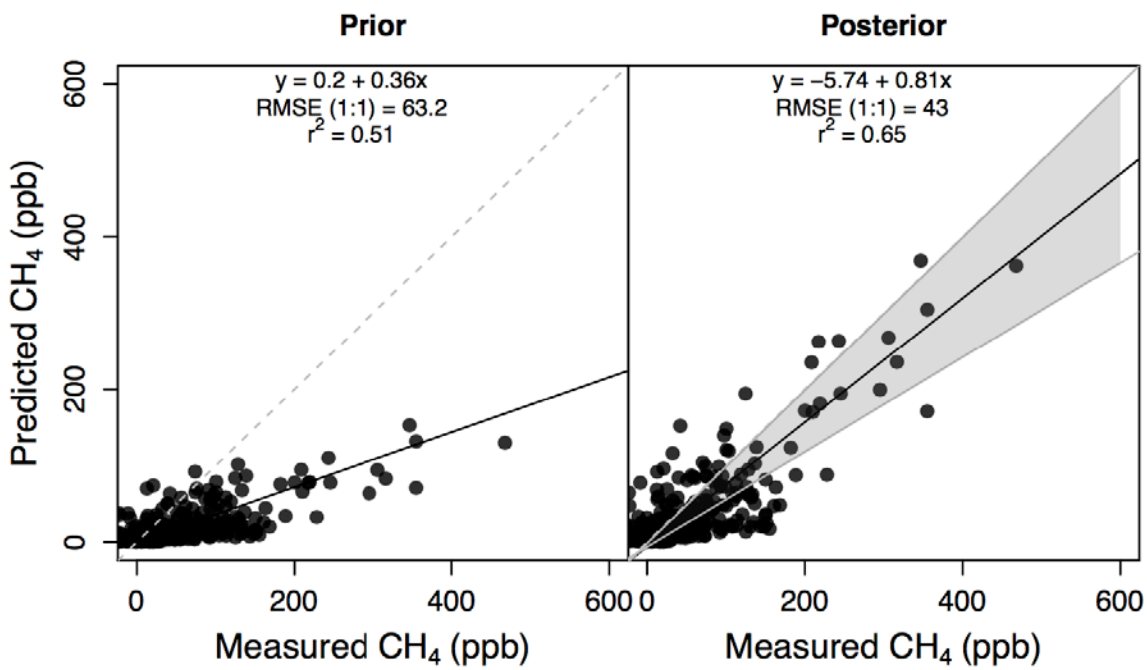

Comparison of predicted and measured CH_4 mixing ratios before (prior) and after (posterior) inversion for each season. Filled circles represent individual 3-hour data points across different sites used in the inversion. The gray dashed line indicates the 1:1 line, and the black solid line represents the best fit for the data shown. The regression coefficients in the posterior plot were calculated based on the median values of the 20000 MCMC samples. The gray shaded area in the posterior plot represents the 95% uncertainty region for the regression analysis using the 20000 MCMC samples.

APPENDIX I:
Correlation between the Landfill to Total Emission Ratios and the LF Emissions for SFBA

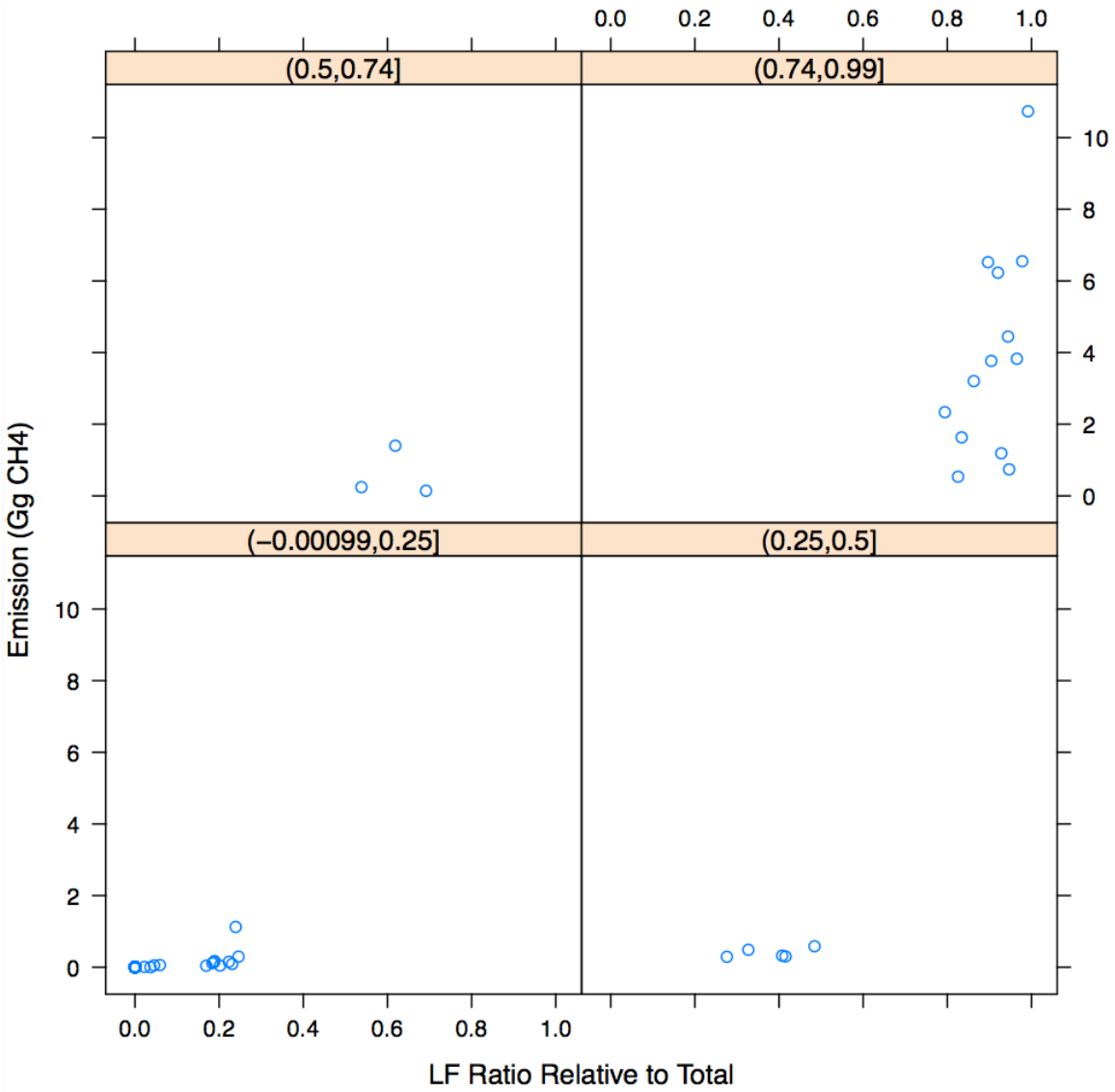

The correlation between the landfill (LF) to total emission ratios (X-axis) and the LF emissions (Gg CH_4/yr, Y-axis) for those pixels with non-zero LF emissions. Each data point represents the pixel with LF point source emissions (LF area source emissions (< 5 Gg in total) are not included), and the sum of these data points is 57 Gg CH_4 (see Table 2.3 in Chapter 2). Each panel shows the correlation plot for approximately each quarter of the ratio (between 0 and 1). Large emissions occur in the pixels with high ratios (of LF to total), and they are correlated. For example, for those pixels with the LF ratio of <0.74, the LF emissions are less than 2 Gg CH_4 whereas most of the large emissions are shown in the 0.74 – 0.99 ratio range.

APPENDIX J:
Evaluation of SFBA Atmospheric Transport Using Carbon Monoxide

The transport model is assessed using carbon monoxide (CO) measurements coupled with the gridded California Air Resources Board (CARB) CO emissions inventory. Anthropogenic CO emissions are tightly coupled to emissions from fuel combustion, which are inventoried for air quality control by CARB. Also, CO has few poorly constrained natural sources in California with wildfire being a major natural source (Pfister et al., 2005), which are easily identifiable and of limited duration. Because of these properties, bottom-up estimates of CO emissions are assumed to be associated with low uncertainty relative to bottom-up estimates of GHG emissions. Brioude et al. (2013) found that a comparison of measured and predicted CO (using the WRF-FLEXPART model) agreed to within about 15% for aircraft flights over SoCAB conducted in May and June, 2010. To generate CO emissions for our entire modeling domain, we combine hourly CO emissions data (~4 km × 4 km) for 2012 provided by CARB and the recent 2008 Emission Database for Global Atmospheric Research (EDGAR, the European Commission Joint Research Joint Research Centre and Netherlands Environmental Assessment Agency) for regions outside California. The EDGAR emissions are annual averages and available at ~10 km resolution.

In this study, CO is measured at all of our GHG sites except for LVR, where CO measurements are not available during our study period. To represent the LVR site where other gases are used for analysis, we use CO measurements from Sandia National Labs (SNL; latitude = 37.67°, longitude = -121.71°), which is located within 10 km of the LVR site. We use daily CO measurements for all sites except for SNL where hourly CO measurements are available. For CO upstream background concentrations, we use CO measurements from the THD site, as we do for VOCs.

Figure A.J1 shows the linear regression of predicted vs. measured CO for each site during September – December 2015. As with other gases, in this analysis we do not include the data points that do not meet the background criteria, which evaluate whether the majority (80% in this study) of the STILT particles for a given simulation time reach our western domain boundary (130°W). Predictions for BWT, SNL, and SJSU agree well with measurements in those sites within standard error (at 68% confidence). The prediction for STR is slightly higher than the measurement while the prediction for WGC is somewhat underestimated compared to the measurement. The regression result for OAK shows that the prediction is lower than the measurement although a few low predictions affect the overall fitting.

To estimate the overall bias in predicted CO during the study period, we combine data points across the sites and compare them (Figure A.J2). We use the potential bias in CO, which is assumed to represent the bias in atmospheric transport, to correct the CH_4 emissions estimate. Figure A.J2 (A) shows that the combined predicted CO mixing ratios are only slightly lower than the measurements, given the estimated error (at 68% confidence) in the regression analysis.

We also estimate the weighted best-fit slope using the normalized mean mixing ratio signal for each site, which represents the relative weights of individual sites on the weighted best-fit slope estimate (Figure A.J2(B)). Using a Monte Carlo method (sample size = 5×10^4), we estimate the weighted best-fit slope is 0.93±0.08, which suggests that predicted CO is consistent with the measurement within error. The normalized signal weights are shown in Figure A.J2(C) along with the best-fit results for all sites.

Using the weighted Monte Carlo analysis result, we estimate that on a seasonal basis the uncertainty associated with atmospheric transport of CO across SFBA is 7%±8% (at 68%), assuming no errors in the CO emissions maps. We assume that atmospheric inversions of CH_4 may share similar levels of uncertainty and can be usefully estimated with the WRF-STILT transport because the *a priori* emissions uncertainties are likely larger. If the CO analysis is applicable to CH_4 inversions, our CO analysis indicates that the posterior CH_4 emissions are overestimated by 7%±8% (at 68%) because of the transport bias. We add this uncertainty estimate to the uncertainty estimated from inversions to incorporate potential biases in atmospheric transport. We also note that the prior emissions are unlikely to completely capture fine scale spatial and temporal variations in actual CO emissions across SFBA.

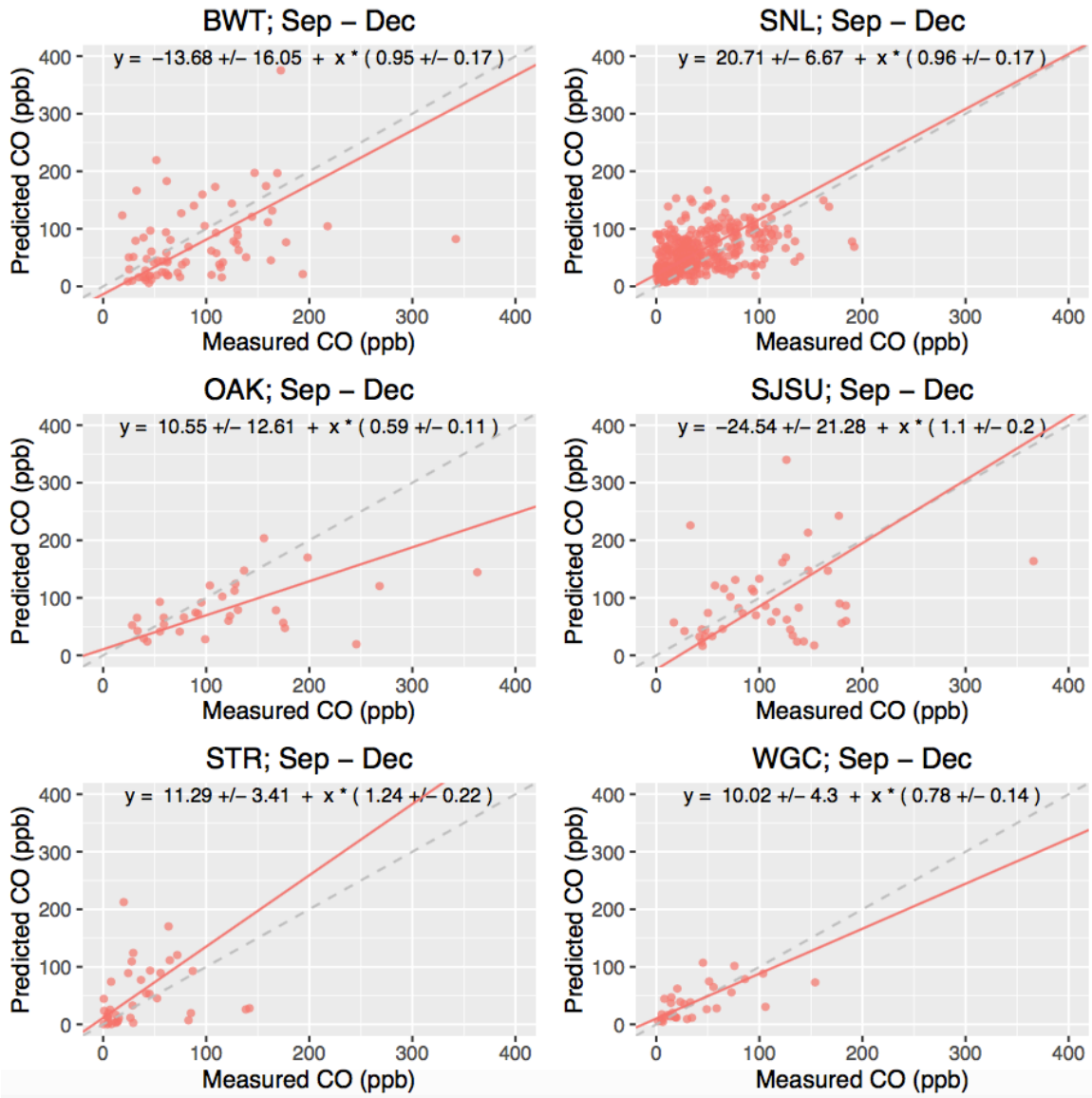

Figure A.J1. Comparison of predicted vs. measured CO during afternoon hours (12 – 17 PST) by site. Hourly CO data are available for SNL whereas only daily data are available for the other sites.

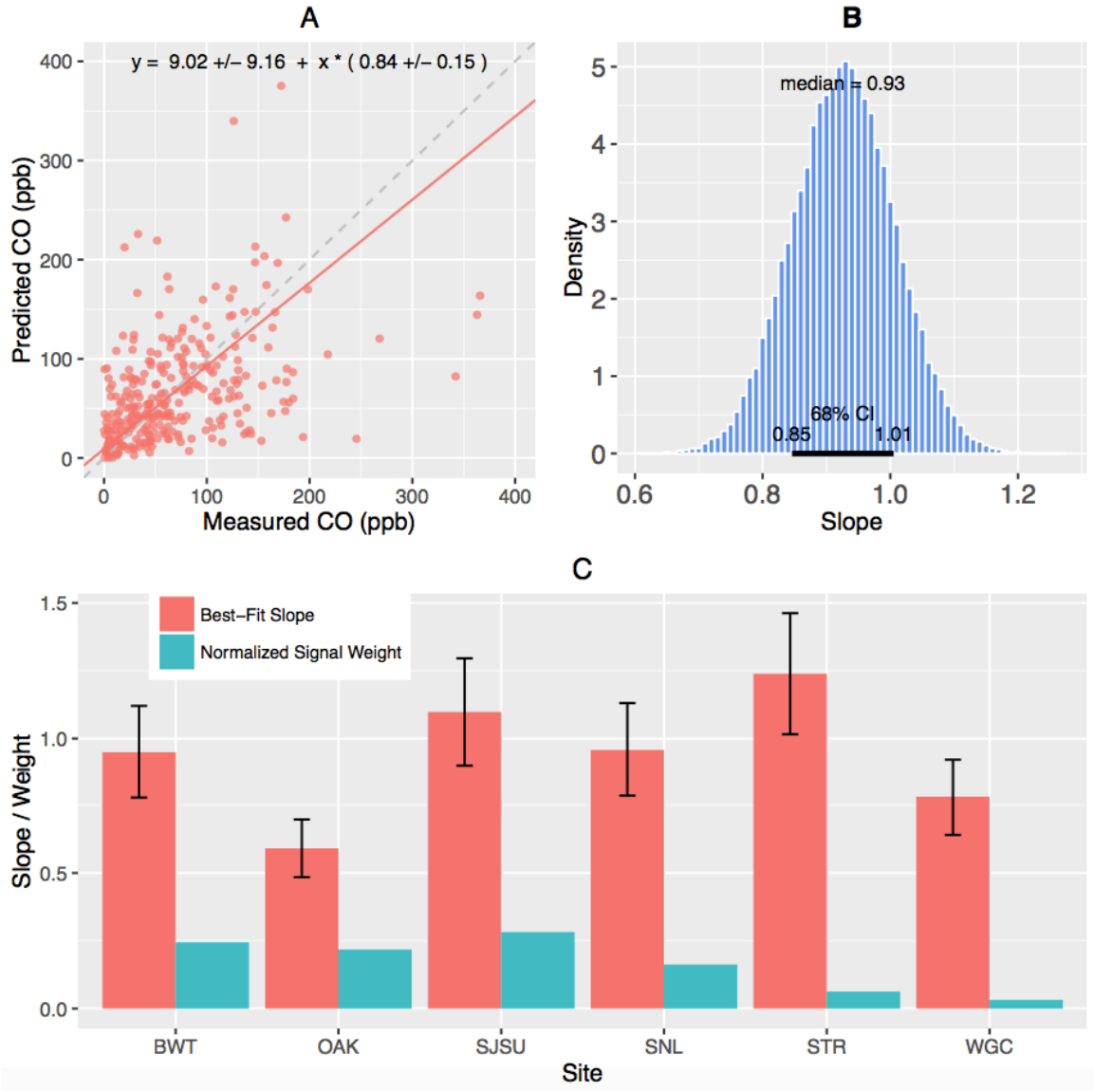

Figure A.J2. Analysis results of predicted and measured CO: (A) Comparison of predicted vs. measured CO, (B) probability distribution of the overall best-fit slope (across the sites) after taking into account the relative mixing ratio signals as weights shown in (C) and simulating the weighted mean slope using a Monte Carlo method, and (C) best-fit slopes and normalized (mean) mixing ratio signals by site. For the scatter plot in (A), we use CO data from SNL for the ~14 PST hour only, i.e., the time at which all other sites have data, to avoid the over-influence of SNL data in the fitting (note we have hourly data for SNL and daily data in the other sites). In (C), the error bar for the best-fit slope represents the standard error (i.e., 68% confidence) and the normalized weights sum to 1. The mean slope for each site is weighted by the normalized signal to estimate the overall mean best-fit slope for all sites shown in (B).

APPENDIX K:
High-resolution Methane Emission Model for SFBA

A high-resolution (~1 km × 1 km) methane emission model was developed for SFBA, and the method is described by sector. We estimate sector emissions for 2011 or 2012, depending on the data availability.

Dairy Livestock

Dairy livestock CH_4 emissions were estimated using the USDA 2012 cattle inventory (http://www.nass.usda.gov/Statistics_by_State/California/Publications/County_Estimates/2013lvsceF.pdf, Accessed January 2015) and the emission factors, which are based on the CH_4 emissions from the California Air Resources Board (CARB, http://www.arb.ca.gov/cc/inventory/inventory.htm, March 2014 version, Accessed January 2015). The USDA cattle inventory dataset provides dairy cow statistics for each county. For counties where county-level dairy cow data are not available, we use the USDA 2012 county cattle data from recent 2012 USDA Census Data (http://www.agcensus.usda.gov/Publications/2012/, Accessed January 2015), which are updated every five years. For spatial disaggregation, the dairy population data for 2005 by Salas et al. (2009) were used. We adjusted the dairy population from Salas et al. (2009) to match the data in the USDA 2012 cattle inventory by county.

The emission factors for dairy livestock (manure management and enteric fermentation) are derived based on the ratio of the state total emissions to the state total number of dairy cows (~1.78×10^6 from the USDA cattle inventory). The derived emission factors are shown in Table A.K1. For counties (e.g., Alameda, Sonoma) where dairy farms do not exist (Salas et al., 2009), we apportioned CH_4 emissions uniformly across the county, based on the dairy livestock population in the USDA cattle inventory.

Table A.K1. Emission Factors for the Dairy Livestock Sector

Subsector	State Total Emission (Tg* CH_4/yr)	Emission Factor† (Mg** CH_4/head)
Manure Management	0.410	0.230
Enteric Fermentation	0.329	0.185
Total	0.739	0.415

†A total of 1,779,870 dairy cows in the USDA cattle inventory were used to derive this emission factor.
*Tg = 10^{12} g.
**Mg = 10^6 g.

Non-dairy Livestock

Non-dairy emissions were estimated using county-level activity data and estimated emission factors. The major non-dairy (excluding poultry) sector includes emissions from non-dairy cattle, sheep, goat, horse, and swine. For non-dairy cattle, activity data were obtained from the USDA cattle inventory as with the dairy sector (http://www.nass.usda.gov/Statistics_by_State/California/Publications/County_Estimates/2013lvsceF.pdf). For sheep, goat, horse, and swine, USDA Census data (http://www.agcensus.usda.gov/Publications/2012/, Accessed January 2015) were used. The emission factors were derived based on statewide CH_4 emissions from CARB (CARB, 2014) and activity data from the USDA Census database. The derived emission factors include both enteric fermentation and manure management (Table A.K2).

Table A.K2. Major Non-dairy Emission Factor (Mg CH_4/head)

Type	Cattle	Sheep	Goat	Horse	Swine
Emission factor	0.036	0.007	0.005	0.115	0.017

In addition to major non-dairy emissions, poultry emissions were estimated. The poultry sector includes broiler, turkey, layers, and pullets. To obtain county-level activity data, we adjusted the county activity data from the 2000 CARB animal husbandry statistics (http://www.arb.ca.gov/ei/areasrc/fullpdf/FULL7-6.PDF) to match the 2012 state-level total in CARB (2014) because the current inventory does not have county-level data.

The spatially explicit emissions for domestic and other animals (i.e., dog, cat, deer, and wild pig) are also generated based on the county-level emissions estimates from BAAQMD. BAAQMD provides emissions estimates for each subsector by county, and we apportioned them uniformly across county by subsector, matching a total of 0.5 Gg CH_4/yr for the entire sector.

Landfill

Landfill emissions were estimated for point sources at the facility level and area sources. Landfill point source emissions were estimated based on the recent (year 2012) landfill emissions dataset from CARB (CARB, 2014), which is similar to that used in Jeong et al. (2013). Using this landfill emissions dataset, we estimate the total landfill emissions for BAAQMD is 56.9 Gg CH_4/yr. This value is similar to BAAQMD's estimate for landfill point sources, which is 57.2 Gg CH_4/yr. For the fugitive area source sector, we use the 2011 landfill CH_4 emissions estimated by BAAQMD because we don't have a separate estimate for this sector. BAAQMD estimates the total CH_4 emissions from landfill fugitive sources for 2011 are 4.6 Gg CH_4/yr. To

obtain spatially explicit emissions, we apportioned the total emissions for each county uniformly.

Natural Gas

Spatially explicit natural gas emissions were generated for eight subsectors using the emissions estimated by BAAQMD (BAAQMD, 2015). Among the eight subsectors, the emission map for the natural gas point source sector was prepared at the facility level. For the other subsectors, BAAQMD's total emissions were apportioned by population density (see Figure A.K1). Using a similar method to that of Jeong et al. (2013, 2014), for example, the emission map for "Other Fuel Use" (see Table A.K3), which represents fugitive emissions in the natural gas distribution system, was generated by distributing a total of 17.2 Gg CH_4 according to the population density map for BAAQMD.

Table A.K3. Summary of CH_4 Emissions for the Natural Gas Sector Estimated by BAAQMD (2015)

Sector	Subsector	Emissions (Mg CH_4/yr)
Natural Gas Distribution	Power Plant Fuel Use	4
	Other Fuel Use	17213
	Space Heating	70
Domestic Natural Gas	Water Heating	47
	Cooking	5
Other External Combustion	Natural Gas (point source)	32
	Industrial	68
	Commercial	60
Total		**17499**

Refinery

Refinery emissions were estimated based on CARB's facility-level refinery emissions dataset for 2009 (Jeong et al., 2013). We scaled individual facility emissions such that the total CH_4 emissions from all facilities match CARB's recent (March 2014 version, http://www.arb.ca.gov/cc/inventory/doc/doc_index.php, accessed in January 2015) state total emissions for the refinery sector (3.6 Gg CH_4/yr for 2012). For BAAQMD, we estimate the total CH_4 emissions for the refinery sector are 1.9 Gg CH_4/yr.

On-road Mobile

On-road mobile emissions were estimated based on the traffic volume data for 2011 (http://www.dot.ca.gov/hq/tsip/gis/datalibrary/Metadata/AADT.html, accessed July 2015). The traffic volume data represent annual average daily traffic (AADT, total volume for the year divided by

365 days) recorded at count locations on the California state highway system, which include state highways and major local roads. Because the AADT data are available only at limited locations on the state highway system, linear interpolation was applied to estimate AADT for the pixels on the 1-km grid for which recorded AADT data are not available. Then, we used the largest AADT count within a given 1-km pixel to represent the pixel's AADT, constructing a 1-km traffic density map. Distributing the total on-road emission (2.2 Gg CH_4/yr) estimated by BAAQMD (2015) proportional to the traffic density, we generated an on-road CH_4 emission map. In this study non-major roads were not included to generate the traffic density map.

Wastewater

Wastewater emission maps were prepared for the domestic and industrial wastewater subsectors by incorporating BAAQMD's emissions estimates. The domestic wastewater emissions (5.0 Gg CH_4/yr) are provided in three different categories: (1) anaerobic digesters, (2) centralized anaerobic treatment, and (3) septic systems. The anaerobic digester emission map was generated using the biogas production information at the facility level (BAAQMD, 2015), and for centralized anaerobic and septic systems, the total emissions were apportioned proportional to the population density.

Emission maps for the industrial wastewater sector were generated by incorporating the estimated CH_4 emissions (total = 2.0 Gg CH_4/yr) from BAAQMD (2015) and apportioning the estimated emissions for each county uniformly. For the pulp processing subsector, the total emissions (0.5 Gg CH_4/yr) were equally assigned to the two facilities in Santa Clara County. For refinery wastewater emissions, we apportioned the total CH_4 emissions (1.0 Gg CH_4/yr) in proportion to the refinery CH_4 emissions (described above). This approach assumes that the refinery wastewater emissions occur within the 1-km pixel where individual refining facilities are located.

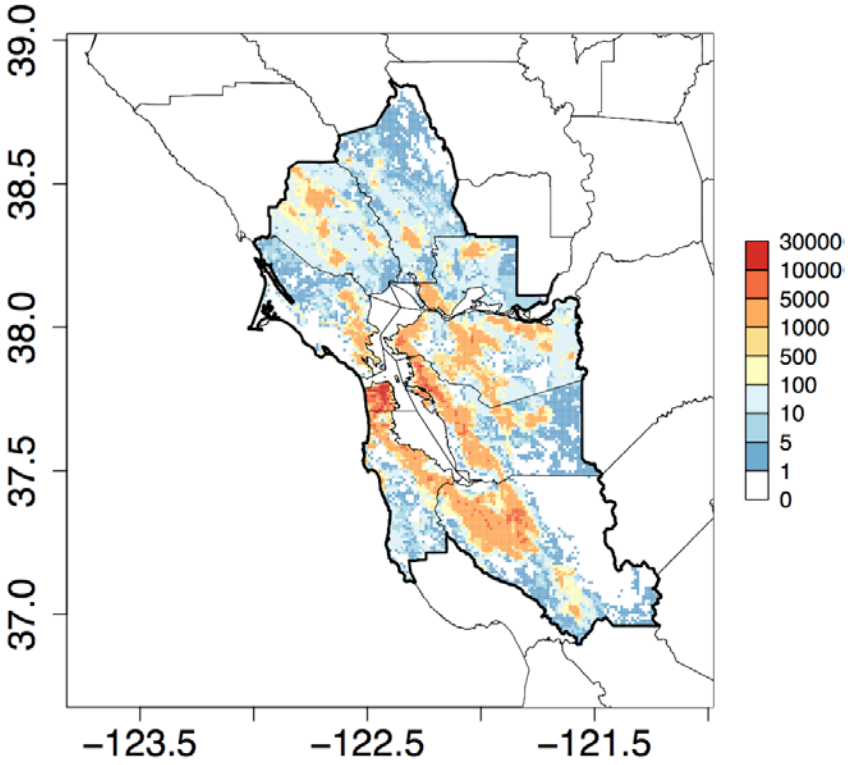

Figure A.K1. 1-km population density (persons/km^2) map for BAAQMD. This map was generated by aggregating the 30-m population map for 2000 available from http://geography.wr.usgs.gov/science/dasymetric/data.htm. The aggregated 1-km population map was adjusted by county to represent the 2010 census data (http://www.bayareacensus.ca.gov/bayarea.htm).

APPENDIX L:
Details of Hierarchical Inversion Method

We used a hierarchical Bayesian inversion (HBI, Ganesan et al. (2014)) method to estimate regional CH_4 emissions in California. In this work we develop an HBI method with more complex structure in representing the model-measurement mismatch matrix than Ganesan et al. (2014) for regional CH_4 emissions quantification.

We start with Bayes' rule and describe each probability distribution in the hierarchical structure of parameters that include the scaling factor (a set of factors used to adjust prior emissions, denoted as $\boldsymbol{\lambda}$). Generally, Bayes' rule can be applied to multiple parameters at different levels as

$$p(\boldsymbol{\phi}, \boldsymbol{\theta}|\boldsymbol{D}) \propto p(\boldsymbol{D}|\boldsymbol{\phi}, \boldsymbol{\theta})p(\boldsymbol{\phi}, \boldsymbol{\theta}) \qquad \text{(A1)}$$
$$= p(\boldsymbol{D}|\boldsymbol{\phi})p(\boldsymbol{\phi}|\boldsymbol{\theta})p(\boldsymbol{\theta})$$

where $\boldsymbol{\varphi}$ and $\boldsymbol{\theta}$ represent the generic parameters in vector form, and **D** is data used to estimate the parameters. The first line in Equation A1 simply states the posterior probability is proportional to the likelihood function and prior distribution. The re-factorization in the second line of Equation A1 holds because the data **D** depend only on the parameter $\boldsymbol{\varphi}$ (thus $\boldsymbol{\theta}$ is factored out), and the values of $\boldsymbol{\varphi}$ depend on the values of $\boldsymbol{\theta}$, constructing a hierarchical structure. The transition of $p(\boldsymbol{\phi}, \boldsymbol{\theta})$ to $p(\boldsymbol{\phi}|\boldsymbol{\theta})p(\boldsymbol{\theta})$ is by the property of a conditional probability, given the dependence of $\boldsymbol{\varphi}$ on $\boldsymbol{\theta}$. Any probabilistic model that can be factorized in chains, as shown in Equation A1, is a hierarchical model (Kruschke, 2015).

The general model in Equation A1 can be applied to estimate surface emissions and their uncertainties. For GHG applications, the parameter vector $\boldsymbol{\varphi}$ can represent scaling factors for emissions adjustment (or surface emissions themselves). The vector $\boldsymbol{\theta}$ can represent a set of parameters, including the hyper-parameters (e.g., mean) that determine the distribution for the scaling factor or surface emissions.

We use the following linear model for estimating scaling factors for regional emissions (Zhao et al., 2009; Jeong et al., 2012a; 2012b; 2013; Wecht et al., 2014)

$$\mathbf{y} = \mathbf{K}\boldsymbol{\lambda} + \mathbf{v} \qquad \text{(A2)}$$

where **y** is the measurement vector ($n \times 1$), which represents the 3-hourly local mixing ratio time series after subtracting background values, **K** = **FE** (an $n \times k$ matrix), **F** is the footprint ($n \times m$), **E** is prior emissions ($m \times k$), $\boldsymbol{\lambda}$ is a $k \times 1$ vector for scaling factors with a covariance matrix **Q** ($k \times k$), and **v** is a vector representing the model-measurement mismatch with a covariance matrix **R** ($n \times n$).

For the model in Equation A2, the joint parameters we need to estimate are

$$\boldsymbol{\Theta} = \{\boldsymbol{\lambda}, \boldsymbol{\mu}_{\boldsymbol{\lambda}}, \boldsymbol{\sigma}_{\boldsymbol{\lambda}}, \boldsymbol{\sigma}_{\boldsymbol{R}}, \eta, \tau\} \qquad \text{(A3)}$$

where $\boldsymbol{\lambda}$ is the scaling factor, $\boldsymbol{\mu}_{\boldsymbol{\lambda}}$ is the prior mean for $\boldsymbol{\lambda}$, σ_λ is the uncertainty for $\boldsymbol{\lambda}$ (i.e., square root of diagonal elements of **Q**), σ_R, η, and τ are the parameters used to construct the model-

measurement mismatch matrix **R** (see below for the representation of **R**). The diagonal elements of **R** represent the total model-measurement mismatch errors that are propagated through the inversion, and **Q** is used to define the uncertainty level for the prior emissions. These two quantities need to be either prescribed with known values or estimated. In HBI we estimate the joint parameter set simultaneously, using the measurements only once. This joint estimation is different from previous approaches (e.g., Jeong et al. (2013)) where the covariance matrix **R** was prescribed via explicit estimation without using atmospheric measurements. It is also different from other methods where atmospheric measurements were used to optimize **R**, and measurements were thereafter also used for inversions (e.g., Michalak et al., (2005)).

With the parameter set identified, we need to write out the posterior probability up to the likelihood function and prior densities (not including the evidence in the denominator in Bayes' rule). We apply the identified joint parameter (i.e., $\boldsymbol{\Theta}$) to the general formulation of a hierarchical model in Equation A1 to get the posterior probability as

$$p(\boldsymbol{\lambda}, \boldsymbol{\mu_\lambda}, \boldsymbol{\sigma_\lambda}, \boldsymbol{\sigma_R}, \eta, \tau | \boldsymbol{y}) \propto p(\boldsymbol{y} | \boldsymbol{\lambda}, \boldsymbol{\sigma_R}, \eta, \tau) p(\boldsymbol{\lambda} | \boldsymbol{\mu_\lambda}, \boldsymbol{\sigma_\lambda}) p(\boldsymbol{\mu_\lambda}) p(\boldsymbol{\sigma_\lambda}) p(\boldsymbol{\sigma_R}) p(\eta) p(\tau) \quad \text{(A4)}$$

where the right-hand side shows the likelihood function and the prior distribution for each parameter. In Equation A4 all variables are in vector form except for η and τ. To build Markov-chain Monte Carlo (MCMC) samplers for the posterior distribution in Equation A4, the JAGS system (just another Gibbs sampler, Plummer (2003)) is used together with the R statistical language (https://cran.r-project.org/). JAGS has been widely used for statistical inference studies in many fields including ecology and genetics (Korner-Nievergelt et al., 2015; McKeigue et al., 2010). The individual distributions in Equation A4 require explicit consideration and are described below.

First, for the likelihood function we use

$$p(y | \boldsymbol{\lambda}, \boldsymbol{\sigma_R}, \eta, \tau) \sim N(\boldsymbol{K\lambda}, \boldsymbol{R}) \qquad \text{(A5)}$$

where N is the normal distribution (here multivariate truncated normal, Miller et al. (2014); Michalak (2008)) with mean $\boldsymbol{K\lambda}$ ($n \times 1$) and covariance $\boldsymbol{R}$ ($n \times n$). Note that $\boldsymbol{y}$ is conditionally independent of all other parameters given $\boldsymbol{\lambda}$, $\boldsymbol{\sigma_R}$, η, and τ.

In order to estimate parameter values with Bayesian inference, prior uncertainty needs to be specified. In the hierarchical model, we need to include prior uncertainty for the joint parameter set $\boldsymbol{\Theta}$ using a series of distributions. The scaling factor $\boldsymbol{\lambda}$ is sampled from a normal distribution instead of a fixed value (e.g., Jeong et al. (2013), Wecht et al., (2014)) as

$$p(\boldsymbol{\lambda}) \sim N(\boldsymbol{\mu_\lambda}, \boldsymbol{\sigma}_\lambda) \quad \text{(A6)}$$

where $\boldsymbol{\mu_\lambda}$ itself is sampled from a truncated normal distribution (Miller et al., 2014; Michalak, 2008) with a mean of 1 and a standard deviation of 0.5 so that 68% of the samples are within 50 ~ 150% from the mean, which is a similar set-up to that of Ganesan et al. (2014). $\boldsymbol{\sigma}_\lambda$ is modeled using a half Cauchy distribution, which is one of the recommended distributions for model variances (Gelman and Hill, 2007; Gelman et al., 2014; Korner-Nievergelt et al., 2015). The

hyper-parameterization ("hyper" meaning the upper level in the hierarchy) for $\boldsymbol{\sigma_\lambda}$ can formally be expressed as

$$\boldsymbol{\sigma_\lambda} \sim hCauchy\ (0,1) \quad \text{(A7)}$$

where *hCauchy* is the half-Cauchy distribution. Note we take the absolute value from the Cauchy distribution so that we consider the positive values only (i.e., half Cauchy). Equation A7 suggests that, if we generate random samples (large enough) from Equation A7, we get a median value close to 1. Thus, the use of 1 for the half Cauchy scale parameter (the larger the scale parameter, the more spread out the distribution) is similar to assuming the uncertainty for $\boldsymbol{\lambda}$ is 100% in the classical Bayesian inversion (e.g., Zhao et al., (2013), Jeong et al., (2013)). The difference is that in this study $\boldsymbol{\sigma_\lambda}$ is sampled from a distribution with a heavy tail so that $\boldsymbol{\sigma_\lambda}$ can be optimized from a broad distribution (instead of being a fixed value, such as 50% of the mean emissions).

For the model-measurement covariance matrix $\boldsymbol{R}$, we use a popular exponential covariance function, which can be written in general form as (Rasmussen and Williams, 2006)

$$R_{i,j} = \eta^2 \exp\left(-\frac{1}{\tau}|t_i - t_j|\right) + \delta_{i,j}\sigma_{R_s}^2 \quad \text{(A8)}$$

where η, τ, and σ_{R_s} are parameters that define the covariance function, t is the measurement time, and δ is the Kronecker delta function (value of 1 if $i = j$, otherwise zero). We use two terms in Equation A8 to ensure the positive definiteness of $\boldsymbol{R}$ (see Figure A.L1 below for posterior estimates), which is often violated with the first term only (Stan Development Team, 2015). Here we use the L_1 norm (i.e., $|t_i - t_j|$) as in Ganesan et al. (2014). The subscript s in σ_{R_s} indicates that σ_R is estimated for each site as was done in Jeong et al. (2013) for their multi-tower analysis.

We model σ_{R_S} using the half Cauchy distribution as in σ_λ (Gelman and Hill, 2007; Gelman et al., 2014; Korner-Nievergelt et al., 2015). The scale parameter (in the hyper-parameter sense) for the half Cauchy distribution for σ_{R_S} is calculated using the first order approximation method following Jeong et al. (2012a; 2012b; 2013) and used as

$$p(\sigma_{R_s}) \sim hCauchy(0, \sigma_{R_{p|s}}) \quad \text{(A9)}$$

where $\sigma_{R_{p|s}}$ is the first-order estimate for σ_{R_s} and includes errors from several sources (e.g., transport and background errors) combined in quadrature.

For η, we use non-informative prior as

$$\eta \sim unif(0, L) \quad \text{(A10)}$$

where η is allowed to vary from 0 to L with an equal probability of $1/L$. In this study we use $\sigma_{R_{p|s}}$ as an upper limit for L to ensure the positive definiteness of the $\boldsymbol{R}$ covariance matrix, which is an important property of $\boldsymbol{R}$ (Stan Development Team, 2015).

Following Ganesan et al. (2014), we use the exponential distribution for τ as

$$\tau \sim \exp\left(\frac{1}{\tau_p}\right) \quad \text{(A11)}$$

where τ_p is the hyper-parameter for τ, which is assumed to be 7 days (typical synoptic time scale for transport, Ganesan et al. (2014)).

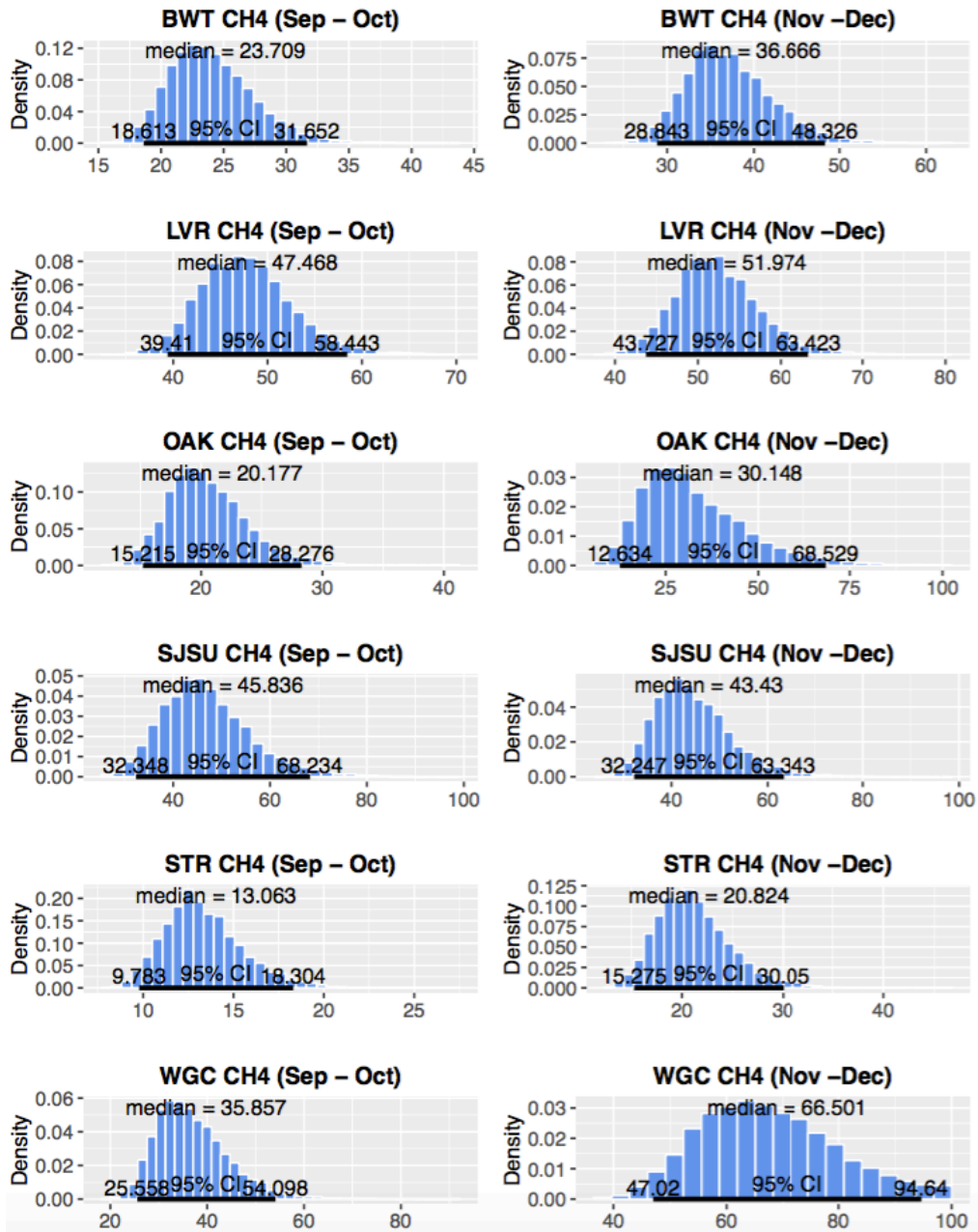

Figure A.L1. Model-measurement mismatch uncertainty. The values estimated here represent the diagonal terms in Equation A8.

APPENDIX M: Summary of Airborne Facility Measurements

Site	Date	Latitude	Longitude	Wdsp (m/s)	Wind con.	# of loops	NON-DIM	CH4	Quality	Frac below	Total Uncer	Binning uncer	Frac Error	C2H6	Frac below	C2H6 Uncer	Et:Me (molar)
Bellridge	4/17/14	35.4681	-119.7275	1.84	0.70	11	3.52	1953.5	0.40	0.46	717.9	131.6	0.07	NA	NA	NA	NA
Bellridge	6/17/14	35.4706	-119.7254	0.69	0.15	8	11.81	464.6	0.04	0.48	268.6	46.5	0.10	-6.2	NA	NA	-0.01
Bellridge	11/3/15	35.4639	-119.7225	3.84	0.94	6	3.90	63.2	0.19	1.11	42.2	16.4	0.26	-21.5	0.00	7.13	-0.18
Benicia	2/16/15	38.0674	-122.1385	3.26	0.90	7	0.97	700.0	0.41	0.31	272.1	65.3	0.09	NA	NA	NA	NA
Benicia	5/13/15	38.0714	-122.1356	8.34	0.95	16	0.28	315.4	0.71	0.56	76.0	30.3	0.10	50.3	0.54	4.61	0.08
Benicia	5/15/15	38.0718	-122.1340	8.83	0.98	19	0.27	220.1	0.81	0.34	32.4	11.6	0.05	44.7	0.29	2.64	0.11
Benicia	6/16/15	38.0715	-122.1355	4.52	0.91	5	0.52	231.2	0.35	0.78	91.1	16.1	0.07	45.8	0.82	3.97	0.11
Benicia	5/20/16	38.0678	-122.1300	10.65	0.99	21	0.31	583.9	0.85	0.39	78.4	35.9	0.06	131.7	0.36	7.62	0.12
Benicia	5/23/16	38.0674	-122.1301	6.75	0.99	31	0.48	293.0	0.91	0.35	31.9	19.4	0.07	27.5	0.29	1.67	0.05
Benicia	6/10/16	37.9888	-121.4748	8.10	0.97	10	0.30	329.2	0.55	0.29	98.0	24.2	0.07	14.3	0.36	1.63	0.02
Blythe	9/3/16	33.6055	-114.6420	5.62	0.99	8	0.31	234.9	0.37	0.48	160.9	87.2	0.37	17.7	0.43	5.15	0.04
Burney	9/10/16	40.8966	-121.6366	4.63	0.93	28	0.41	73.2	0.84	0.36	11.2	5.5	0.08	6.0	0.32	0.41	0.04
Elk Hills	11/5/15	35.2778	-119.4755	2.48	0.89	19	0.89	333.6	0.73	0.11	69.9	25.7	0.08	158.0	0.25	8.16	0.25
Elk Hills	6/9/16	35.2792	-119.4775	2.02	0.88	37	2.43	532.6	0.81	0.29	78.3	28.9	0.05	NA	NA	NA	NA
Gill Ranch	5/13/16	36.7914	-120.2529	6.28	0.99	27	0.15	4.6	0.28	2.09	4.9	3.3	0.71	1.7	0.48	0.09	0.19
Gill Ranch	5/22/16	36.7897	-120.2451	2.52	0.91	39	0.95	58.8	0.63	0.01	28.8	17.9	0.30	2.8	0.09	0.13	0.03
Gill Ranch	6/10/16	36.7893	-120.2462	4.60	0.99	18	0.48	35.9	0.51	1.07	25.1	16.2	0.45	4.0	0.34	0.34	0.06
Hanford	9/2/16	36.0718	-120.0909	1.24	0.77	20	1.53	2.8	0.43	2.40	1.9	1.1	0.40	1.2	0.15	0.06	0.22
Honor Rancho	6/9/16	34.4562	-118.5942	4.94	0.95	18	0.64	834.6	0.74	0.44	207.0	99.5	0.12	NA	NA	NA	NA
Honor Rancho	9/15/16	34.4562	-118.5936	2.00	0.65	59	0.97	-20.7	-0.51	-0.05	21.4	37.0	-1.79	3.2	0.27	0.69	-0.08
Kirby	2/16/15	38.1605	-121.9177	3.69	0.98	4	0.85	150.1	0.35	0.44	50.9	1.9	0.01	NA	NA	NA	NA
Kirby	5/12/15	38.1626	-121.9132	11.11	0.95	6	0.24	103.9	0.40	0.69	40.2	9.0	0.09	9.3	0.61	0.52	0.05

Kirby	5/13/15	38.1626	-121.9121	10.08	0.95	8	0.29	51.6	0.36	0.69	35.4	18.9	0.37	4.5	0.52	0.77	0.05
Kirby	6/16/15	38.1619	-121.9105	2.01	0.53	13	0.93	33.3	0.11	1.36	38.9	24.1	0.72	0.2	4.09	0.32	0.00
Kirby	5/13/16	38.1644	-121.9131	12.29	1.00	6	0.21	-10.2	0.37	0.00	-0.6	2.6	-0.26	-1.5	0.00	0.27	0.08
Kirby	5/17/16	38.1639	-121.9120	8.91	0.99	17	0.30	25.8	0.71	0.61	8.8	5.0	0.19	0.2	2.40	0.63	0.00
Kirby	5/20/16	38.1644	-121.9134	9.12	0.99	12	0.29	33.0	0.64	0.27	7.1	1.2	0.03	1.8	0.21	0.10	0.03
Lagoleta	5/26/16	34.4210	-119.8322	2.97	0.92	23	1.22	215.3	0.80	0.57	42.2	20.5	0.10	9.3	0.57	1.19	0.02
Lodi	5/13/16	38.2074	-121.2121	7.51	0.99	15	0.26	-89.6	0.65	-0.46	4.7	20.6	-0.23	-20.1	0.00	2.18	0.12
Los Medanos	5/17/16	38.0278	-122.0071	5.89	0.99	10	0.52	31.0	0.56	0.13	9.9	3.1	0.10	2.3	0.07	0.27	0.04
Los Medanos	5/20/16	38.0286	-122.0058	8.93	0.99	14	0.38	24.3	0.48	0.12	16.8	10.5	0.43	2.1	0.13	0.93	0.05
Los Medanos	5/22/16	38.0293	-122.0032	6.18	0.98	9	0.59	38.4	0.36	0.93	28.8	16.5	0.43	0.4	1.93	0.61	0.01
Martinez	5/13/15	38.0268	-122.0665	7.56	0.90	8	0.35	283.2	0.45	0.59	94.2	15.9	0.06	23.2	0.63	1.98	0.04
Martinez	5/15/15	38.0281	-122.0668	7.23	0.97	11	0.37	238.7	0.58	0.56	69.5	19.8	0.08	17.5	0.53	1.85	0.04
Martinez	5/23/16	38.0286	-122.0669	4.69	0.95	35	0.55	258.3	0.88	0.41	35.0	19.3	0.07	17.0	0.46	1.84	0.04
Mcdonald	6/16/15	37.9910	-121.4780	3.88	0.93	15	0.64	461.1	0.69	0.29	90.2	17.6	0.04	18.9	0.27	0.98	0.02
McDonald	5/13/16	37.9874	-121.4780	7.04	0.97	21	0.28	260.9	0.79	0.58	63.6	36.1	0.14	23.2	0.59	3.24	0.05
McDonald	5/14/16	37.9875	-121.4772	6.11	0.97	25	0.34	260.4	0.86	0.34	40.6	22.4	0.09	21.4	0.34	1.59	0.04
McDonald	5/18/16	37.9885	-121.4777	4.79	0.97	47	0.48	432.7	0.89	0.16	59.1	34.8	0.08	35.1	0.17	3.24	0.04
McDonald	6/10/16	38.0673	-122.1300	8.40	0.99	40	0.38	348.0	0.90	0.43	47.9	30.4	0.09	43.5	0.29	1.42	0.07
McDonald	5/12/15	37.9905	-121.4765	8.21	0.90	5	0.26	21.9	0.19	0.88	19.9	11.0	0.50	6.5	0.74	1.31	0.16
McDonald	5/12/15	37.9909	-121.4772	6.53	0.85	10	0.29	93.2	0.49	0.51	27.7	3.8	0.04	10.1	0.51	0.53	0.06
McDonald	5/13/15	37.9900	-121.4775	5.75	0.89	18	0.40	187.4	0.72	0.48	38.4	11.9	0.06	17.6	0.46	0.87	0.05
McDona	5/15/15	37.9894	-121.4769	4.63	0.92	14	0.51	184.3	0.65	0.41	44.7	12.3	0.07	NA	NA	NA	NA

ld																	
McDonald	6/6/14	37.9905	-121.4831	4.13	0.98	5	1.05	99.3	0.37	0.57	41.0	9.9	0.10	NA	NA	NA	NA
McDonald	9/26/14	37.9891	-121.4784	3.90	0.97	8	0.50	107.2	0.48	0.53	38.1	10.1	0.09	7.0	0.55	0.72	0.03
Mettler	9/2/16	35.0612	-119.0284	1.53	0.78	22	1.17	92.7	0.69	0.26	19.2	4.7	0.05	5.0	0.39	0.42	0.03
Moreno	9/3/16	33.9094	-117.1201	2.38	0.84	20	0.85	42.5	0.72	0.14	7.0	1.0	0.02	3.3	0.19	0.06	0.04
Needles	9/3/16	34.6967	-114.6101	7.08	0.97	11	0.31	12.2	0.52	0.26	5.9	3.0	0.24	2.0	0.28	0.19	0.09
Newberry	9/15/16	34.7803	-116.5962	3.67	0.94	31	0.47	71.9	0.87	0.29	9.6	4.9	0.07	3.8	0.27	0.21	0.03
Panoche	9/13/16	36.6507	-120.5805	4.15	0.97	16	0.39	158.0	0.74	0.38	29.8	9.4	0.06	1.7	0.41	0.11	0.01
Pleasant Creek	9/26/14	38.5496	-122.0020	2.48	0.92	11	0.71	22.2	0.55	0.78	7.1	2.2	0.10	2.2	0.72	0.25	0.05
Pleasant Creek	6/16/15	38.5476	-121.9949	1.41	0.63	15	1.38	8.8	0.46	0.55	3.2	0.8	0.09	-0.1	-0.02	0.03	-0.01
Pleasant Creek	5/17/16	38.5513	-122.0035	8.97	0.98	10	0.22	24.0	0.53	0.58	9.8	4.1	0.17	1.4	0.55	0.20	0.03
Pleasant Creek	5/20/16	38.5507	-122.0039	5.01	0.97	13	0.40	8.0	0.66	0.38	1.7	0.3	0.04	0.6	0.43	0.06	0.04
Princeton	5/17/16	39.3842	-122.0307	10.17	1.00	13	0.17	43.4	0.66	0.61	12.2	4.8	0.11	0.1	2.20	0.58	0.00
Rodeo	2/16/15	38.0422	-122.2511	2.61	0.86	7	1.37	271.3	0.28	0.98	207.3	109.8	0.40				0.00
Rodeo	5/12/15	38.0447	-122.2516	9.24	0.96	7	0.25	487.8	0.44	0.76	179.4	41.8	0.09	49.2	0.75	4.87	0.05
Rodeo	5/15/15	38.0455	-122.2513	8.37	0.98	10	0.29	221.5	0.49	0.83	113.6	57.3	0.26	18.8	0.91	5.89	0.05
Rodeo	6/16/15	38.0457	-122.2519	4.35	0.95	7	0.53	526.6	0.42	0.74	218.1	66.7	0.13	40.8	0.71	4.70	0.04
Rodeo	5/23/16	38.0442	-122.2524	4.24	0.98	30	0.63	22.8	0.70	0.39	9.9	6.4	0.28	2.3	0.37	0.42	0.05
Wild Goose	5/12/15	39.3238	-121.8834	1.32	0.37	15	1.41	-2.9	0.22	0.00	-0.2	0.9	-0.31	0.2	0.35	0.03	-0.03
Wild Goose	6/16/15	39.3243	-121.8822	2.81	0.75	15	1.28	105.0	0.52	0.11	42.2	16.9	0.16	1.3	0.08	0.16	0.01
Wild Goose	5/17/16	39.3239	-121.8835	9.20	0.99	6	0.14	2.3	0.41	0.12	0.9	0.2	0.10	0.2	0.60	0.01	0.04
Wild Goose Compressor	9/11/16	39.3500	-121.8175	5.40	0.98	23	0.32	166.6	0.80	0.54	41.5	25.2	0.15	12.3	0.52	1.78	0.04